VERIFICATION AND MATLAB IMPLEMENTATION OF THE INVERSE DYNAMICS MODEL OF THE METU GAIT ANALYSIS SYSTEM

A THESIS SUBMITTED TO
THE GRADUATE SCHOOL OF NATURAL AND APPLIED SCIENCES
OF
MIDDLE EAST TECHNICAL UNIVERSITY

BY

KORAY SAVAŞ ERER

IN PARTIAL FULFILLMENT OF THE REQUIREMENTS
FOR
THE DEGREE OF MASTER OF SCIENCE
IN
MECHANICAL ENGINEERING

FEBRUARY 2008

Approval of the thesis:

VERIFICATION AND MATLAB IMPLEMENTATION OF THE INVERSE DYNAMICS MODEL OF THE METU GAIT ANALYSIS SYSTEM

Submitted by **KORAY SAVAŞ ERER** in partial fulfillment of the requirements for the degree of **Master of Science in Mechanical Engineering Department, Middle East Technical University** by**,**

Prof. Dr. Canan ÖZGEN _____
Dean, Graduate School of **Natural and Applied Sciences**

Prof. Dr. Kemal İder _____
Head of Department, **Mechanical Engineering**

Asst. Prof Dr. Ergin Tönük _____
Supervisor, **Mechanical Engineering Dept., METU**

Assoc. Prof. Dr. Sibel Tarı _____
Co-Supervisor, **Computer Engineering Dept., METU**

Examining Committee Members:

Prof. Dr. Mehmet Çalışkan _____
Mechanical Engineering Dept., METU

Asst. Prof. Dr. Ergin Tönük _____
Mechanical Engineering Dept., METU

Assoc. Prof. Dr. Sibel Tarı _____
Computer Engineering Dept., METU

Prof. Dr. M. Kemal Özgören _____
Mechanical Engineering Dept., METU

Asst. Prof. Dr. Senih Gürses _____
Engineering Sciences Dept., METU

Date: 07.02.2008

I hereby declare that all information in this document has been obtained and presented in accordance with academic rules and ethical conduct. I also declare that, as required by these rules and conduct, I have fully cited and referenced all material and results that are not original to this work.

Name, Surname: Koray Savaş Erer

Signature:

ABSTRACT

VERIFICATION AND MATLAB IMPLEMENTATION
OF THE INVERSE DYNAMICS MODEL
OF THE METU GAIT ANALYSIS SYSTEM

Erer, Koray Savaş
M.Sc., Mechanical Engineering Department
Supervisor: Asst. Prof. Dr. Ergin Tönük
Co-Supervisor: Assoc. Prof. Dr. Sibel Tarı

February 2008, 133 Pages

The METU Gait Analysis System employs a computer program called Kiss-GAIT for the calculation of joint angles, moments and powers using force plate data and marker trajectories as input. Kiss-GAIT was developed using Delphi and is confined to calculations related to the standard gait protocol. Because the code lacks the flexibility required to carry out various test cases, the inverse dynamics formulation being used could not be verified and the extent of the error propagation problem could not be determined so far.

The first aim of this study was to develop a code for the inverse dynamics model of the METU Gait Analysis System making use of the flexible programming environment provided by MATLAB. Verified and more reliable analysis results, obtained by reformulating the inverse dynamics algorithm in a new code, are presented. Secondly, data smoothing and differentiation techniques conventionally used in gait analysis were critically reviewed. A common tool used for filtering marker trajectories is the Butterworth digital filter. This thesis presents a modified, adaptive version of this classical tool that can handle non-stationary signals owing to its coefficients which are functions of local signal structure.

The results of this thesis indicate the dominancy of ground reactions as compared to inertial effects in normal human gait. This implies that the accuracy needed in body segment inertial parameter estimation is not a critical factor. On the other hand, marker trajectories must be as accurate as possible for meaningful kinetic patterns. While any smoothing and differentiation routine that produces reasonable estimates is sufficient for joint moment calculation purposes, the estimation performance becomes a key requirement for the calculation of joint powers.

Keywords: Gait Analysis, Inverse Dynamics, Butterworth Filter, Non-stationary Signals.

ÖZ

ODTÜ YÜRÜYÜŞ ANALİZİ SİSTEMİ
EVRİK DİNAMİK MODELİNİN
DOĞRULANMASI VE MATLAB ORTAMINA AKTARILMASI

Erer, Koray Savaş
Yüksek Lisans, Makine Mühendisliği Bölümü
Tez Yöneticisi: Y. Doç. Dr. Ergin Tönük
Ortak Tez Yöneticisi: Doç. Dr. Sibel Tarı

Şubat 2008, 133 Sayfa

ODTÜ Yürüyüş Analizi Sistemi, eklem açılarını, momentlerini ve güçlerini, kuvvet platformu ve işaretleyici yörüngeleri bilgilerini kullanarak hesaplayan Kiss-GAIT adlı bir yazılım ile çalışmaktadır. Delphi ile geliştirilen Kiss-GAIT yazılımı, standart yürüyüş analizi hesaplamaları ile sınırlıdır. Şu andaki kodun çeşitli testlere izin verecek esnekliğe sahip olmaması nedeniyle kullanılan evrik dinamik biçimlendirmesi doğrulanabilmiş değildir ve sistemindeki hata yayılım sorununun boyutları belirlenememektedir.

Bu çalışmanın ilk amacı ODTÜ Yürüyüş Analizi Sistemi için, MATLAB tarafından sağlanan esnek programlama ortamından yaralanarak, bir kod geliştirmekti. Evrik dinamik algoritmasının yeni bir kodun içinde tekrar biçimlendirilmesiyle elde edilen doğrulanmış ve daha güvenilir analiz sonuçları sunulmaktadır. İkinci olarak, yürüyüş analizinde kullanılagelmekte olan veri düzleme ve türevleme teknikleri eleştirel bir bakış açısıyla irdelenmiştir. İşaretleyici yörüngelerinin süzülmesinde yaygın olarak kullanılan araçlardan biri Butterworth sayısal süzgecidir. Bu klasik aracın, durağan-olmayan sinyalleri, yerel sinyal yapısının işlevi olan katsayıları sayesinde süzebilen, uyarlanır bir biçimi bu tezde sunulmaktadır.

Bu tezin sonuçları, normal insan yürüyüşündeki yer tepkilerinin ataletsel etkilere kıyasla baskınlığına işaret etmektedir. Bu, uzuv ataletsel değiştirge tahmininde ihtiyaç duyulan doğruluk oranının ciddi bir etmen olmadığını gösterir. Öte yandan, anlamlı kinetik desenler için, işaretleyici yörüngeleri mümkün olduğunca doğru olmalıdır. Anlamlı tahminler ürüten herhangi bir düzleme ve türevleme uygulaması eklem momentlerini hesaplama amacı için yeterli olurken; tahmindeki başarım, eklem güçlerinin hesaplanmasında anahtar bir gereksinim haline gelmektedir.

Anahtar Kelimeler: Yürüyüş Analizi, Evrik Dinamik, Butterworth Süzgeci, Durağan-olmayan Sinyaller.

ACKNOWLEDGEMENTS

The author thanks to Prof. Dr. Turgut Tümer for providing the opportunity to work in the field of gait analysis.

The author thanks to Asst. Prof Dr. Ergin Tönük for his support during the final phases of the work.

The author thanks to Assoc. Prof. Dr. Sibel Tarı for her understanding.

The author acknowledges all those who contributed to the completion of this work in this or that way.

National Scholarship for MSc Students provided by TÜBITAK is also acknowledged.

TABLE OF CONTENTS

CHAPTER 1

INTRODUCTION

One of the best aspects of doing scientific study is that most of the work can most probably be established upon what has been clarified by former researchers; scientific progress is made possible by such accumulation of technical knowledge. This work, whose foundations are available in the extensive literature on gait analysis, is no exception.

Walking is the most direct means of human locomotion and has unsurprisingly been subject to extensive research. The specialized area of research associated with human walking is called gait analysis. The dictionary meaning of gait is *a particular way of walking*. As its name implies, gait analysis aims to unveil the mechanisms of human gait; in other words, it tries to shed light upon the manner in which human beings walk.

Gait analysis is composed of attempts to quantify human walking. It has a multi-disciplinary nature and is by definition far from being purely theoretical. Analysis of human gait involves cooperation of specialists from medical and engineering sciences. Information gained through investigation of how the real biosystem, the human body, accomplishes the task of walking provides invaluable insight into real problems.

Identification of pathological gait is perhaps the most direct application of gait analysis. Quantification of human gait provides clinicians with objective means for distinguishing between normal and abnormal gait. Gait analysis also plays an important role in decision making. Analysis results may imply potential injury, in which case preventive action can be taken. And if injury has occurred, gait data can lead to correct selection between treatment options, obviating unnecessary surgical

operation. Moreover, effectiveness of a treatment can be assessed by comparing pre- and post-treatment analysis outputs. In addition to these medical applications, a non-medical example might be retrieved from the field of robotics: Gait analysis can supply useful information about kinematics and kinetics of human walking to be used in the design and manufacturing of humanoid robots. In short, it is likely that there is a lot of potential in gait analysis, which has not yet been fully utilized.

Basically, gait analysis aims to arrive at mathematical relationships that govern the task of walking. For this purpose, it uses information extracted from the human body. One commonly adopted information extraction method is to record trajectories of body landmarks while ground reactions are simultaneously measured. Markers attached to various locations on the body facilitate this trajectory recording process and force plates provide ground reaction readings.

1.1. Motivation

The METU Gait Analysis Laboratory is one of many laboratories in the world equipped with cameras and force plates. The laboratory has been in the service of academic and clinical gait analysis applications for nearly a decade. In spite of this seemingly long duration, there are several issues that have not yet received the necessary attention.

This thesis is one of many studies about the METU Gait Analysis System called **Kiss** (**K**as **is**kelet **s**istemi in Turkish, **Ki**nematic **s**upport **s**ystem in English). The very first works were completed during the initialization of the set-up and involve information on hardware and software that are still being used in the laboratory (Güler, 1998) and on trajectory generation algorithms employed by the system (Shafiq, 1998). Later studies assess marker tracking capabilities of the system (Karpat, 2000) and reliability / repeatability of the adopted analysis protocol (Söylemez, 2002). Another early work concerns with effects produced by skin induced deviation of markers (Afşar, 2001). Recently, comparison of kinematic results of the system with those of a commercial system was presented (Civek, 2006). Another recent study is about sensitivity / compatibility of the analysis

protocol to variations in experimental methodology (Kafalı, 2007). Except for that of Güler (1998), none of the works listed here includes evaluation of kinetic results produced by the system. The corresponding dissertation of Güler (1998) evaluates results from a former, inferior hardware configuration which was not representative of the current configuration.

The inverse dynamics model of Kiss is originally embedded in the software program Kiss-GAIT, which has been used to process marker trajectories to obtain kinematic as well as kinetic gait variables. The problem is that Kiss-GAIT was developed using the development tool Delphi (Borland Software Corporation), which does not provide a flexible programming environment in current standards. The calculation routine in Kiss-GAIT is therefore confined to a previously coded form which does not allow tests to be carried out to verify the existing inverse dynamics formulation and to determine the extent of the error propagation problem.

This work intends to give a full and coherent investigation of kinetic analysis capabilities of the system. The inverse dynamics model utilized by Kiss-GAIT was examined in the course of the study and several modifications to improve its reliability and traceability are proposed in this text. Examinations firstly revealed that there were complications inherent in the smoothing and differentiation algorithms, which adversely affect joint power results produced by Kiss-GAIT. Secondly, it was seen that kinematic computations were realized in a circuitous manner, which requires a certain deal of computational effort and which, more importantly, is not straightforward to understand and to implement.

1.2. Scope

With the aim of devising a consistent smoothing and differentiation algorithm for Kiss, filtering methods mentioned in the related literature were critically reviewed. During the process, it was realized that the conventional Butterworth filter, the actual potential of which is underestimated by Kiss-GAIT, was a suitable noise suppression tool for gait analysis purposes. It is nevertheless undeniable that this tool, like all conventional filters, is poor in performance when it comes to

processing non-stationary signals. Experimentations conducted in this direction resulted in a modified version of the Butterworth filter, which is described in this text. This work shows that employment of either the conventional or modified version of this filter, followed by a numerical differentiation routine, ensures more reliable joint power curves. The reason why joint powers, not joint moments, are improved is the fact that powers are obtained by multiplication of moments with angular rates. Due to the dominancy of ground reactions in human gait, the effect of the performance of a filtering technique is limited in moment calculations. On the contrary, the filtering technique directly determines the quality of estimated rates; in other words; the quality of estimated joint powers. Moreover, an improvement for kinematic computations is suggested here. This improvement is merely a reformulation of the algorithm using a direct computational approach so that the corresponding section of the source code is more traceable than that of Kiss-GAIT.

Various tests on previously acquired gait data were executed making extensive use of the flexible programming environment MATLAB (The MathWorks, Inc.) provides. Considering that the first aim of this thesis was to develop a MATLAB code for the inverse dynamics model of the METU Gait Analysis System, the graphical user interface KissGaitM developed during the course of the study serves this purpose.

1.3. Outline

Chapter 2 is a concise overview of techniques used in kinetic analysis of gait.

Chapter 3 briefly introduces the METU Gait Analysis System and then discusses some important features about the system.

Chapter 4 is an investigation of spectral behaviours of selected signals that may be regarded as representatives of gait data for purposes of designing and testing filter routines.

Chapter 5 is devoted to the second order Butterworth filter. Its regular and adaptive formulations are presented and their performances are evaluated.

Chapter 6 includes the introduction of a gait analysis program that runs in the MATLAB environment. Several newly developed algorithms are described in detail and results are presented.

Chapter 7 discusses several issues and tries to reach conclusions based on the discussions. Suggestions for further work are also presented.

.

CHAPTER 2

AN OVERVIEW OF KINETIC ANALYSIS OF GAIT

Objective assessment of gait is possible with quantitative availability of angular joint variables. It naturally follows that the primary concern of gait analysis is to reveal these variables. Gait analysis tries to accomplish this via two specialized tools: kinematic analysis and kinetic analysis, the prerequisite of the latter being the former. Kinematic analysis reveals how joint angles vary throughout the gait cycle. Joint moments, by means of which such angular motion is realized, are the outputs[1] of kinetic analysis, or inverse dynamics analysis in its current meaning.

There are several problematic issues of kinematic analysis such as determination of joint centres[2] and construction of marker coordinates. On top of difficulties related to kinematic analysis, inverse dynamics analysis has inherent complications that render the issue more problematic. Although the methods of inverse dynamics are well defined and easily applicable, it is not as straightforward to obtain the inputs it requires. This routine is basically an estimation process, where inertial parameters and accelerations of body segments must be calculated. Estimation is the correct word here as these are almost never directly known. The tools of estimation are numerous and will be briefly described in what follows after several points about inverse dynamics are discussed.

2.1. Inverse Dynamics

As opposed to direct dynamics, which is used to generate movement trajectories by manipulating known forces and moments applied on a mechanical system, inverse

[1] Joint forces are also calculated in the process. Joint powers and work done by joints can also be computed.

[2] There are no biological rotation centres in reality; joint centres are just mechanical idealizations.

dynamics proceeds in a direction opposite to natural flow of events (Yamaguchi et al., 1991). It is the task of calculating forces and moments using acquired trajectory information, estimated body segment inertial parameters (BSIP), and frequently, measured external reaction forces and moments.

Inverse dynamics is a very powerful tool for gaining insight into kinetics of motion; yet, it is well known to be prone to errors when applied to human motion. Errors arise from a number of sources among which are inaccuracies in estimated BSIP, inherent noise in observed marker trajectories and in ground reaction measurements, inaccuracies in locating joint centres, and unavoidable relative motion between markers affixed to skin and underlying bones (Riemer et al., 2007). A broader perspective may be assumed by claiming that there is a fundamental inconsistency present in analysis methods in that data from actual biosystems are used in mathematical models whose dynamic behaviours are not representative of the actual systems (Hatze, 2002). From whichever point of view the issue might be observed, the conclusion to be drawn is that each and every attempt to perform inverse dynamics analysis of gait will inevitably result in errors of varying degrees.

Although far from being the most adequate one, the customary approach in motion analysis is to model the human body as a system of rigid objects, i.e. body segments, connected to each other by means of mechanical joints. Segmental interactions of such a system can easily be calculated by employing the Newton-Euler formulae in a recursive manner. Calculations are initiated from segments with known boundary conditions, recursively progressing to neighbouring segments. This way, it is possible to obtain all forces and moments in joints as well as unknown external reactions provided that there are as many known variables as there are unknowns[3].

When no inputs other than observed trajectories and estimated BSIP are available, inverse dynamics is known to yield poor results as it relies on accelerations

[3] Human running and gait in swing phase are examples of such determinacy, where ground reactions do not act on both feet simultaneously. Weight lifting might be another example; although both feet are in contact with ground, reactions may be assumed to be equally distributed owing to symmetry considerations.

obtained by double differentiation of noisy displacement data (Kuo, 1998). One remedy would be introducing additional information in the form of force plate measurements, which are almost always more precise than acceleration estimates. Calculations are performed in a bottom-up fashion; and naturally, zero boundary conditions are expected for the head, the top-most segment. However, this requirement is very likely to be violated. Inverse dynamics failure, which manifests itself as residual forces and moments, is generally inevitable (Kuo, 1998). The failure can be prevented by realizing that the system becomes over-determinate, i.e. known variables outnumber unknown ones, after the introduction of force plates. Such a state of redundancy may be exploited by applying optimization methods for improved inverse dynamics results (Cahouët et al., 2002; Kuo, 1998). Besides force plate usage, it is obvious that utilization of additional sensors such as accelerometers and gyros is useful (Dariush et al., 2001; Zijlstra and Bisseling, 2004). However, this solution would be expensive because of additional tools used and also, movement patterns of the (especially pathological) subjects could be altered by the presence of equipment.

The most commonly utilized way of observing human gait is the one that is performed via assistance of cameras tracking markers affixed to certain landmarks on the body and of force plates. As can be inferred, this practice results in an over-determinate set of equations in case of whole body analysis. However, the over-determinate nature vanishes if the researcher is interested only in lower extremity, which is often the case. Markers are placed on lower portions of the body and inverse dynamics calculations are performed up to hip joints. In this case, boundary conditions, which are hip joint forces and moments, are not readily available because of the usually non-invasive nature of gait analysis. Hence, the resulting mathematical system is a determinate one and does not allow the use of optimization techniques; one has to settle for the outputs of classical Newton-Euler solution. The results are always far less accurate for hip joint than for ankle joint, and in between for knee joint (Kuo, 1998). The fact that ankle joint solutions are quite satisfactory is immediately attributed to direct measurement of ground reactions.

If a better model representing the real biosystem is not available, the only way to decrease inverse dynamics errors is to perform better in estimation processes. Estimated BSIP are likely to represent the actual parameters poorly due to several reasons such as financial constraints and scarcity of time. Typically, accelerations must be estimated after filtering noisy displacement measurements, which is a notoriously difficult task and must be handled by proper data conditioning techniques. In the following paragraphs, these estimation techniques are briefly introduced and the ones that are most suitable for the purposes of this study are indicated.

2.2 BSIP Estimation

Experimental assessment and prediction are techniques through which BSIP can be estimated (Cappozzo and Berme, 1990). A historical overview of most of these techniques can be found in Bjørnstrup (1995). In summary, experimental assessment is subject specific, time-consuming and most of the time expensive; yet, it produces the most accurate results. Prediction techniques are classified into two as geometrical approximation and regression equations. In geometrical approximation, shapes of body segments are represented with standard geometrical forms, for which inertial parameter calculations are quite straightforward. On the other hand, regression equations are available through previous statistical analysis of data from sample populations. Both of these prediction techniques dictate anthropometric measurements be taken, the numbers of which for geometrical methods often by far exceeding those for regression methods. Despite the fact that regression equations produce the least accurate results as compared with experimental assessment and geometrical approximation, it is the most commonly employed method owing to its superiority in terms of ease of use (Best and Begg, 2006). However, care must be taken when using regression equations; it is an accepted rule that equations derived using data from a certain population are not representative for members of other populations (Bjørnstrup, 1995; Cappozzo and Berme, 1990; Durkin and Dowling, 2003).

There were notable efforts to adjust previously reported BSIP estimations so that they conform to conventional definitions. One of these is the manipulation of the comprehensive set of data obtained by Zatsiorsky et al. (1990a) with a gamma-scanner method (Zatsiorsky et al., 1990b) by de Leva (1996). Another was performed by Dumas et al. (2007) to adjust data reported by McConville at al. (1980) and Young et al. (1983). In the former study, parameters originally referenced to bony landmarks are referenced to joint centres or other commonly used landmarks. The scope of the latter work is similar and it also includes orientations of principal axes of inertias. Dumas et al. (2007) express that their findings are consistent with those obtained by de Leva (1996).

Prediction methods found in the literature produce substantial variations in BSIP estimates (Durkin and Dowling, 2003; Pearsall and Costigan, 1999; Rao et al., 2005). Influence of these methods on inverse dynamics analysis results was studied by several investigators. Pearsall and Costigan (1999) advocate that differences in results produced by various techniques are small for human gait. They conclude that these differences, despite being small, would become more important in applications requiring higher accelerations such as running. On the contrary, Rao et al. (2005) show that significant differences might arise especially in hip joint moments even when slow gait is concerned. Variations between methods are most of the time larger in swing phase, where gait is not dominated by ground reactions, than those in stance phase.

The comparative work of Durkin and Dowling (2003) investigates performances of several prediction methods from literature. They developed their own regression equations after calculating frontal plane BSIP using dual energy x-ray absorptiometry. They show that the new regression equations are superior to existing methods; however, these equations are not generally applicable since they are only valid for the frontal plane. The authors state in conclusion that the regression equations from Zatsiorsky et al. (1990a) may be the best to be used for prediction purposes, especially since equations for both males and females are available.

As mentioned above, equations from Zatsiorsky et al. (1990a) were adjusted by de Leva (1996). Owing to segment end point definitions, these adjusted versions are directly applicable to the inverse dynamics methods used in this thesis work. Therefore, these equations are used for BSIP estimation, as is the practice by other authors (Ren et al., 2005, 2007; Riemer et al., 2007; Schache and Baker, 2007; Schache et al, 2007).

2.3. Filtering of Noisy Gait Data

In a general context, the word filtering means to enhance data quality by separating errors from signals. Data acquisition is almost always followed by some kind of filtering since captured signals are unavoidably contaminated by various error types. Errors present in gait data are discussed in detail in a number of studies (Lanshammar, 1982b; Hatze, 1990; Woltring, 1985, 1990, 1995; Wood, 1982). To summarize, these errors may in general be divided into two as systematic and non-systematic errors. The former group is composed of camera calibration errors, deviations of skin-fixed markers from their intended positions, operator errors in setting up the equipment, electrical interference, etc. while the latter refers to random errors, namely noise, mainly arising due to quantization process such as analog to digital conversion. Noise is assumed to be additive, normally distributed, uncorrelated and to occupy a wide frequency band whereas systematic errors may arise even in the form of constant biases. It depends on circumstances which kind of error is more harmful. In an experiment, where most of systematic errors are prevented and/or eliminated, random errors would be the primary factor to be got rid of. However, if, for example, marker displacement caused by soft tissue movement beneath is at excessive levels, there is no point in wasting time with trying to suppress noise (Macleod and Morris, 1987).

In a narrower context, filtering is increasing signal-to-noise ratio by means of noise suppression. There are a large number of filters available with different features. It is a crucial task to select a suitable one depending on requirements dictated by the application. Whenever exact power spectra of signal and noise are known, use of the Wiener filter is the optimal approach (D'Amico and Ferrigno, 1990; Woltring,

1985, 1990, 1995). This, however, is certainly not the case for gait analysis. Only assumptions can be made regarding the characteristics of these two. The first assumption, as stated above, is that noise is located on a wide frequency band. Secondly, it is assumed that gait signals are band-limited (D'Amico and Ferrigno, 1990; Lanshammar, 1982b; Wood, 1982). It automatically follows these assumptions that spectra of signal and noise do unavoidably overlap and that outside the region where they overlap, i.e. on intervals of high frequency, noise dominates the spectrum. Figure 1 shows power spectra of typical gait signal and noise.

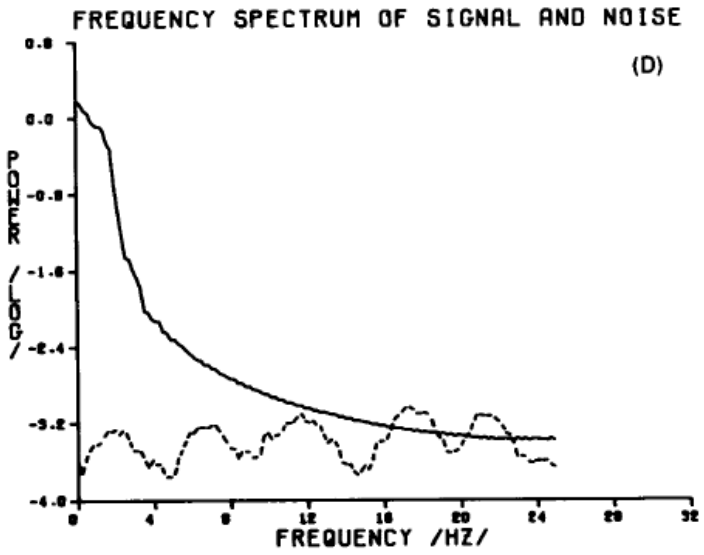

Figure 1. Power spectra of typical gait signal (solid line) and noise (dotted line) (Wood, 1982).

It is this nature that renders the art of filtering a highly problematic process. For demonstration purposes, a displacement signal contaminated by noise is considered here. The magnitude of high frequency noise is negligible as compared to that of the signal. Such a situation might be represented as below:

$$y(t) = \sin(\omega t) + 0.01\sin(20\omega t).$$

When differentiated twice, the expression for the acceleration signal becomes:

$$\ddot{y}(t) = -\omega^2 \sin(\omega t) - 4\omega^2 \sin(20\omega t).$$

As seen, the result is dominated by amplified noise and the obtained signal is far from the original acceleration. Figure 2 illustrates this amplification phenomenon. It is therefore apparent that high frequency noise present in acquired data must be suppressed before any further signal processing.

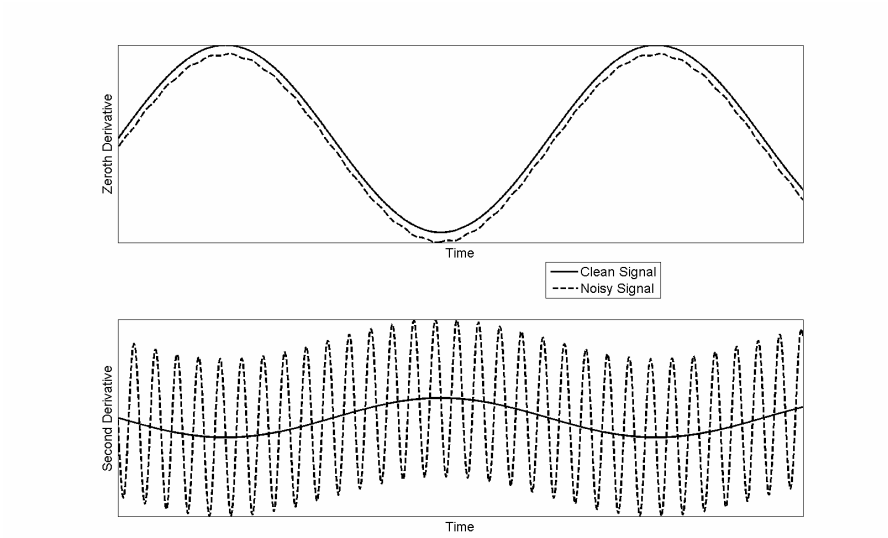

Figure 2. Comparison of clean and contaminated signals. Displacement signals are deliberately shifted for the sake of visual intelligibility.

Complete elimination of noise from contaminated measurement is very difficult, if not impossible; yet, significant noise suppression can be achieved by convenient signal conditioning. The theoretical precision limit attainable by any smoothing and differentiation technique is (Lanshammar, 1982b):

$$\sigma_k^2 \geq \frac{\sigma^2 \omega^{2k+1}}{f_s \pi (2k+1)}.$$

Here, σ_k and σ are the standard deviations of noise in k^{th} and 0^{th} derivatives, respectively; ω is the bandwidth of the signal; and f_s is the sampling frequency. It is immediately seen that noise contribution in derivatives can be suppressed more

when signals are sampled at higher rates[4]. This naturally necessitates more expensive equipment. Even if such acquisition systems are affordable, it is subject to questioning how a reduction in sampling interval affects the amount of noise passed to signals (Woltring, 1995). Therefore, the best way to make sure that least possible amount of noise leaks to higher derivatives seems to be applying efficient noise reduction after data have been acquired. Therefore, researchers have resorted to various filtering techniques in the history of biomechanics.

2.3.1. Conventional Tools

These are methods that have been used since the beginning of biomechanical studies by researchers who sought quick solutions to eliminate unwanted components inherent in captured biomechanical signals. An extensive review of these techniques is available in Wood (1982). Conventional tools for smoothing can be examined under four main groups described below.

Polynomials: Fitting of polynomials to signals in least squares sense has been one of the most useful tools in experimental data analysis. A single, global polynomial can be utilized to represent the entire signal (Wood, 1982) or multiple, local polynomials can be fitted to a number of successive data points (Lanshammar, 1982b). The derivative can then be obtained by analytical differentiation. Polynomial fitting is definitely a useful approach when the aim is to gain preliminary insight into some behaviour; however, it lacks flexibility; that is, as the name implies, it is confined to a certain, predefined mathematical form. Whenever the phenomena under investigation dictate signals of polynomial nature, such as the trajectory of a falling object, least squares polynomial fitting is a natural candidate for data representation. Since this is seldom the case in reality, even if polynomials may still be used to represent the original signals themselves, derivative calculations following polynomial fitting could lead to detrimental results as it tends to over-smooth inputs (Simons and Yang, 1991).

[4] The lower limit for the sampling rate a signal must be sampled at is twice the highest frequency component present in the signal, as dictated by the sampling theorem (Nyquist, 1928; Shannon 1949).

Smoothing Splines: The need for more flexible functional representations which can accommodate time-varying curvatures better than polynomial functions do, led researchers to explore spline functions (Wood, 1982). When globally viewed, a spline function is a single continuous function whereas it is actually a combination of a number of different polynomials. It can either be made to pass through data points or, by adjusting its least squares constraint (smoothing factor), it is possible to obtain smooth versions of contaminated signals. As splines are mathematical functions, their derivatives are analytically available.

Fourier Analysis: Representing a signal as a sum of trigonometric functions enables the user to gain insight into the frequency domain characteristics of any occurrence. Such representation of digital data is made possible by discrete Fourier transform (Cooley and Tukey, 1965), which is a powerful tool that transforms signals in time domain into their spectral counterparts. Digital filtering in frequency domain can be achieved by application of various windowing techniques (Gold and Rader, 1969; Wood, 1982). A detailed account of windows used in harmonic analysis can be found in Harris (1978). While harmonic analysis may be used as a forerunner of digital filter design, it also provides economic means of storing data since complete time history can be represented by a few Fourier coefficients (Wood, 1982). As is the case with polynomials and splines, Fourier series representation provides analytical derivatives.

Digital Filters: Digital filtering may indicate any form of digital signal processing. In the current narrow context, the term refers to discrete-time low-pass smoothing, which has been an essential tool in biomechanics (Robertson and Dowling, 2003). Digital filters may either be recursive or non-recursive, the difference being in that the recursive filters use not only raw but also filtered data points to filter raw data points. Recursive filters consequently have more memory than non-recursive ones, which combine only raw data points in calculations. Since non-recursive filters usually require many coefficients, recursive formulation is often preferred (Wood, 1982). It should be noted that data need to be fed both in forward and backward directions to recursive digital filters for phase shift elimination. Another problem inherent in recursive filtering is the need for previously filtered data points, which

are not available in the beginning of the process. Several approaches are available to overcome this difficulty. Initial values may be assumed zero, filtering may be initiated from a sufficient number of points ahead, or padding techniques may be applied (Derrick, 1998; Giakas et al., 1998; Smith, 1989; Vint and Hinrichs, 1996). Unlike the three methods above, digital filtering does not yield analytical results; time series it provides must be numerically differentiated to obtain signal derivatives. First or second order central differences are generally preferred for derivative calculation.

Each filtering technique briefly described above has its own key parameter that influences its smoothing behaviour. In spline filtering, a smoothing factor should be selected and for frequency domain methods, shape of the window should be determined (Woltring, 1985). As for digital filtering, one must decide on the cut-off frequency. The former parameters, namely the smoothing factor and the window type, are equivalents of the latter. It was indeed shown that spline smoothing and digital filtering were identical for special cases of these two methods (Craven and Wahba, 1979). And since digital filters are often derived by analogy to continuous forms, the link between frequency domain windows and cut-off frequency is obvious. The key point here is that there are many algorithms which in theory lead to identical filters (Gold and Rader, 1969).

2.3.2. Automatic Determination of Filter Parameters

As mentioned above, estimating derivatives of noisy data is an ill-posed problem, meaning that the estimation process is quite sensitive to errors in measurements; that is why acceleration patterns obtained by differentiation could be totally different while estimated displacement data produced by various filter configurations might be virtually identical (Woltring, 1985). This indicates that if kinetic analysis of motion is to be performed, filter parameters must be sufficiently well adjusted. If performed manually, such adjustment procedure is based on trial and error as the operator must evaluate the outputs before proceeding; moreover, it potentially leads to non-homogeneous results because subjective user opinion is employed in the process (D'Amico and Ferrigno, 1990). To be able to avoid manual

adjustment of filter parameters, several automatic filtering techniques were developed. These techniques estimate optimal filtering parameters based usually on statistical or power spectrum information of signals (Giakas and Baltzopoulos, 1997a).

One popular technique is generalized cross-validation which provides an estimate for the smoothing parameter to be used with splines (Craven and Wahba, 1979; Dohrmann et al. 1988). A second spline method is least squares cubic splines that, as obvious from its name, combines the concepts of least-squares and splines (Simons and Yang, 1991). Another technique is the use of regularized Fourier series that makes use of the periodogram of the data sequence (Hatze, 1981). The method called model-based bandwidth-selection allows automatic shaping of filter windows (D'Amico and Ferrigno, 1990). The technique of residual analysis (Winter, 1990) and the works of Capello et al. (1996) and Yu et al. (1999) describe how to define the optimal cut-off frequency to be used with Butterworth digital filter[5]. A comparative assessment of these automatic filtering techniques was performed by Giakas and Baltzopoulos (1997a). Their results show that bandwidth-selection followed by Butterworth filtering and spline methods perform best with walking data. They conclude by stating that there is no optimal solution for biomechanical data filtering and limitations of each method and signal characteristics in time and frequency domains should be examined.

2.3.3. The Concept of Non-stationary Signals

Although it is not entirely incorrect to claim that an automatic filtering technique can handle the smoothing process in an optimal manner, it is only as efficient as the conventional method it improves. The main assumption that the conventional methods are based upon is that signals to be processed are stationary (Woltring, 1990, 1995). This might be valid for various applications; but, is not always the case for gait analysis. In spite of the fact that gait signals are mostly contained within a relatively narrow band of frequencies (Angeloni et al., 1994; Winter,

[5] Butterworth filters (Butterworth, 1930), introduced to the field of biomechanics by Winter et al. in 1974, find wide acceptance owing to their simplicity and acceptable performance.

1990), force transients associated with impacts tend to violate this basic assumption (Woltring, 1990, 1995). In typical gait, as an example, an ankle marker comes to rest soon after heel-strike, stays nearly motionless until heel-off, after which it swings in the air. In other words, in certain portions of the gait cycle, the signal contains more high-frequency components than others, meaning that its power changes in time; that is why it would be incorrect to regard it as stationary. Another example is running, which unquestionably involves impacts. As demonstrated by van den Bogert and de Koning (1996), conventional filtering overlooks the correct, non-stationary nature of this phenomenon, which, in turn, results in unacceptable errors in inverse dynamics results.

The discussion above dictates that filters which aim to smooth non-stationary signals must accommodate time dependent changes in signal structure. This issue was previously addressed by Dowling (1985) and Lanshammar (1982a): to be able to have effective noise removal while preserving the correct acceleration pattern, it is necessary to change the filtering method according to the interval being processed. It should hence be noted that usefulness of conventional filters against non-stationary signals is quite limited since they cannot always accommodate changes in local signal structure regardless of them being optimized or not.

2.3.4. Advanced Tools

Based on such inadequacy of conventional filters, new filtering methods were introduced to the field. These were all adapted from existing techniques and are said to able to process non-stationary signals. The first of such studies employed wavelet transform, which can be described as an alternative to Fourier transform (Ismail and Asfour, 1999). The results greatly varied depending on the selected mother wavelet function and decomposition level. Another method involves the use of Wigner function (Georgakis et al., 2002a; Giakas et al., 2000). The method effectively represents the signal in both time and frequency domain; however, it impractically requires five parameters to be defined, one of which is the time of impact. For low-impact signals, the procedure was shown to yield inferior results compared to conventional filtering even when the parameter selection is automated (Georgakis et

al., 2002b). Thirdly, singular spectrum analysis based on multivariate statistics was proposed (Alonso et al., 2005a). The algorithm decomposes the original signal into components of decreasing weight. A window length and number of components to be used for reconstructing the decomposed signal must be determined, which is a manual process. The last technique is the usage of Hodrick-Prescott filter which is a standard tool used to decompose a macroeconomic time series into non-stationary and stationary components (Alonso et al., 2005b). Smoothing with this filter, which requires a single parameter to be set, was shown to yield similar results to those of generalized cross-validated quintic spline method.

These methods are certainly promising. Respective publications reveal that they almost always perform better than conventional filters, especially in case of non-stationary signals. However, these are not yet fully established and need further improvement in the sense that selections of their parameters need to be settled on more solid basis. Only one of them is said to be automatic. So, it would be difficult for a user to tune their parameters if he/she is not acquainted with what constitutes the technical base behind these filters.

A part of this thesis work is devoted to a new filtering technique introduced by Erer (2007)[6], which is a modified, adaptive version of the Butterworth digital filter. Applied to benchmark data, the adaptive filter was shown to produce best results found in the literature. Unlike advanced filters, this method remains within the bounds of classical digital filtering approach while it can handle non-stationary data, unlike conventional filters. After lower and upper bounds for cut-off frequencies are specified by the user, this semi-automatic algorithm determines how individual cut-off frequencies are varied throughout the data sequence based on estimated velocity and acceleration information[7]. In other words, the filter has a

[6] The corresponding article can be found in Appendix F.

[7] Most automatic filtering techniques based on digital filtering retrieve information only from displacement data (Giakas and Baltzopoulos, 1997b).

variable cut-off frequency distribution defined for each data point. Since the distribution is determined by local signal characteristics, the filter is able to adapt itself to changes in frequency content.

CHAPTER 3

A BRIEF OVERVIEW OF THE METU GAIT ANALYSIS SYSTEM

The METU Gait Analysis Laboratory (Figure 3), located at the Department of Mechanical Engineering, is the first gait analysis laboratory of Turkey. The METU Gait Analysis System, a.k.a. Kiss, is a non-commercial system which is equipped with six cameras and two force plates for data acquisition purposes. The system has the necessary software programs that operate during and after the data acquisition process. The final outputs of the system are kinematic and kinetic data which enable assessment and interpretation of gait patterns on quantitative bases.

Figure 3. Overview of the laboratory.

This chapter concentrates on some components of the METU Gait Analysis System that are relevant to the scope of this work. More detailed discussions on various

aspects of the system can be found elsewhere (Afşar, 2001; Civek, 2006; Güler, 1998; Kafalı, 2007; Karpat, 2000; Shafiq, 1998; Söylemez, 2002).

3.1. Collection of Data

All data collection routines during any Kiss experiment are governed by a program called Kiss-DAQ. The standard collection protocol is composed of two main parts: the static trial and the dynamic trial. During both of the trials, images of a number of reflective markers attached to various landmarks on lower extremities are captured at 50[8] Hz by default. Considering the low-pass nature of human gait, this value may safely be accepted to be more than twice of the highest frequency value possible for human gait. So, the sampling theorem (Nyquist, 1928; Shannon, 1949) is not violated.

The static trial requires the subject to stand still for a specified duration so that data required for further calculations can be obtained with high reliability. The dynamic trial, on the other hand, is the phase of the experiment where the subject actually walks. During the dynamic trial, force plate data (the default sampling frequency is 500 Hz) synchronized with camera images are collected. Marker configurations for the static and dynamic trials are respectively seen in Figure 4 and Figure 5.

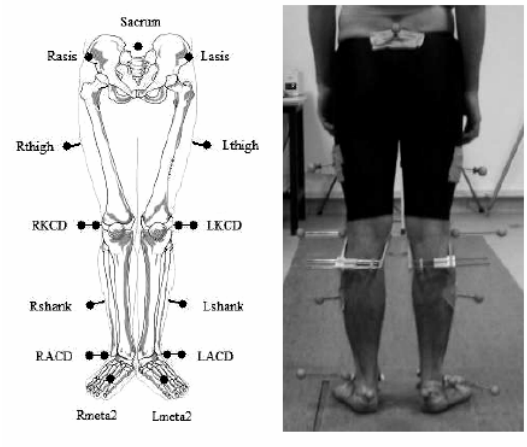

Figure 4. The static trial (adapted from Kafalı (2007)).

[8] A discussion on the fact that this value is only the apparent sampling frequency is available below.

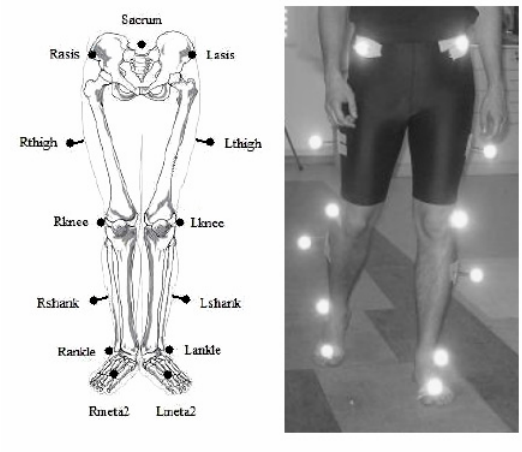

Figure 5. The dynamic trial (adapted from Kafalı (2007)).

The static trial is practised to be able to relate technical reference frames observed in the dynamic trial to non-observable anatomical reference frames. It involves employment of 19 markers, 13 of which are those used in the dynamic trial. Extra information supplied by the remaining 6 markers enables hip, knee and ankle joint centres to be estimated. It is thereafter possible to construct the assumedly constant transformation matrices that are used to obtain anatomical reference frames from technical ones. Supplied with such crucial transformation data from the static trial, dynamic trial data are processed to obtain kinematic (angles) and kinetic (moments, powers) joint variables.

3.2. Processing of Data

After image data are acquired, static and dynamic marker trajectories are extracted via the program Motion Tracking. It should be noted that this trajectory extraction is partly a manual process, which requires user proficiency. Force plate data become readily available after the acquisition process and do not need post-processing. Before the trajectories and force plate data are fed into Kiss-GAIT, the gait analysis program of Kiss, they must be packed together with the experimental setup file by the intermediate piece of code named BVD Filer.

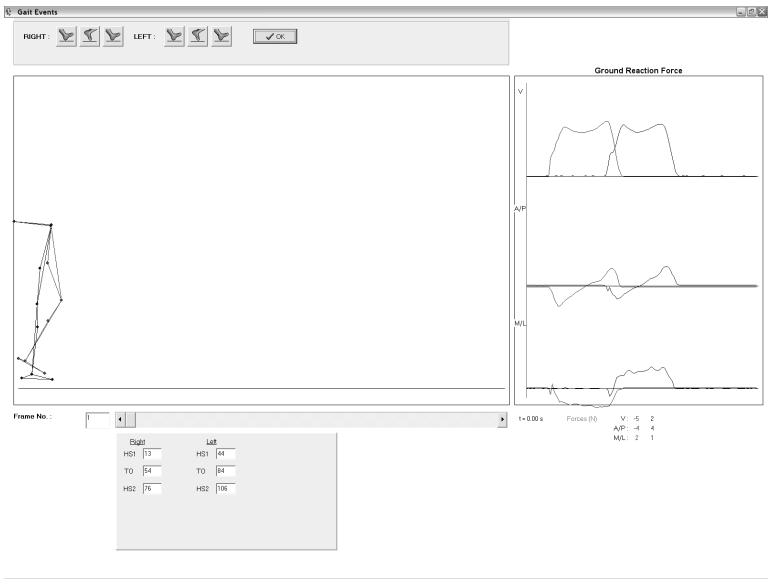

Figure 6. A screenshot from Kiss-GAIT.

As inputs, Kiss-GAIT accepts the data package mentioned above and the subject's anthropometric data, i.e. weight and height of the subject and several distances measured on the subject. The analysis process needs to be initiated with user specification of the gait events which are heel-strikes and toe-offs. The gait events can be specified making use of the walking stick-man animation and ground reactions plots, as seen in Figure 6. After this manual step, the code is ready for automatic calculation several gait variables: time distance parameters, joint angles, joint moments and joint powers. Sample outputs of Kiss-GAIT are included in Appendix E.

Because the primary aim of this thesis study is to develop a computer code to assess inverse dynamics model of Kiss, it is convenient here to present some key points in calculation routines of Kiss-GAIT that are unjustified. The thing that complicates the issue is the absence of a complete reference about these routines. The information below was extracted partly from the dissertation of Güler (1998), partly from the source code of Kiss-GAIT, and partly through personal communication.

3.2.1. Question Marks on Calculation Routines of Kiss-GAIT

Kiss-GAIT initiates the mathematical manipulation of marker trajectories by employing a digital filter for noise suppression purposes. The filter is a dual pass second-order Butterworth filter[9] whose cut-off frequency was found (through inverse solution of filter coefficients) to be equal to 11.1 Hz. This; however, is only the first part of a dual smoothing process. Filtered marker trajectories are used in the construction of anatomical reference frames. These frames are then utilized to obtain joint angles. At this point, the second smoothing process is applied. 9th order polynomials are fitted in least-squares sense to joint angle histories such that each time point in a series is assigned a polynomial whose coefficients are determined using 41 (20 on either side) data points. Obviously, first and last 20 data values remain unchanged. This dual smoothing approach certainly yields smooth (probably over-smooth) patterns. However, it is not clear why such a method was preferred; a single smoothing process having solid spectral background should be sufficient most of the time.

Figure 7 demonstrates that Kiss-GAIT introduces temporal shift in the course of this dual processing. The raw angle is the sagittal plane hip joint angle derived after the first filtering process and integrated velocity refers to the same angle calculated by integrating the joint angular velocity which is obtained after the second filtering process. The reason why the program behaves so is unknown.

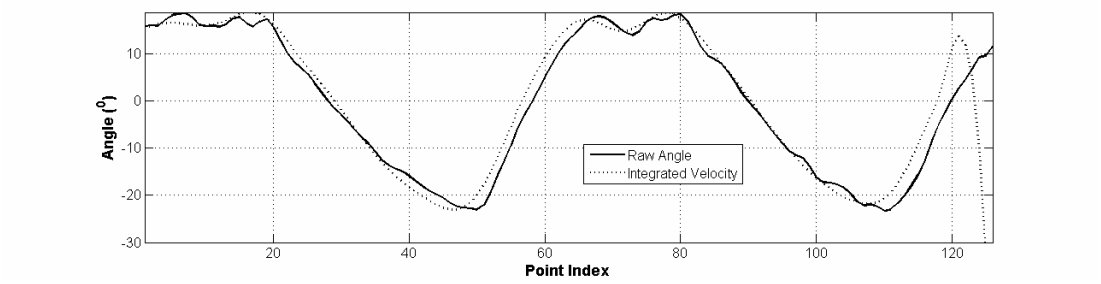

Figure 7. Time shift introduced by Kiss-GAIT.

[9] A detailed account for the second-order Butterworth filter is presented in Chapter 5.

Another unjustified action of Kiss-GAIT is how it calculates joint kinematics. The program feeds the Newton-Euler (N-E) equations with kinematic variables obtained with a recursive algorithm that suits best for robot manipulators (Fu et al., 1987). In fact, the joint model used by Kiss gives the impression that such an approach is the direct way for kinematic calculations. However, the computational burden can be decreased by utilizing the obvious method which is calculating kinematic variables directly from marker data[10]. Furthermore, the assumption of Kiss-GAIT that the pelvis frame remains parallel to the global frame is needles, if not intolerably wrong. The angular velocity of the pelvis segment can indeed be calculated using the pelvis-to-global transformation matrix.

A third problematic issue is the BSIP estimation method of Kiss-GAIT. The source code reveals some regression equations which are not the ones presented by Güler (1998). The origin of these equations is unknown. Instead of relying on such untrustworthy information, usage of the aforementioned regression equations (de Leva, 1996) is adopted in this work.

3.3. Mathematical Joint Model

Kiss adopts a three degree-of-freedom joint model to express joint variables. The rotation sequence between a proximal and a distal segment is defined as shown in Figure 8. Such a sequence can be represented by the Hartenberg-Denavit (H-D) convention (Özgören, 2004). Unit vectors of the frames defined by the H-D representation are also given in the figure.

In this convention, Frame 0 is attached to the proximal and Frame 3 is attached to the distal segment. There are two more segments which only virtually exist ($d_1 = d_2 = 0$). Having Frame 1 and Frame 2 attached on, they only facilitate the mathematical solution of joint variables. Table 1 summarizes the variables of the H-D convention valid for this specific case[11].

[10] Chapter 6 includes a step-by-step definition of this algorithm.

[11] Assuming that the proximal segment is the stationary base with respect to which the other segments rotate through three angles may facilitate understanding of the rotating sequence.

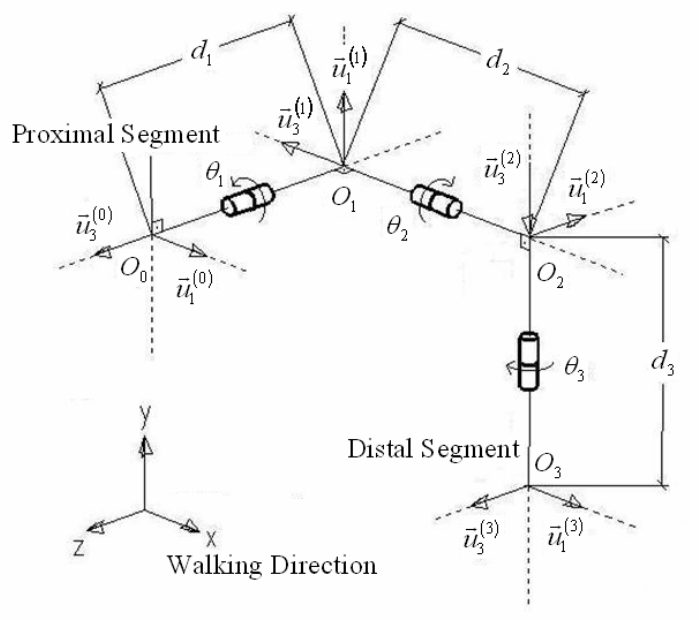

Figure 8. Joint model used by Kiss.

Table 1. H-D parameters of the joint model. [*F*: frame number, θ: rotation about $\vec{u}_3$, α: rotation about $\vec{u}_1$, *d*: offset in direction of $\vec{u}_3$, *a*: offset in direction of $\vec{u}_1$]

F	1	2	3
θ	joint var.	joint var.	joint var.
α	$-\pi/2$	$-\pi/2$	$-\pi/2$
d	$-d_1$	$-d_2$	$-d_3$
a	0	0	0

The distal-to-proximal transformation matrix $\hat{C}^{(p,d)}$ [12] that transforms vector quantities expressed in the distal frame (Frame 3) into their equivalents in the proximal frame (Frame 0) is expressed in terms of exponential rotation matrices as:

$$\hat{C}^{(p,d)} = e^{\vec{u}_3\theta_1} e^{-\vec{u}_1\frac{\pi}{2}} e^{\vec{u}_3\theta_2} e^{-\vec{u}_1\frac{\pi}{2}} e^{\vec{u}_3\theta_3} e^{-\vec{u}_1\frac{\pi}{2}}.$$

When written in open form, the expression becomes:

[12] The hat indicates a square matrix.

$$\hat{C}^{(p,d)} = \begin{bmatrix} c\theta_1 c\theta_2 c\theta_3 + s\theta_1 s\theta_3 & c\theta_1 s\theta_2 & -c\theta_1 c\theta_2 s\theta_3 + s\theta_1 c\theta_3 \\ s\theta_1 c\theta_2 c\theta_3 - c\theta_1 s\theta_3 & s\theta_1 s\theta_2 & -s\theta_1 c\theta_2 s\theta_3 - c\theta_1 c\theta_3 \\ -s\theta_2 c\theta_3 & c\theta_2 & s\theta_2 s\theta_3 \end{bmatrix} = \begin{bmatrix} C_{11} & C_{12} & C_{13} \\ C_{21} & C_{22} & C_{23} \\ C_{31} & C_{32} & C_{33} \end{bmatrix},$$

where *s* and *c* stand for sine and cosine functions, respectively. The transformation matrix above is obtained through multiplication of two transformation matrices derived using marker trajectories. The multiplication is:

$$\hat{C}^{(p,d)} = \hat{C}^{(p,g)} \hat{C}^{(g,d)}.$$

The above expression states that the distal-to-proximal transformation matrix is obtained when the transpose of the proximal-to-global[13] transformation matrix is pre-multiplied with the distal-to-global transformation matrix.

Once the transformation matrix between the segments is available, the three joint angles may then be solved for as below:

$$\theta_1 = \text{atan}_2\left(C_{22}, C_{12}\right),$$
$$\theta_2 = \text{acos}\left(C_{32}\right),$$
$$\theta_3 = \text{atan}_2\left(C_{33}, -C_{31}\right).$$

This inverse kinematics solution cannot be applied for $\theta_2 = 0$ and $\theta_2 = \pi$. Such a configuration implies the distal segment becoming horizontal, i.e. parallel to the ground, which is obviously never realized during human gait.

It should finally be noted that all three angles are $\pi/2$ for an ideal upright posture and their clinical equivalents for joints on either side of the human body are:

- θ_1 : Flexion (both for right and left sides),
- θ_2 : Abduction / Adduction (right / left),
- θ_3 : External / Internal Rotation (right / left).

3.4. Extent of Noise in Kiss

Like all data acquisition systems, Kiss-DAQ is only able to capture contaminated versions of signals instead of the signals themselves. It is well known that noise

[13] The laboratory frame is the global frame.

present in acquired data may adversely affect final outputs if not dealt with properly; and, the first condition of being able to take proper measures is being aware of the extent of noise contamination in recorded data. This section, therefore, aims to shed some light upon time and frequency domain behaviours of Kiss marker and force plate signals. Data investigated here are from one specific gait trial; however, unless the system configuration is modified, generalized conclusions about the extent of noise in Kiss may be drawn based on the results.

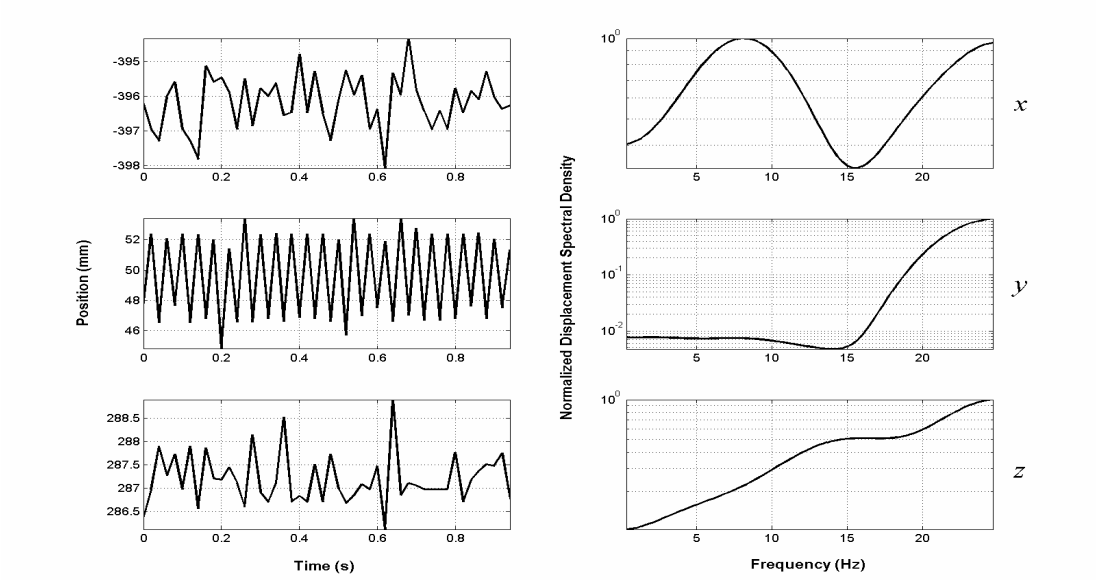

Figure 9. Time and frequency domain behaviours of displacement signal of a stationary marker.

The first column of plots in Figure 9 show recorded global coordinates of a stationary marker; coordinates of a marker placed on the second metatarsal recorded during a static trial to be more specific. It is seen that the measurements are contaminated by certain amount of noise as expected (the corresponding standard deviations can be found in Table 2). The issue which is of particular importance; however, is that *y* coordinates behave markedly different than *x* and *z* coordinates do. It seems that measurements in *y* axis contain not only random noise but also certain type of systematic error that manifests itself as harmonic noise contribution. When examined closely, it is seen that the spikes seen in *y* coordinates are

positioned exactly 0.04 s apart (positive-to-positive or negative-to-negative peak distance) from each other, which indicates a frequency of 25 Hz. This is the result of separate usage of even and odd fields of camera images (Karpat, 2000; Shafiq et al., 2000); as a result, it is a deliberate contribution for rather than contamination. The natural price paid for such an action is a decrease in visual smoothness of trajectory curves. Other than that, the modification is harmless as it introduces harmonic components oscillating exactly at a certain frequency which can easily be dealt with by filtering. The phenomenon is also clearly visible in the provided spectral density plots. The components located at 25 Hz dominate the spectrum for all coordinates, not only for *y* coordinates. The reason why this effect is more pronounced in *y* axis can be attributed to the location where the static trial is executed; tracking qualities of Kiss vary depending on where in the calibration volume a marker is positioned (Karpat, 2000).

The situation is not different for a dynamic marker trajectory. Figure 10 shows trajectory components of the same metatarsal marker during gait. Since the range of *x* coordinates is large, the effect of noise is not seen at this scale. On the other hand, for *y* and *x* readings, whose ranges of values are at the same order of magnitude, noise contamination is visible. As in the case of static data, oscillations at 25 Hz are most apparent in *y* axis.

Figure 11 presents spectral densities of the trajectory components. Dominated by the frequency content of the motion itself, the 25 Hz contributions are not prominent for *x* and *z* axes. On the contrary, data in *y* axis are visibly affected in spite of their relatively (with respect to data in other axes) higher harmonic content.

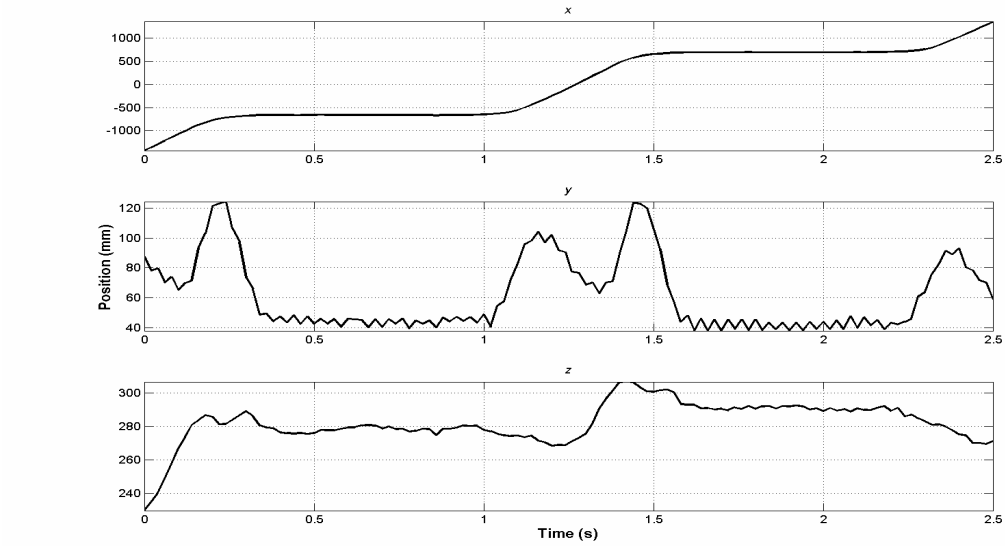

Figure 10. Trajectory components of a metatarsal marker.

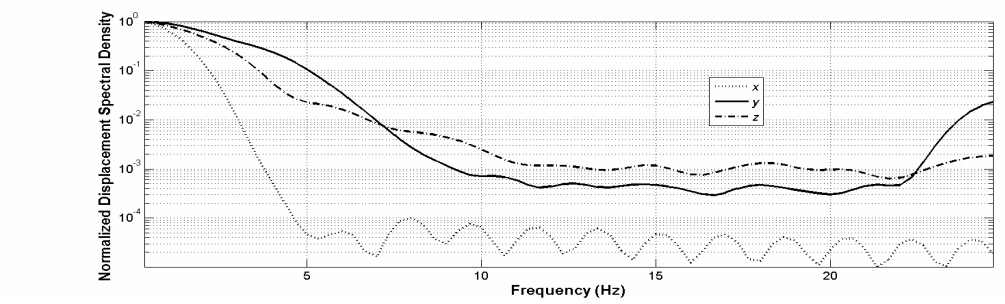

Figure 11. Spectral contents of trajectory components of a metatarsal marker

Although they are visually dominated by the oscillations at 25 Hz, it needs to be indicated that effects of random noise in measurements are still the most detrimental constituents considering the differentiation process that is applied on marker trajectories. A separate investigation of effects of random noise is very difficult, if not impossible[14], here since these two types of errors are superposed in the measurements.

[14] An ideal filter approximation with a cut-off frequency of less than 25 Hz might be tried; however, the action may not be justified due ringing effects the filter will produce.

It might be subject to question how the above demonstrated contamination in Kiss influences its marker tracking accuracy. A simple test is to track two markers the distance between which is known. Without the need for specialized setup, such a test can be performed using standard static and dynamic trial data. An ankle marker is assumed to be located both on the foot and shank segments since it is placed on the joint between. Thus, the distance between an ankle marker and a metatarsal marker on the same foot is nearly constant during gait. Likewise, the distance of a knee marker to an ankle marker on the same shank is assumed to remain the same throughout the whole gait cycle. Successful approximations to these distance values can be extracted from static trial coordinates and the dynamic accuracy of the system may then be judged accordingly. Such an assumption is likely to hold because the static trial gives the opportunity of recording marker coordinates while they are almost motionless; the averaging process should effectively eliminate the random noise in readings. Moreover, it is known that marker tracking performance of Kiss at the centre of the calibration volume, which is where static trials are executed, is acceptable (Karpat, 2000).

Time variations of calculated distances between the markers are shown in Figure 12. What is immediately seen is that the dynamic accuracy of the system is worse than its static accuracy (mean and standard deviation values of the curves are presented in Table 2). Another important issue regarding dynamic accuracy, which is obvious in the estimation of the distance between the knee and ankle markers, is that estimation patterns are sensitive to the gait phase the subject is in. The interval approximately between 1 and 1.35 s corresponds to the swing phase of gait. During this phase, the ankle marker gains considerably higher velocity values compared to those of the knee marker. The poorness of estimation during this interval implies that fast moving markers are relatively difficult to be tracked by Kiss. Since the relative velocity between the ankle and metatarsal markers does not increase as much, the distance between them is estimated more consistently. It should finally be noted that the reasoning above neglects skin induced deviations of markers, which may not be altogether negligible (Afşar, 2001).

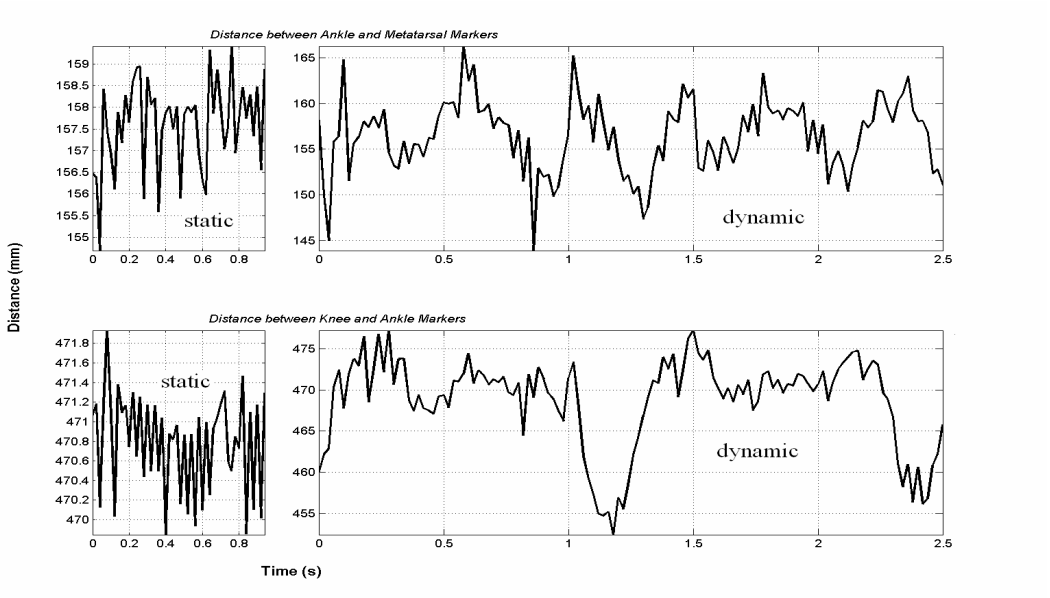

Figure 12. Estimated distances between markers from static and dynamic data.

Table 2 serves as a performance summary of marker tracking capabilities of Kiss. Although the specific values presented here are valid only for the data set examined here, browsing through Kiss database showed consistent behaviour among all sets acquired with the same (default) system configuration[15]. As mentioned above, the assumption with which the table was filled in is that mean values of static measurements include negligible error in representing actual values. As also illustrated in Figure 9 and Figure 12, standard deviation of static marker coordinates is highest for *y* axis and static estimation accuracy of Kiss is quite better than its dynamic accuracy.

[15] There are some data sets which exhibit different characteristics. They were produced with a problematic system configuration that caused the images to be taken at 25 Hz; synchronization failure between force plate and marker data is inevitable.

Table 2. Mean and standard deviation values of estimations.

	Reference	**Estimated**
***x* Coordinate (Static)**	000.00	000.00 ± 0.77
***y* Coordinate (Static)**	000.00	000.00 ± 2.87
***z* Coordinate (Static)**	000.00	000.00 ± 0.54
Distance on Foot (Static)	157.59	157.59 ± 1.04
Distance on Foot (Dynamic)	157. 59	156.44 ± 3.96
Distance on Shank (Static)	470.79	470.79 ± 0.49
Distance on Shank (Dynamic)	470.79	468.70 ± 5.50

Unlike marker data, force plate data do not undergo the differentiation process. This means that noise levels in ground reactions are not as critical as those in marker trajectories since they are not amplified during calculations. Moreover, it is most of the time true that force plate measurements are far accurate than marker coordinates. Based on these facts and knowing that calibrated force plates provide consistent readings, it may not be necessary to investigate ground reaction signals; nonetheless, out of a sense of completeness, time and frequency domain behaviours of a typical vertical ground reaction force signal is presented in Figure 13. Besides being contaminated by random noise and illustrating typical low-pass characteristics consistent with the nature of human gait, local spikes present at 50 Hz and at its integer multiples (harmonics) are distinguished at once. This is nothing but the disturbance coming from power lines, which dominates the spectrum when the force plate is not trod on. This already insignificant error source becomes altogether negligible after force plate signals are downsampled to 50 Hz, which is the frequency at which marker coordinates are sampled.

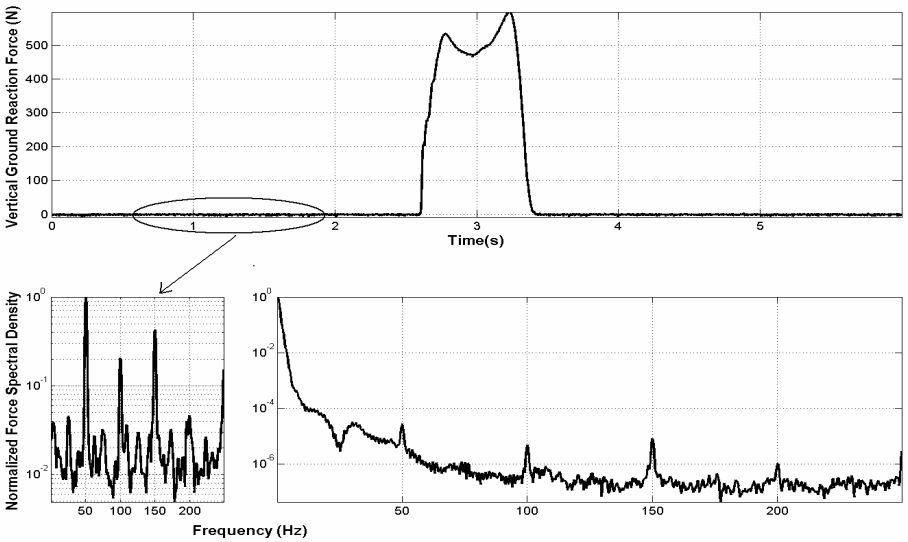

Figure 13. Time and frequency domain behaviours of typical vertical reaction force.

CHAPTER 4

ABOUT SPECTRAL BEHAVIOURS OF REPRESENTATIVE DATA

Gait data, which are among the most studied biomechanical signals, possess low-pass characteristics, meaning that no appreciable components exist above a certain frequency limit (D'Amico and Ferrigno, 1990; Lanshammar, 1982b; Wood, 1982). It should also be noted that depending on gait speed and on which portion of lower extremity the information belongs to, frequency contents of signals may exhibit non-stationary features (Woltring, 1990, 1995). As stated previously, this fact complicates the filtering process necessary to be applied to acquired data before further processing. The quality of calculated acceleration signals are directly determined by the quality of the preferred filtering technique.

It is customary in gait analysis to test smoothing and differentiation techniques on benchmark data, which are assumed to represent biomechanical signals, readily available in the literature to be able to assess their effectiveness.

4.1. Power Characteristics of Representative Data

In this section, four benchmark signals from literature and several gait signals provided by KISS are examined from a spectral point of view. None of the benchmark signals was produced by gait; however, three of them are clearly more challenging since their frequency contents extend to frequency values far higher than those of any possible gait signal; and furthermore, they involve impacts, i.e. severe accelerations of short duration, of varying degrees accompanied by negligible acceleration intervals. In theory, therefore, any filtering technique able to process these non-stationary data should also conveniently handle gait signals. It is common that the first step of filter design is to gain insight into spectral behaviour

of data to be filtered. So, frequency contents of all these sample signals, benchmark and gait, are investigated here using frequency domain methods.

Three of the benchmark studies are experimental and one is a simulation study. In experimental studies, along with observed displacements, accelerations were also captured with accelerometers. On the other hand, gait displacement data were provided by KISS and unfortunately, corresponding acceleration histories are not available. A workaround to this problem might be conventional low-pass filtering of displacement signals (Giakas and Baltzopoulos, 1997b) so that accelerations yielded by double differentiation represent the actual occurrence within reasonable bounds. This, however, brings about the possibility of elimination of high frequency components present in original signals. As the primary aim of this section is to correctly evaluate frequency contents, such an approach is considered to be inappropriate. An alternative is to fit global functions to displacement signals and then to obtain reference accelerations by analytical differentiation, rather than numeric differentiation that would be necessary with the other option. There are nonetheless complications associated with the latter approach: not every signal is possible to be fitted well with analytical functions, at least not without great effort[16]. Therefore, only a few number of gait signals, for which analytical fits were coincidentally applicable, are presented here.

The issue is demonstrated with the help of two types of graphs drawn by making use of methods established in frequency domain. Firstly, spectral density plots (using the built-in MATLAB function *pwelch*) of displacement and acceleration signals are provided to illustrate their low-pass characteristics. The key parameter to be considered in this case is the frequency value below which almost all (e.g. 99 %) power of the signal is contained. The second tool utilized is a method that can be best described as a running, or windowed, fast Fourier transform process. The results are presented in figures, where each value on the vertical axis is a measure of the total power (sum of harmonic magnitudes) of a window whose centre is the corresponding point on the horizontal axis. Window length was manually adjusted

[16] If it was so, the art of smoothing and differentiation would become obsolete!

for each plot to ensure visual intelligibility. This approach is useful in visualizing frequency content as a function of time so that any non-stationary nature of an acceleration signal is revealed. Although the technique is powerful, it exhibits some undesired behaviour. There is always an anti-peak between two peaks. These anti-peaks should not be regarded as indicators of low power. They merely correspond to intervals around local acceleration extrema.

Pezzack et al.'s Data: The angular displacement signal is a modified version of the experimental data provided by Pezzack et al. (1977). The experiment was conducted with an aluminium arm free to rotate in horizontal plane. The authors state that the abduction-adduction tasks performed by the arm are similar to angular movement patterns of body segments. The displacement and acceleration signals were recorded respectively with a potentiometer and an accelerometer. Lanshammar (1982a) later found this angular displacement signal to be too clean to test filtering techniques and he presented a more contaminated version of the signal, which is examined here. The sampling interval is 0.0201 s. The contaminated displacement and the recorded acceleration are seen in Figure 14.

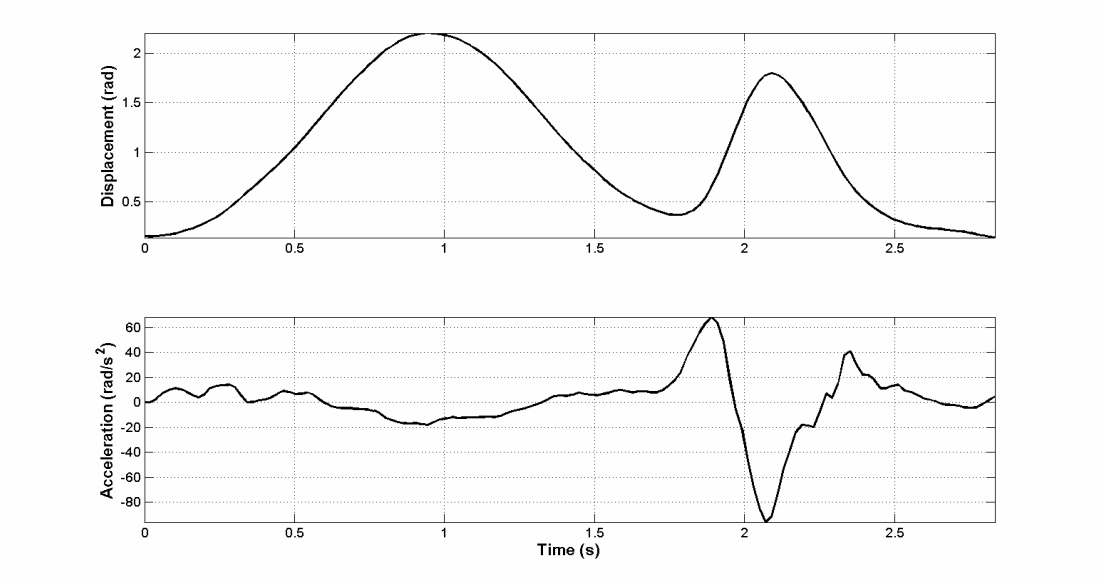

Figure 14. Time variations of the displacement and acceleration signals (Pezzack et al.'s data).

Figure 15 shows frequency spectra of the displacement and acceleration signals. 99 % of the power of the displacement signal is contained within an interval of 2.4 Hz wide while the corresponding value for the acceleration is 6.8 Hz.

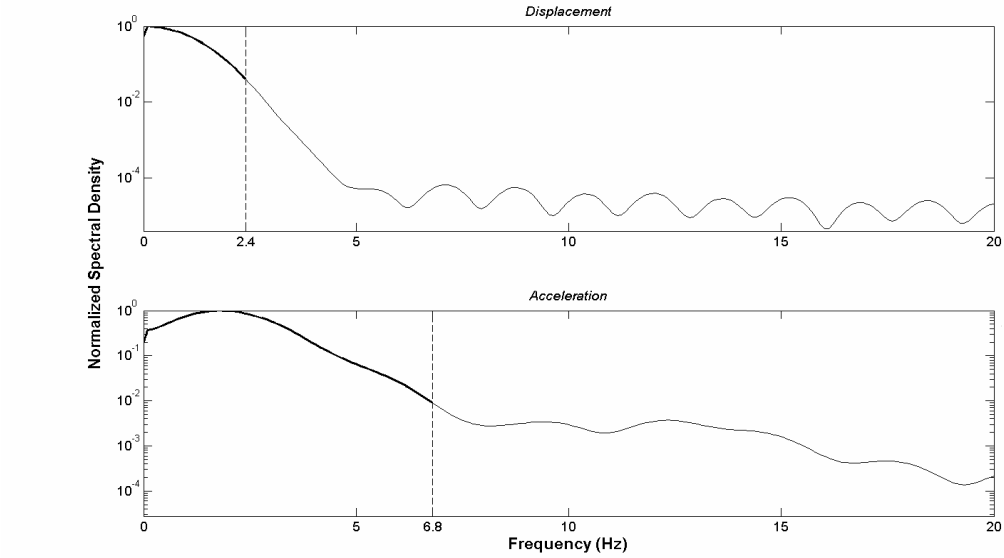

Figure 15. Power spectra of the displacement and acceleration signals (Pezzack et al.'s data).

Figure 16 clearly displays how the power of the acceleration signal increases after 1.5th second, which is an expected result because this interval involves a rather quick angular movement.

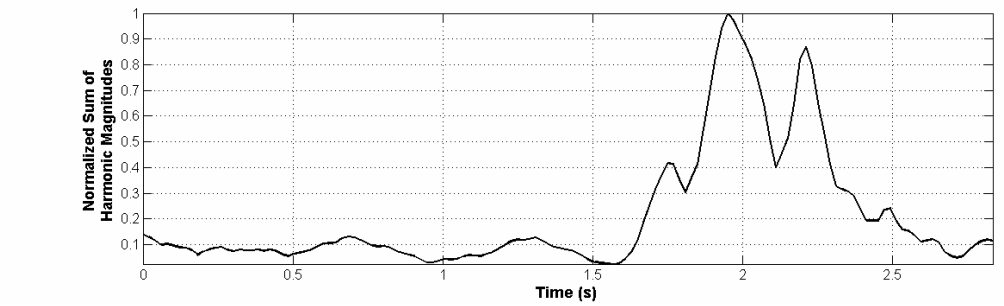

Figure 16. A measure of the power of the acceleration signal as a function of time (Pezzack et al.'s data).

Dowling's Data: Another angular displacement signal is the one provided by Dowling (1985). This is a good example of signals which conventional filtering techniques fail to handle properly. In the corresponding work, the horizontal pendulum experiment involved impact with a barrier, which is why the data are highly non-stationary. As was the practice of Pezzack et al. (1977), the displacement was captured with a potentiometer and the acceleration with an accelerometer (Figure 17). The sampling frequency is 512 Hz.

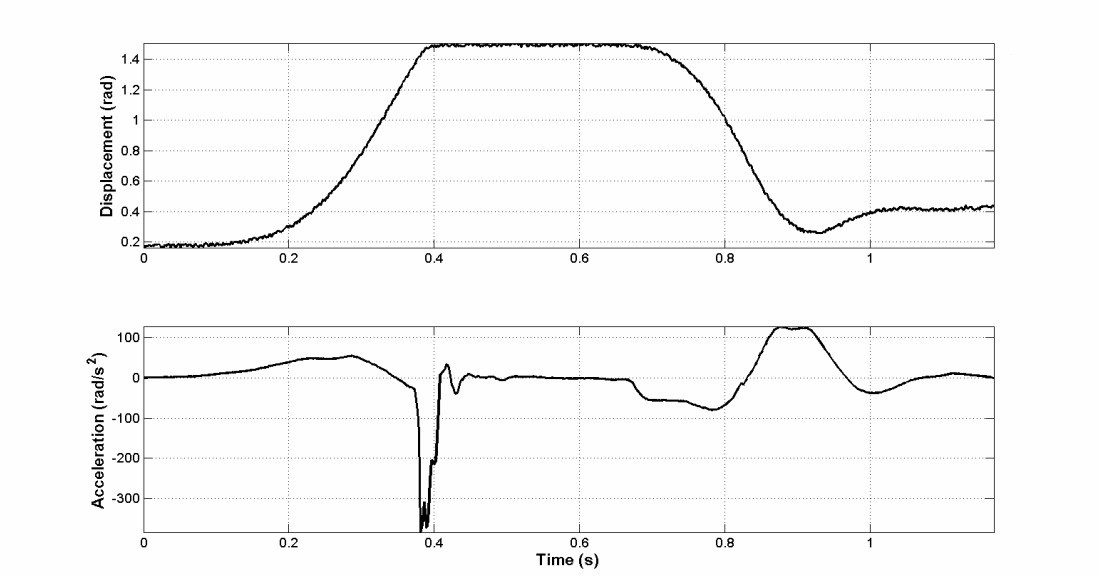

Figure 17. Time variations of the displacement and acceleration signals (Dowling's data).

As seen in Figure 18, the 99 % power limit for the acceleration signal (97.3 Hz) is far higher than the one for the displacement (5.3 Hz). This difference is directly caused by the short interval of severe acceleration caused by the impact.

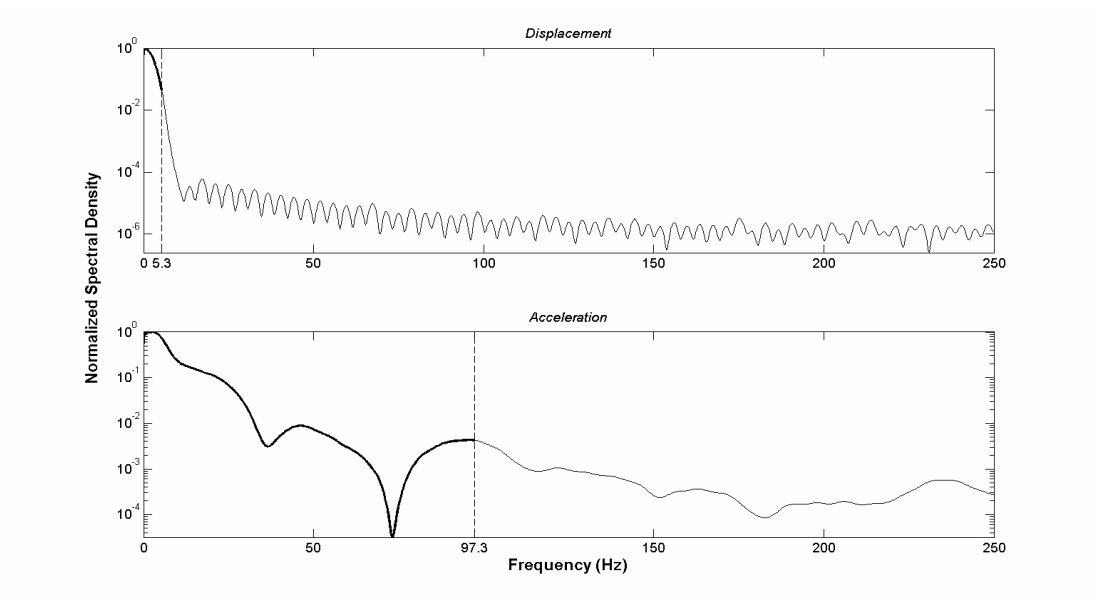

Figure 18. Power spectra of the displacement and acceleration signals (Dowling's data).

A representation of how the power of the acceleration signal changes in time is given in Figure 19. The rapid rise and fall in the neighbourhood of the impact (around 0.4th second) dominates the plot.

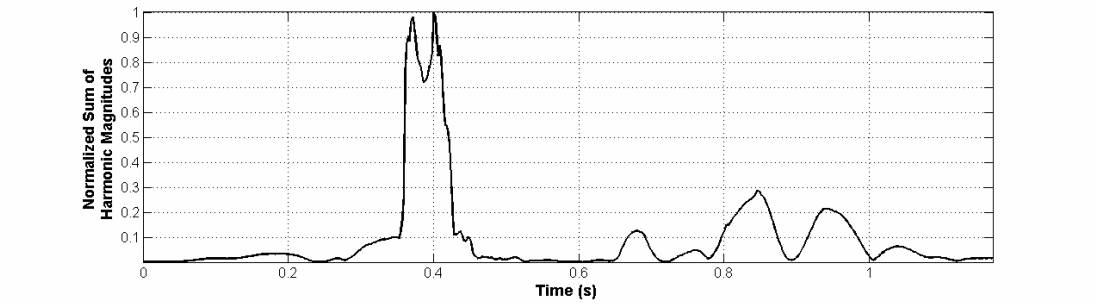

Figure 19. A measure of the power of the acceleration signal as a function of time (Dowling's data).

Foot Impact Data: This is one (S_3) of the non-stationary signals experimentally obtained by Georgakis et al. (2002a). The data represent horizontal displacement that involves impact with an obstacle. The displacement signal was recorded with

cameras tracking reflective markers and the acceleration signal was obtained with an accelerometer. Figure 20 shows these signals. The sampling rates are 1000 Hz.

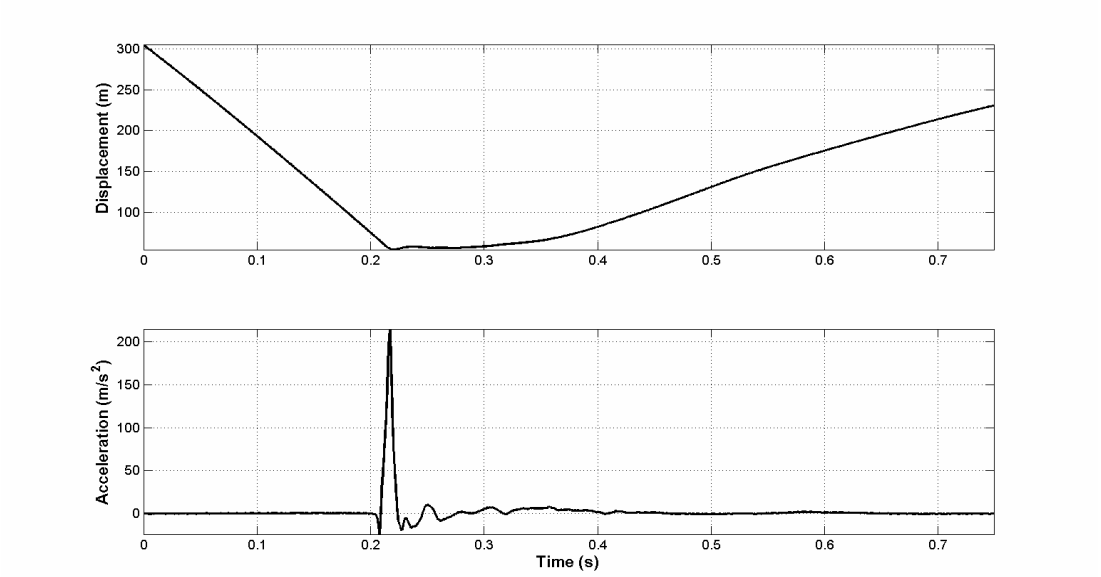

Figure 20. Time variations of the displacement and acceleration signals (foot impact data).

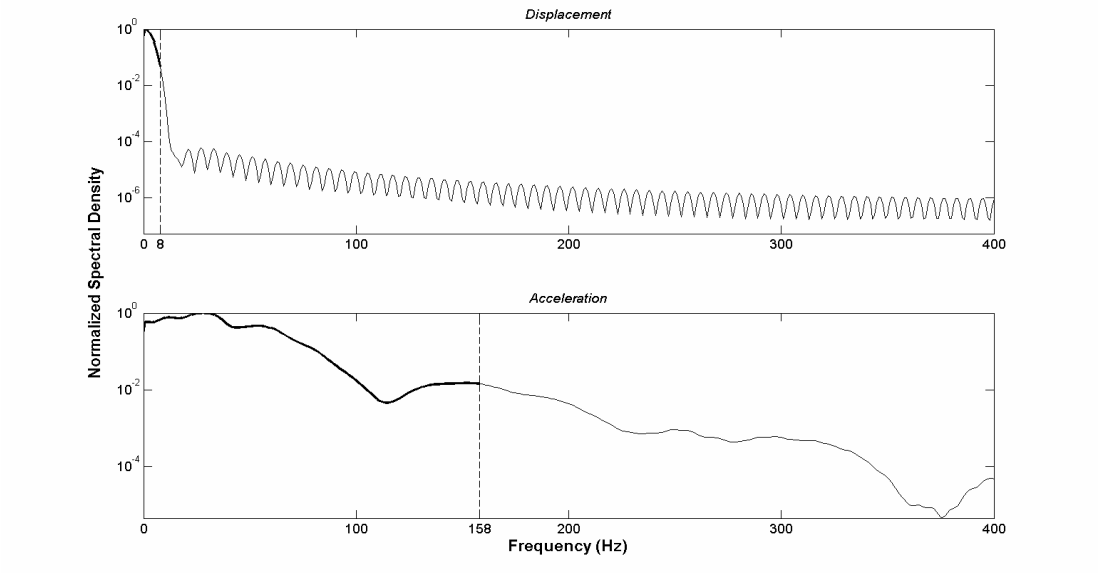

Figure 21. Power spectra of the displacement and acceleration signals (foot impact data).

Figure 21 shows similar trends to those of Dowling's and running simulation data. In this case, the difference between the limiting values (8 vs. 158 Hz) is the greatest among the signals examined in this study.

The impact occurs just after 0.2nd second as presented in Figure 22. What is at once seen is that only the impact is effective throughout the entire acceleration power history.

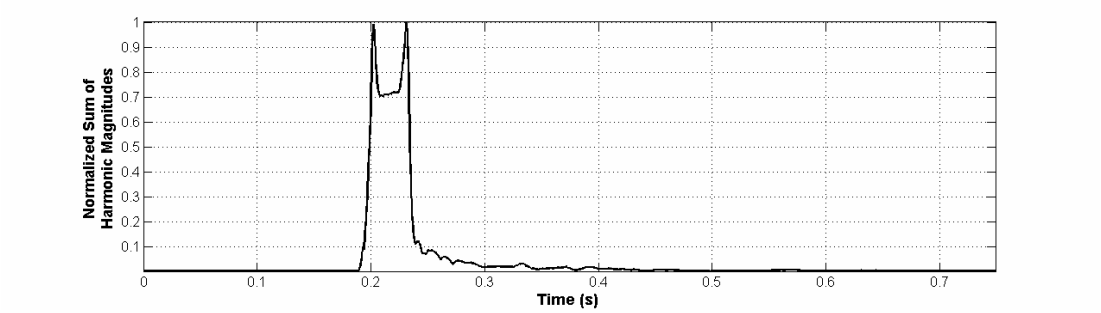

Figure 22. A measure of the power of the acceleration signal as a function of time (foot impact data).

Running Simulation Data: Vertical position history of the ankle resulting from a running simulation done by van den Bogert and de Koning (1996) is a challenging signal to test filters. The 10,000 Hz data were downsampled to 500 Hz to have a more realistic sampling rate and numerically differentiated to have the reference acceleration signal. Figure 23 shows how the displacement and acceleration signals vary in time. Since the application under investigation is running, a very short, yet high magnitude acceleration period exists due to heel strike.

As is the case with the previous example, the frequency limits of the displacement and acceleration signals are quite apart as can be seen in Figure 24. Almost all of the power of the displacement is contained in 10 Hz whereas this value is 86 Hz for the acceleration.

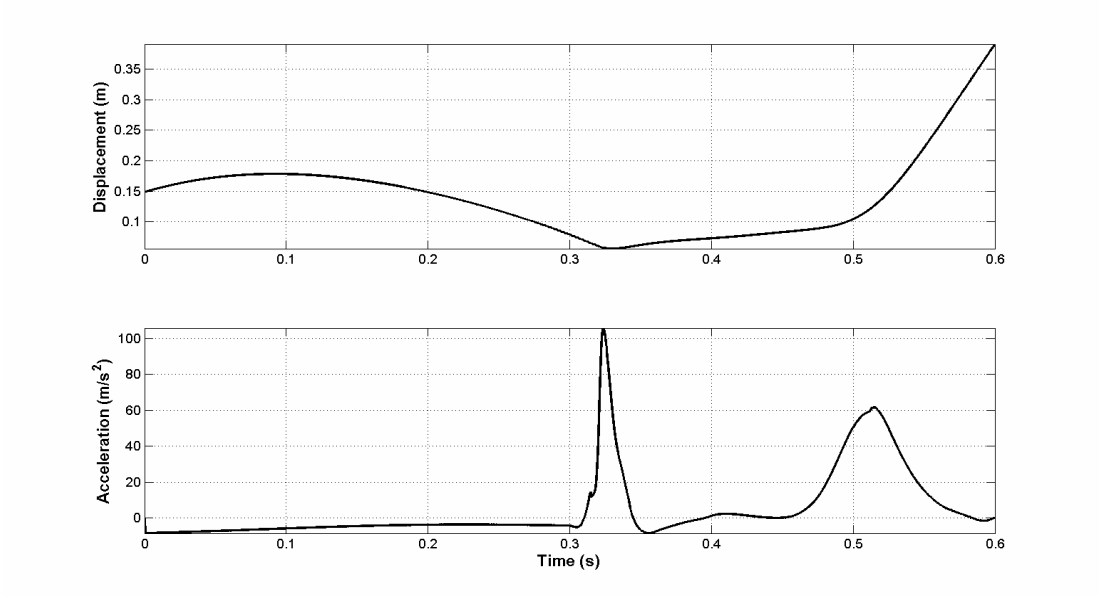

Figure 23. Time variations of the displacement and acceleration signals (running simulation data).

Figure 25 illustrates the expected non-stationary behaviour of the acceleration signal. The power experiences a rapid up and down movement after the heel strike (0.3rd second).

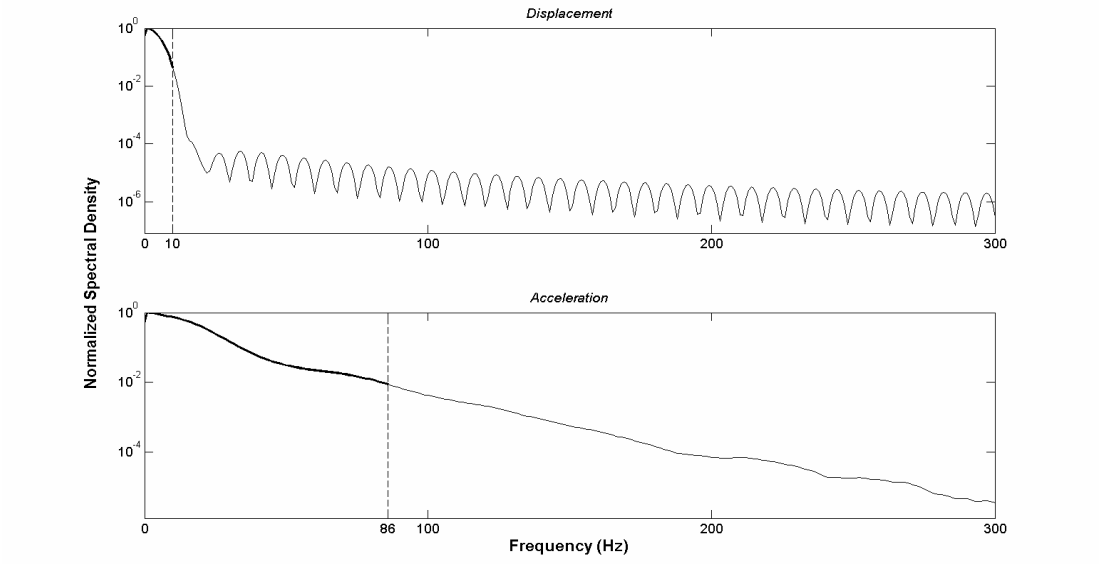

Figure 24. Power spectra of the displacement and acceleration signals (running simulation data).

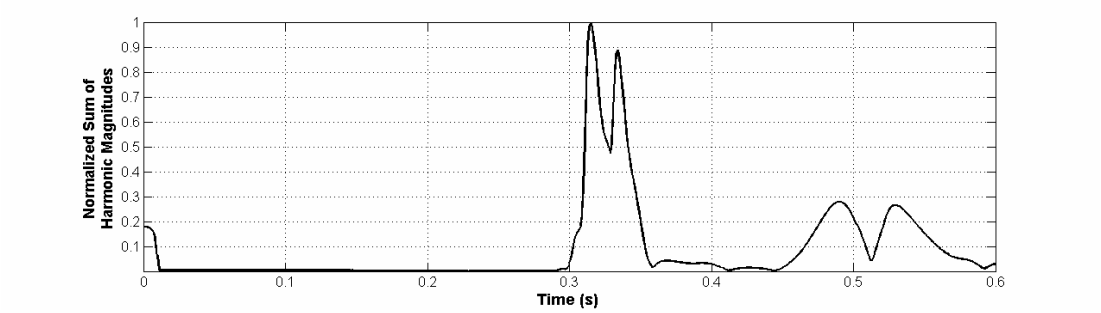

Figure 25. A measure of the power of the acceleration signal as a function of time (running simulation data).

The following three are artificial signals created by manipulating signals of biomechanical origin, which are vertical displacements of markers placed on several landmarks (ASIS, knee, second metatarsal) of lower extremity. The original signals were recorded at 50 Hz during an experiment with KISS and the reference signals were obtained by applying analytical fits using MATLAB's Curve Fitting Tool. The resulting signals were differentiated to get the reference accelerations.

ASIS Marker Data: An eighth order Fourier fit was suitable for the ASIS (Anterior Superior Iliac Spine) marker. The displacement and acceleration curves are plotted in Figure 26.

Spectral densities of the displacement and acceleration signals are given in Figure 27. The values that mark up to which frequency 99 % of power is contained are 2.3 and 4.5 Hz, which indicates a rather small difference when compared to other data investigated above.

As for the temporal power content of the acceleration, the patterns in Figure 28 imply a rather uniform distribution; in other words, the data are stationary.

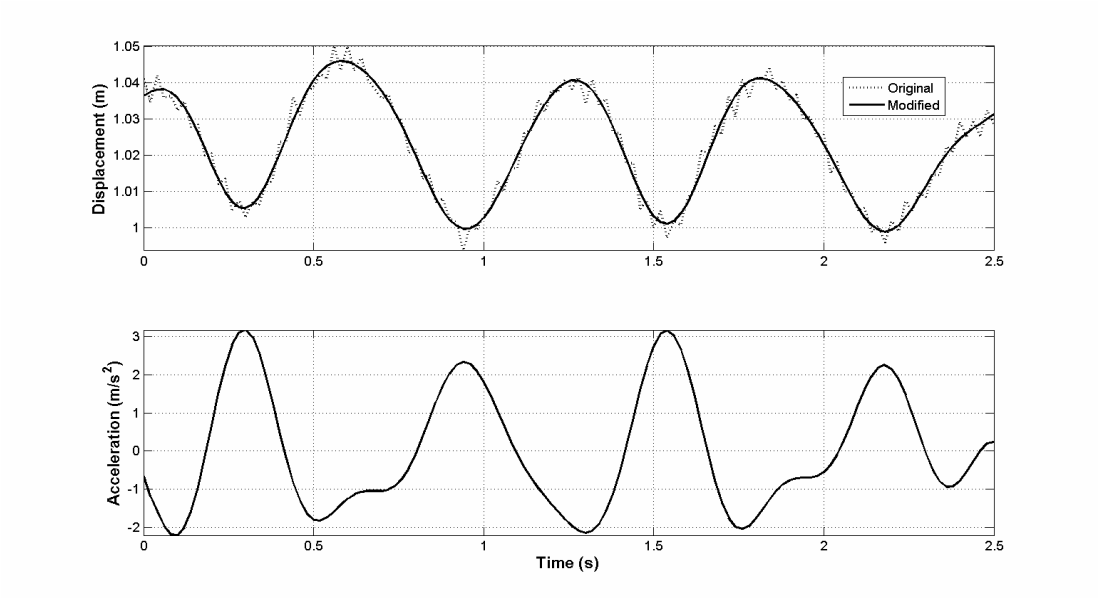

Figure 26. Time variations of the displacement and acceleration signals (ASIS marker data).

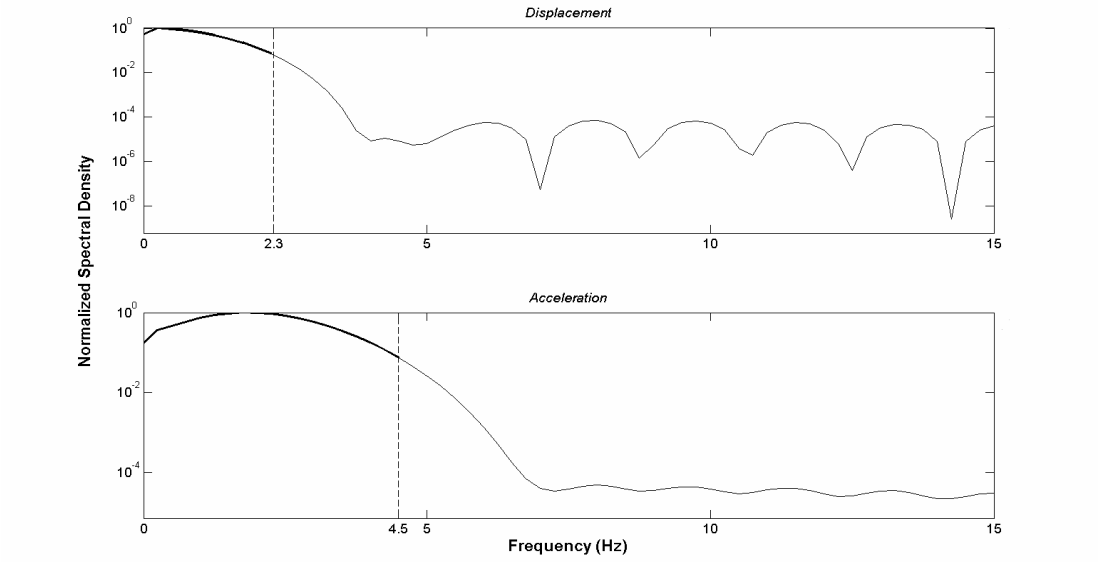

Figure 27. Power spectra of the displacement and acceleration signals (ASIS marker data).

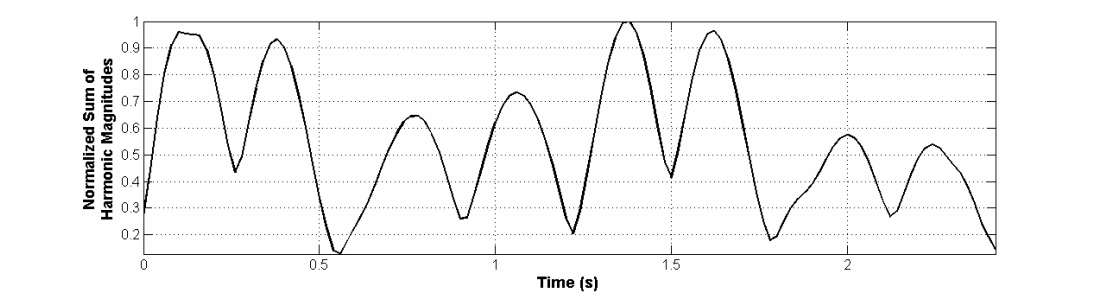

Figure 28. A measure of the power of the acceleration signal as a function of time (ASIS marker data).

Knee Marker Data: In this case, a sum of eight sine functions was appropriate for obtaining the reference signals from the displacement history of the knee marker. These signals can be seen in Figure 29.

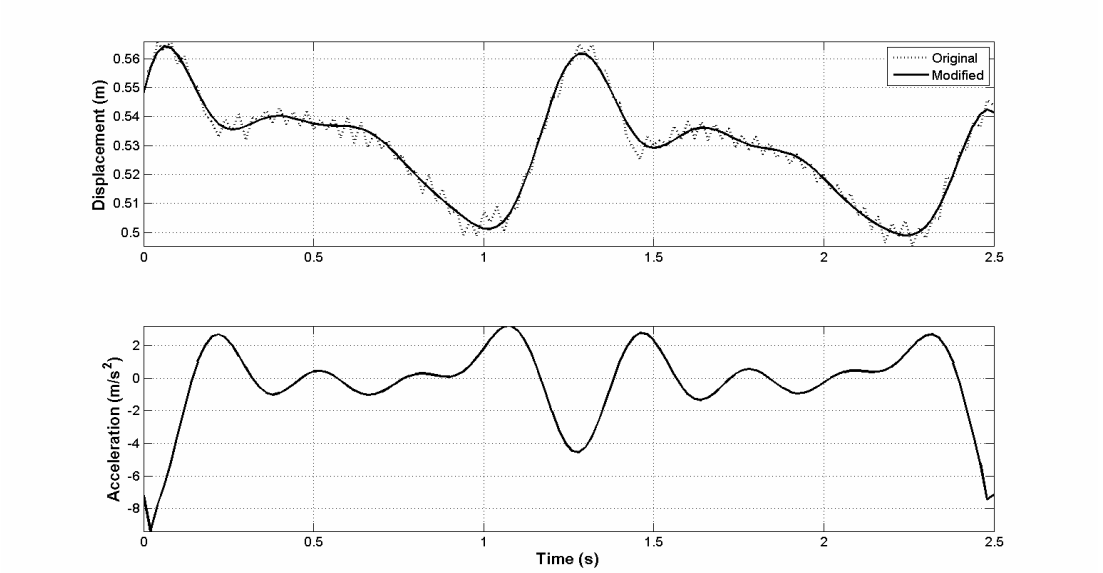

Figure 29. Time variations of the displacement and acceleration signals (knee marker data).

Figure 30 displays spectral density plots of the displacement and acceleration signals. The frequency values are 2.3 and 5 Hz, the difference between being a little larger than that of ASIS marker data.

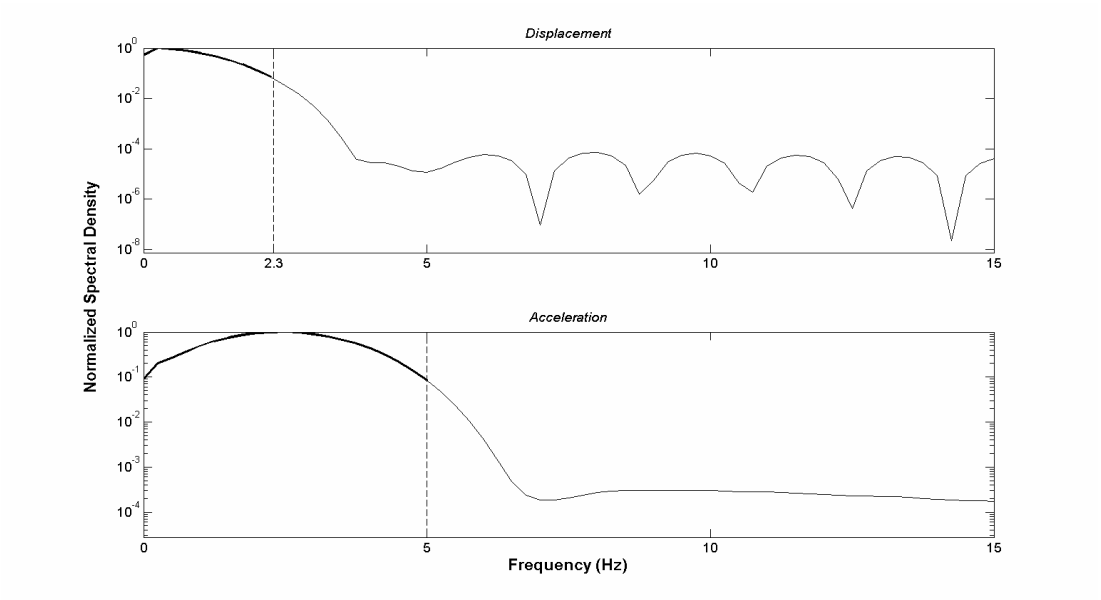

Figure 30. Power spectra of the displacement and acceleration signals (knee marker data).

When Figure 31 is examined, it might be concluded that neither the acceleration signal can be considered stationary nor it is appreciably non-stationary. The power content exhibits variations; yet, the changes are gradual.

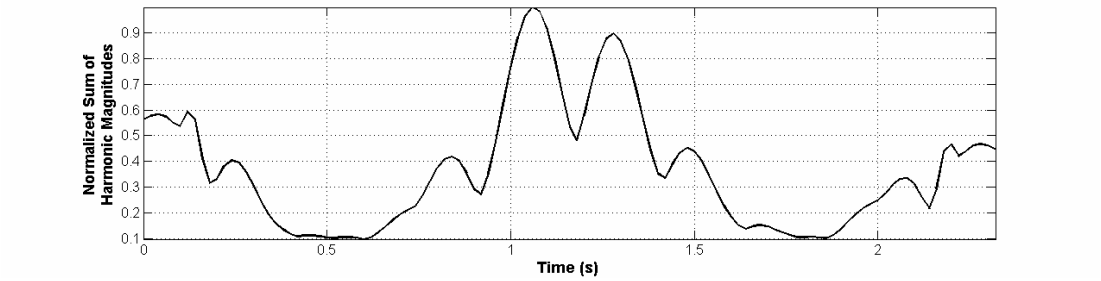

Figure 31. A measure of the power of the acceleration signal as a function of time (knee marker data).

Metatarsal Marker Data: For an accurate representation of the kinematics of the metatarsal marker, an eighth term Gaussian fit was necessary. Figure 32 shows the quality of the fit and the second derivative of the fit.

As seen in Figure 33, the frequency values indicating 99 % coverage of the total power are 4.3 and 8.5 Hz, respectively for the displacement and the acceleration signals. The difference between the values is the greatest among the gait signals presented here.

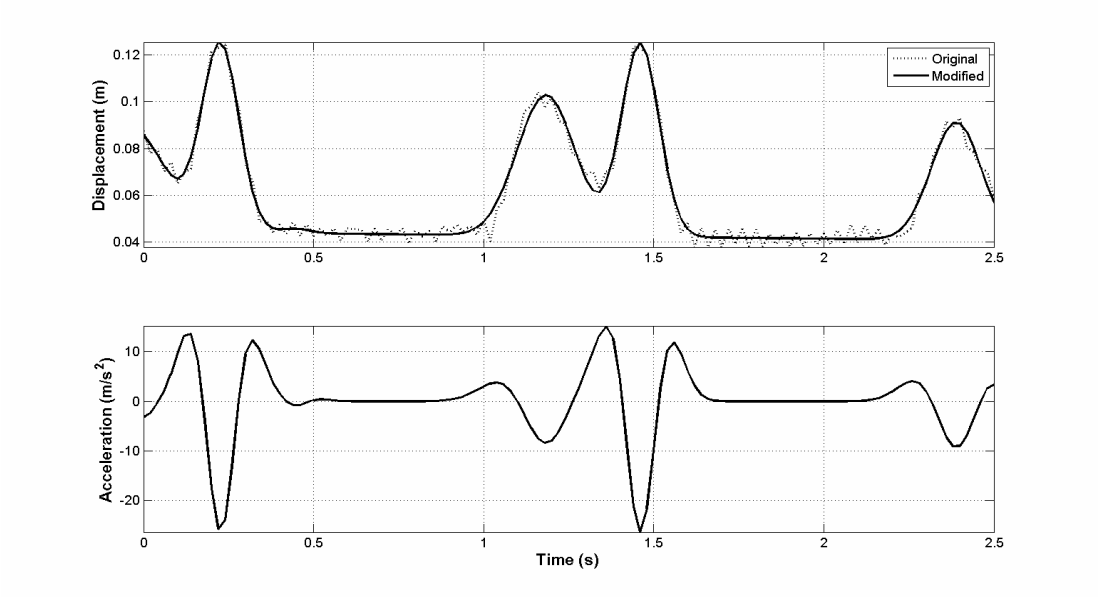

Figure 32. Time variations of the displacement and acceleration signals (metatarsal marker data).

Figure 34 shows the non-stationary nature of the acceleration signal. This is an expected result for a marker located on the foot, which is a segment that comes into contact with the ground after heel strike (impact) and leaves the ground with toe off.

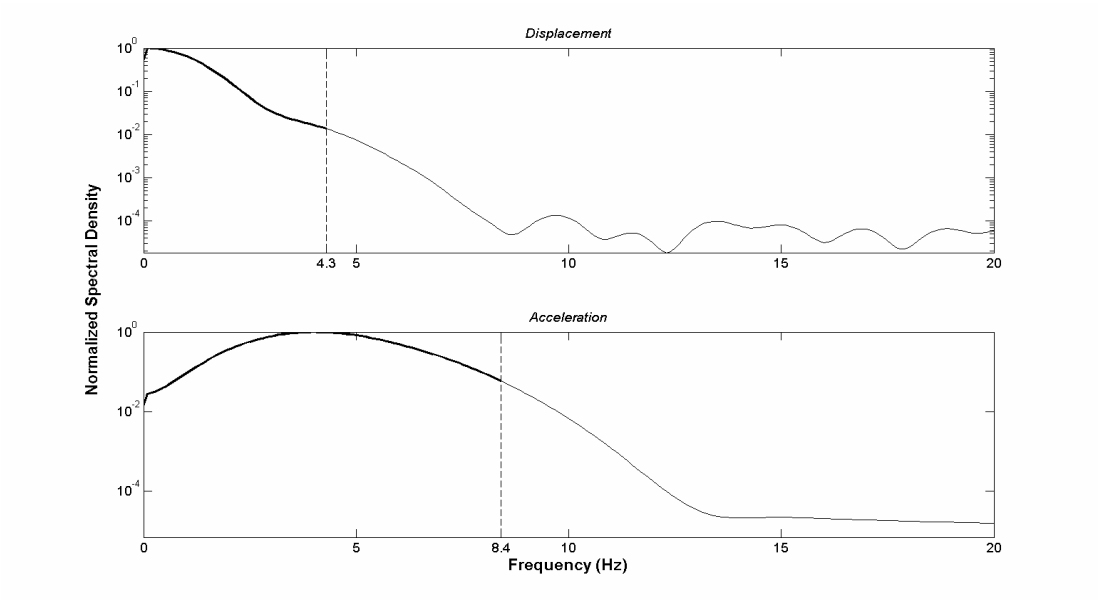

Figure 33. Power spectra of the displacement and acceleration signals (metatarsal marker data).

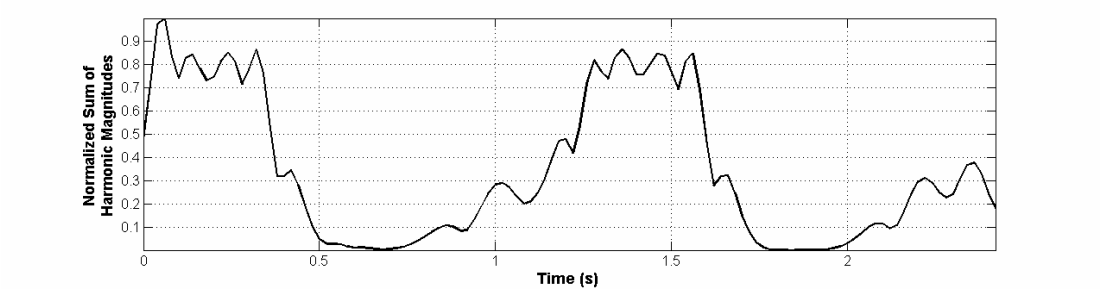

Figure 34. A measure of the power of the acceleration signal as a function of time (metatarsal marker data).

4.2. Discussion on the Results

One implication of the above investigation on frequency contents of various signals is that data from the literature can be used as representatives of gait data for the purpose of testing smoothing and differentiation routines. Like gait data, these are all band-limited; that is, no significant harmonic components are present in their power spectra above certain frequency limits. The other common feature is the variation of signal power in time. Such non-stationary natures have been demonstrated above in the second derivative level and it is true that benchmark

signals possess more power than typical gait data do. Moreover, noise levels found in experimental benchmark data may be accepted to be within bounds that may be faced during any gait trial.

When spectral density plots are examined, it is always seen that the frequency value at which an acceleration signal reaches 99 % of its total power is always higher than the value for the corresponding displacement signal. Amplifying nature of the differentiation process is the mathematical answer here. However, the relative magnitude of these two frequencies is different for each displacement-acceleration couple. There is a positive correlation between the difference of these values and the severity of impact involved in the physical occurrence. This fact is illustrated below. The curves in Figure 35 depict spectral densities of modified accelerations of Dowling's and running simulation data. The modification was such that impact intervals were manually removed from respective acceleration histories[17]. The result is dramatic reduction in limiting frequency values.

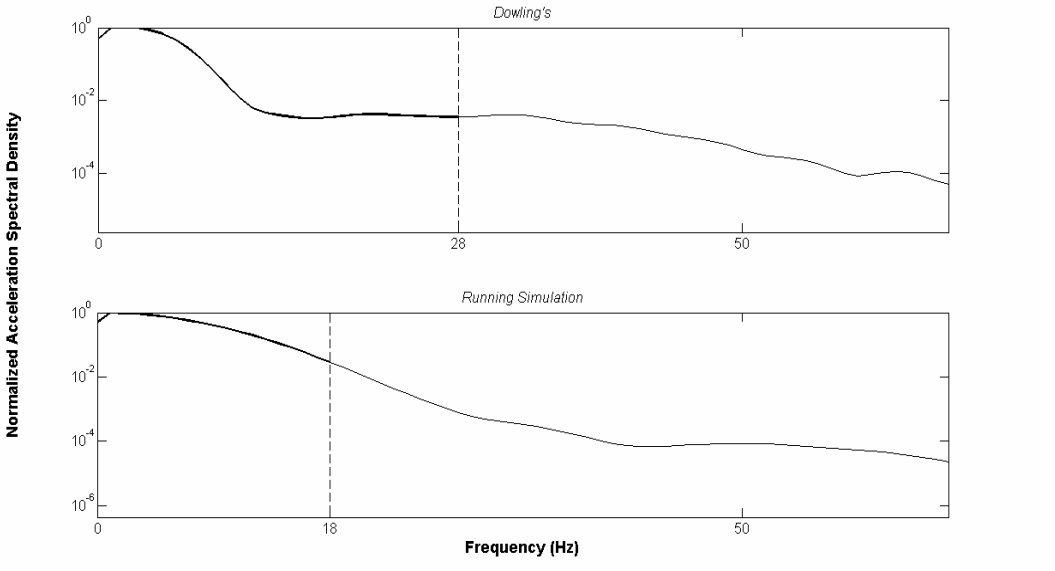

Figure 35. Power spectra of the modified Dowling's and running simulation data.

[17] Foot impact data is not considered since no meaningful signal would remain if its peak acceleration signal was removed.

Here, the conclusion to be arrived is that the difference between the limiting frequency values for a signal and its second derivative is governed by the level of (non-)stationarity of the data. Whereas the difference is fairly low for relatively stationary signals such as Pezzack's and ASIS marker data, this value can reach to considerable amounts when non-stationary signals are concerned.

The discussion above has implications in filtering applications. The frequency value below which a tolerably low amount of information is contained directly takes part in filter window shaping, namely in determination of filter cut-off frequency. It is the primary aim of a filtering process to suppress noise as much as possible while preserving useful signal information. Here, the adjective useful must be well defined. In other words, the question to be answered is what percent of the signal is to be kept as it is, away from the attenuation interval.

If the cut-off frequency is selected as the value below which, for instance, 99 % of the power of the signal is contained, the problem that follows is the need to specify the derivative level whose information content is to be conserved. It has indeed been shown above that frequency, i.e. cut-off frequency, requirements of different derivative levels could be considerably different. This issue was previously raised by Giakas and Baltzopoulos (1997b). The authors assert that different cut-off strategies should be adopted depending on the derivative level the researcher is interested in.

The results obtained in this chapter show that cut-off requirements of non-stationary acceleration signals are likely to be unreasonably high. Utilizing a high cut-off frequency enables peak accelerations to be accurately estimated; but, this constitutes serious complications on intervals where signal power is lower; that is, where relative noise power is higher. The existence of such unfavourable phenomenon is the foundation the next chapter is constructed upon.

CHAPTER 5

ABOUT THE SECOND ORDER BUTTERWORTH FILTER

Butterworth filters are characterized by flat magnitude response curves in pass-band unlike other types of filters such as Bessel or Chebyshev. They may be of any desired order; yet, second order Butterworth filters have been commonly used in biomechanics for smoothing purposes (Robertson and Dowling, 2003). This is why this chapter focuses only on the second order Butterworth filter.

5.1. Continuous Formulation

A second order transfer function is represented in *s* domain as:

$$G(s) = \frac{\omega_n^2}{s^2 + 2\zeta\omega_n s + \omega_n^2}.$$

The transfer function characterizes a Butterworth filter if the damping ratio ζ happens to be $\sqrt{2}/2$. This underdamped system is given as:

$$G_B(s) = \frac{\omega_c^2}{s^2 + \sqrt{2}\omega_c s + \omega_c^2}.$$

Here, ω_c, which replaces the natural frequency ω_n, is the cut-off frequency that indicates the frequency value at which transition from pass-band to stop-band occurs. Magnitude and phase responses of the filter can be shown to be:

$$\mu_B(r) = \frac{1}{\sqrt{r^4 + 1}} \text{ and } \phi_B(r) = -\arctan_2\left(\sqrt{2}r, 1 - r^2\right),$$

where *r* is the frequency ratio defined as ω/ω_c.

It is theoretically true that all harmonic components (except for the harmonic located at zero frequency value) of an incoming signal are attenuated by the filter. The level of attenuation directly depends on relative location of each individual

component with respect to the cut-off frequency value. Magnitude and phase response functions are plotted in Figure 36. It is seen that components in the pass-band ($r \leq 1$) are not attenuated more than $\sqrt{2}/2$ times their original magnitudes while those that are in the stop-band ($r \geq 1$) are suppressed more and more as the frequency ratio increases. As for the phase response, the lag created by the filter increases with r, being 45° when r equals 1.

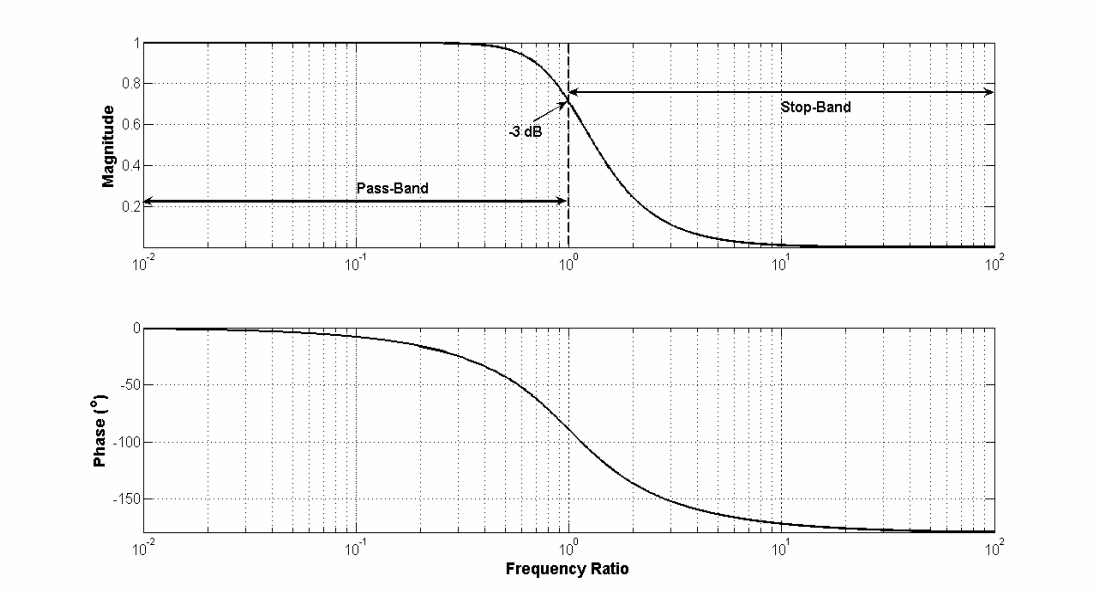

Figure 36. Magnitude and phase responses of a second order Butterworth filter.

Magnitude and phase behaviour of the filter can be demonstrated by means of an online processing example. A sine wave oscillating at 10 rad/s was passed through a second order Butterworth filter with a cut-off frequency of 10 rad/s, in which case r is equal to 1. Simulation results are presented in Figure 37, where attenuation and phase shift values are indicated. Values of the output magnitude and phase shift, from corresponding response functions, are:

$$\mu_B = \frac{1}{\sqrt{2}} = 0.707 \text{ and } \phi_B = -\arctan_2\left(\sqrt{2}, 0\right) = \frac{\pi}{2} \Rightarrow \Delta t = \frac{\phi_B}{\omega} = 0.157\ s\ .$$

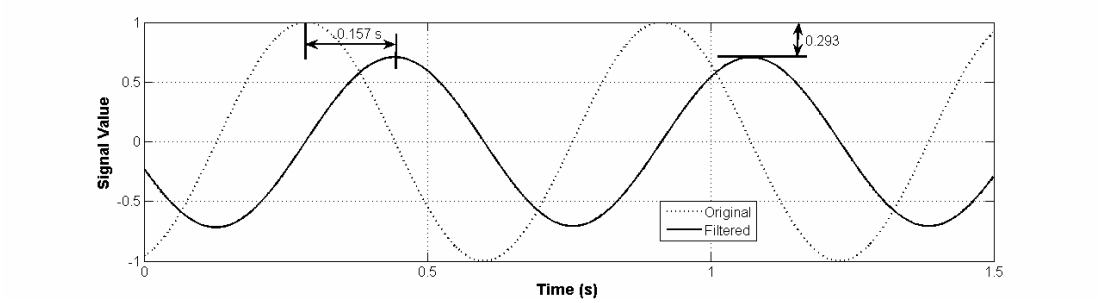

Figure 37. Effects of the Butterworth filter on a harmonic signal oscillating at the same frequency of the filter's cut-off frequency.

This example gives an idea as to how the Butterworth filter works; however, the attenuation and the phase lag created by the filter are at excessive levels, caused by the selected cut-off frequency, which should normally be higher than the highest frequency component present in a signal. Such results are generally not acceptable in filtering applications because the aim of filtering is to obtain a clean version of a contaminated signal. Therefore, the output of a filtering process must deviate as little as possible from the original signal that represents the actual phenomenon. Such a result is only possible with a filter whose magnitude response approximates 1 in the pass-band and 0 in the stop band; and furthermore, the phase lag inevitably created by the filter should be negligible. Since a second order Butterworth filter provides a flat magnitude response, attenuation of useful harmonics is avoidable with a correct selection of ω_c[18]. Although the phase response of the filter is not very acceptable, this is only important in online data processing and has no significance in offline processing as is made clear in the next section.

It is now convenient to present another example that demonstrates the usage of a Butterworth filter as a noise suppressing tool, which is its intended purpose. The sine wave used in the first example was contaminated with Gaussian noise of magnitude 0.02. In a real application there is no option but to work only on the contaminated data. However, since this is a simulated example, the signal and the

[18] This necessitates at least approximate knowledge of the frequency content of the signal to be filtered.

artificial noise may be processed separately and then added[19]. The corresponding Simulink diagram is presented in Figure 38 to provide a visual understanding of the whole process.

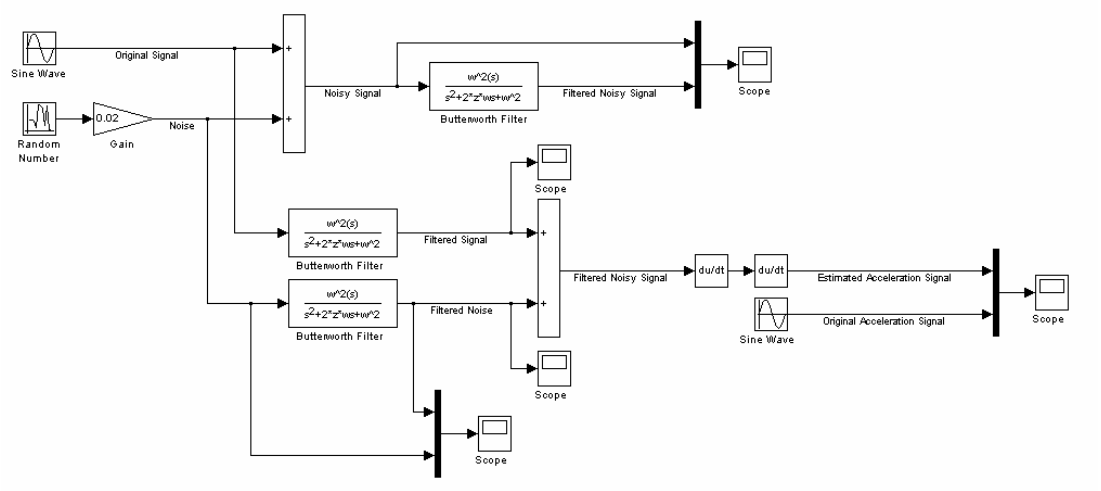

Figure 38. Simulink diagram of an online filtering simulation.

The cut-off frequency is 30 rad/s, which indicates an *r* value of 1/3. The filtered signal is expected to have a magnitude of 0.994 and to lag 0.049 s behind. These values are slightly violated because the behaviour of a filter on a contaminated signal only approximates its behaviour on a clean signal. In Figure 39, it is seen that the direct output of the filter seems to be sufficiently smooth; yet, its second derivative proves otherwise. The differentiation process acts as a high pass filter and amplifies the suppressed noise. A lower cut-off selection would yield better noise suppression, but the price to be paid is more signal attenuation and more phase lag. As mentioned before, the latter disadvantage disappears in offline filtering.

[19] Filtering allows superposition as it is a linear operation.

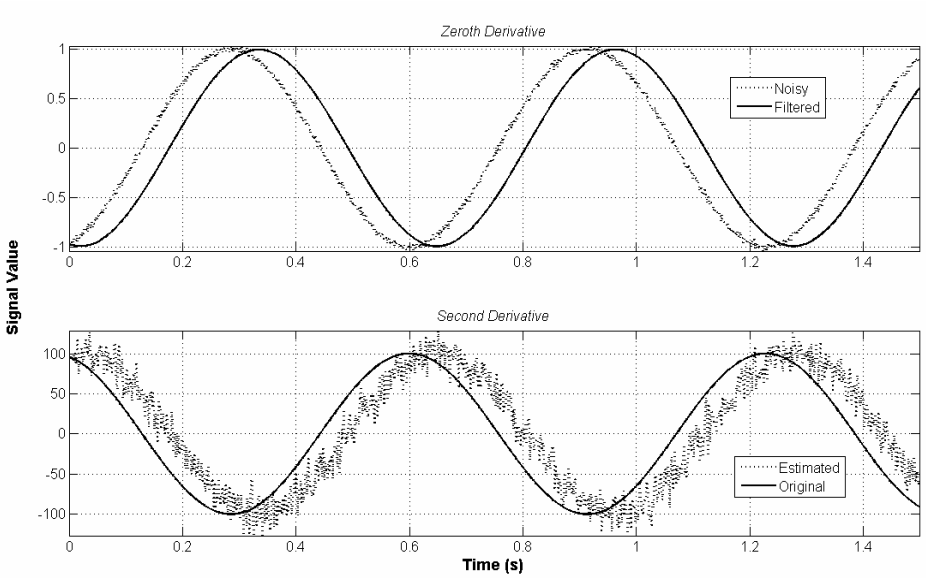

Figure 39. Zeroth and. second derivatives of the signals.

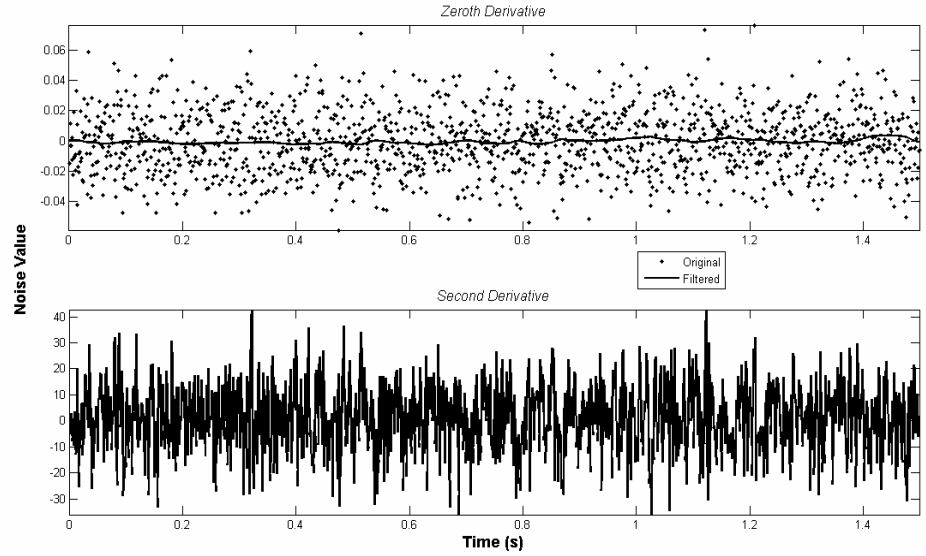

Figure 40. Zeroth and second derivatives of the noise signals.

Better insight into filtering might be gained by examining how noise is affected by the filtering operation. Figure 40 shows the zeroth and the second derivatives of the filtered noise. The noise itself is also included. Its second derivative is not given as it would not be visually meaningful due to excessively oscillatory patterns. It is

obvious that filtering has significant effects on noise; however, it may not output desired results in the second derivative level.

The continuous formulation given in this section is not useful if data are defined in discrete time steps, which is the usual form for digitally acquired signals. The next section is about the regular digital formulation of the Butterworth filter.

5.2. Regular Digital Formulation

A filter defined in Laplace (s) domain can be converted to its equivalent in discrete time domain through the bilinear transformation (Oppenheim and Schafer, 1989). The details are provided in Appendix A.

For a second order filter, the bilinear transformation results in the recursive equation below:

$$y_k = b\left(x_k + 2x_{k-1} + x_{k-2}\right) - a_1 y_{k-1} - a_2 y_{k-2}\,.$$

This equation defines a second order digital filter in discrete time domain. It shows that filtered data points y_k are determined using both previously filtered and raw data points x_k, where k is point index.

In offline processing, which is the kind of processing executed after data acquisition, the phase lag created by the filter can be avoided by feeding the signal in both forward and backward directions (dual pass). This practice; however, results in a fourth order filter. Because the filter order is changed, the coefficients provided by the bilinear transformation become invalid; they must accordingly be adjusted to be able to keep the desired, effective cut-off frequency unchanged. The formulation to calculate second order Butterworth filter coefficients correctly for multiple passes is presented in Appendix B (Robertson and Dowling, 2003).

5.3. The Need for an Advanced Formulation

Based on the discussion in the previous chapter, it should be expected that a Butterworth filter would fail in processing non-stationary signals, the degree of failure being positively correlated with the level of non-stationarity.

Before continuing with an example of such failure, it is convenient to underline that all derivative calculations in this study were performed with second order central differences (Chapra and Canale, 2002) and as a quantitative indicator of failure, Root Mean Squared Error (RMSE) was used. Mathematical definitions are presented in Appendix B.

Failure of the regular Butterworth filter can be demonstrated by making use of the highly non-stationary Dowling's data. Figure 41 shows acceleration histories derived after Butterworth filtering the noisy displacement data with cut-off frequency values of 4, 12, 20 and 28 Hz. The respective RMSE values are 41.9, 26.0, 22.0 and 33.8 rad/s^2. As both qualitatively and quantitatively obvious, none of the curves is able to accurately represent the actual acceleration signal. The output of the filter with 12 Hz cut-off is seen to approximate the overall behaviour the most smoothly; yet, it disturbingly fails around the impact interval. On the other hand, a cut-off frequency of 28 Hz is able to closely replicate the peak acceleration; however, the rest of the output is far from being smooth; intolerable oscillations arise due to unsuccessful noise suppression.

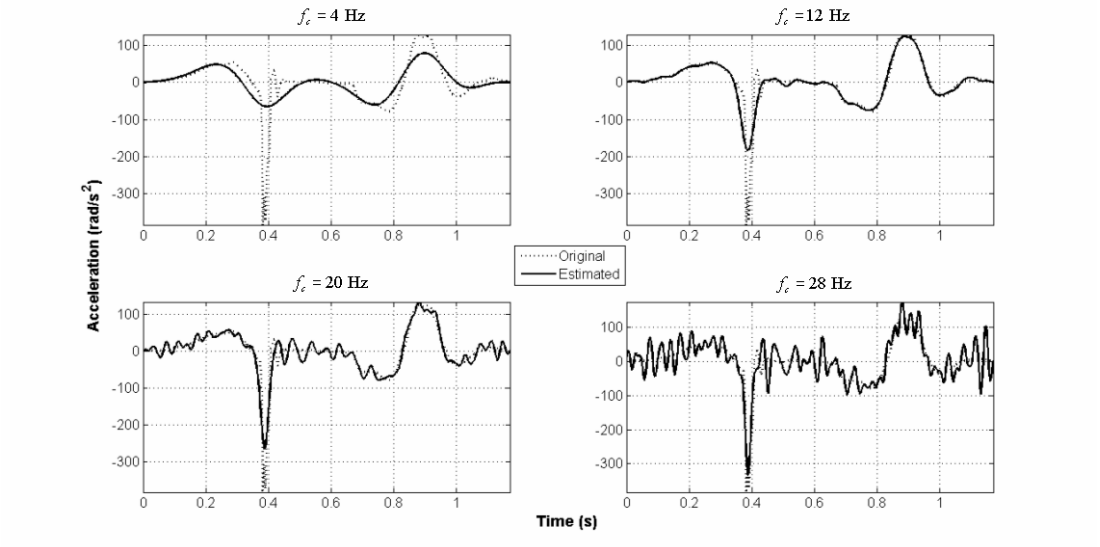

Figure 41. Results of double differentiation of Dowling's displacement signal after filtering it with regular Butterworth filters using increasing cut-off frequencies.

If the researcher intends to settle for a moderate result which neither produces severe oscillations nor highly underestimates extreme accelerations, an intermediate cut-off value, which in the case of Dowling's data is around 20 Hz, should be employed. However, a superior approach would be to process signal segments separately rather than to handle the whole signal at the same time. It is obvious from the above discussion that different intervals in Dowling's data require different cut-off frequencies. This requirement can manually be satisfied by dividing the signal into sections as practised by Dowling in his representative work (1985). There are two swing phases at the beginning and at the end separated by an impact phase followed by an interval of motionlessness. An RMSE of 14.1 rad/s^2 was achieved when cut-off frequency values of 8, 12 and 32 Hz were respectively assigned to motionless, swing and impact phases. The result is similar to what was obtained by Dowling. He reported an RMSE value less than 14 rad/s^2. The small difference can be attributed to the preferred filtering techniques. Dowling used cubic splines and the Butterworth filter in a combined manner whereas the current study employs only the Butterworth filter.

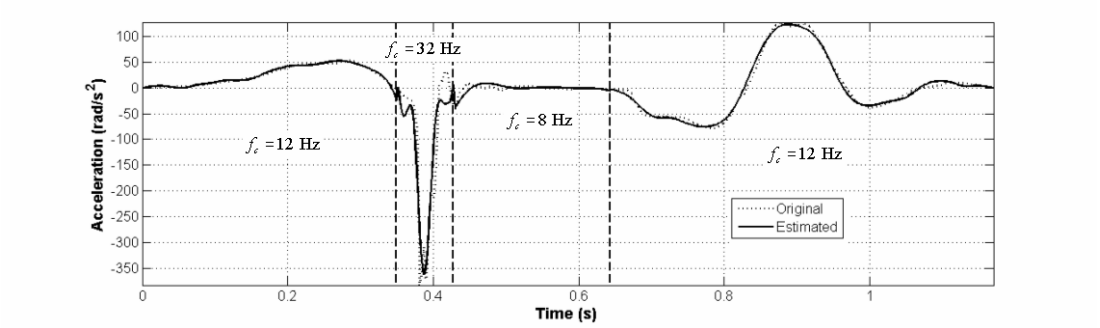

Figure 42. Acceleration response of the regular Butterworth filter applied to the manually segmented Dowling's displacement signal.

The segmentation procedure is definitely superior to the classical approach; nevertheless, it requires certain amount of labour and subjective user decision is involved in the process when performed manually. Also, the method may suffer from the presence of inconsistency between segments because they are processed

separately as though they were not contained in the same signal. Such inconsistency is visible in Figure 42 where there are jumps at the beginning and the end of the impact interval, caused by the large difference between the cut-off values on either side of the transition points.

5.4. Adaptive Digital Formulation

The preceding section shows that neither low nor high cut-off frequencies lead to satisfactory acceleration estimates when non-stationary data are concerned. Manual segmentation could solve the problem; but, an automatic solution is necessary to overcome the difficulties associated with the involvement of user intervention.

Instead of segmenting signals at discrete points, an alternative, automatic approach may be to vary Butterworth cut-off frequencies according to some proper criterion, which should be closely related to local acceleration as it is the acceleration that determines cut-off requirements as demonstrated above. A filter realized in such a way might be called an adaptive Butterworth filter.

At this point, it is proposed that the cut-off frequency distribution be a function of the point which is being processed. One possible solution is:

$f_k = f_1 + f_2 c_k$.

Cut-off frequencies, f_k, assume values between f_1 and $f_1 + f_2$, which denote the minimum and maximum frequency values to be used in the filtering process. Vector c should be formed such that it leads to cut-off frequencies that are closely correlated to local acceleration values. After exhaustive tests on benchmark data, its formulation was empirically determined as:

$d_k = vel_k + acc_k$,

$c_k = d_k + \max(d)$.

vel and *acc* are normalized (ranging between 0 and 1) first and second derivatives of the displacement data derived after filtering the signal. The criterion cannot be solely based on acceleration values because a certain degree of smoothness in the distribution of frequencies is required. Hence, cut-off values of points that have low

accelerations but appreciable velocities (e.g. inflection points) are increased by making use of their velocity values. Filtering process needs to be initiated by prefiltering the signal using a regular Butterworth filter with a cut-off frequency f_p, after which the calculation of the adaptive cut-off frequencies follows.

Experimentation with the new filter indicated that iteration increases the performance as it allows the cut-off frequencies to be determined from improved (derived after adaptive filtering) velocity and acceleration estimates; however, it may tend to distort the smooth variation of the frequency distribution. Hence, low-pass filtering of f is necessary if the adaptive filter is to be used in an iterative manner. This filtering is done by employing an adaptive Butterworth filter that uses the elements of f as its own cut-off frequencies. In other words, f is filtered with itself, resulting in f_s. Adaptive filtering of the frequency distribution does not only eliminate the need for a constant cut-off value to be selected by the user, it also renders the total filtering process nearly insensitive to the choice of the prefiltering cut-off; f_p may safely be set equal to $f_1 + f_2$. It should be noted here that this filtering routine causes the actual limits to be somewhat different from (generally lower than) f_1 and $f_1 + f_2$.

As for the final step, the output of the adaptive filter should be one last time passed through a standard Butterworth filter with a cut-off higher than or equal to the highest element of f_s. This represents a finishing process, smoothing out small irregularities caused by the adaptive usage of the filter. Obviously, the result is an increase in the filter order.

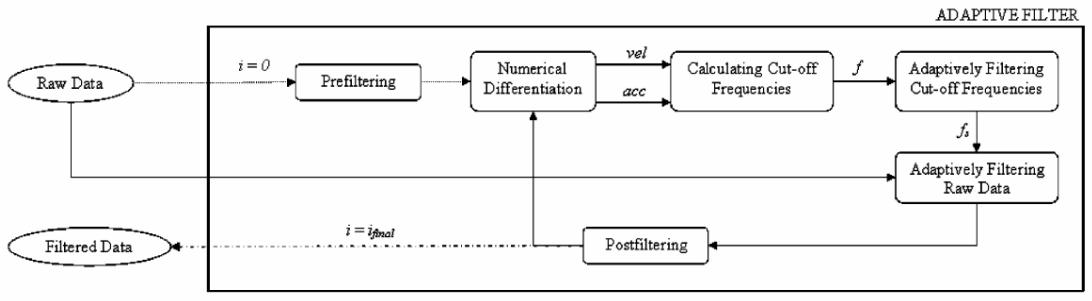

Figure 43. Steps in the application of the adaptive Butterworth filter.

Figure 43 summarizes all the steps described above. All four filter passes are single dual pass and raw data are padded as described by Derrick (1998) to facilitate processing of end regions. The padding is achieved by mirroring left and right halves of a signal. Figure 44 illustrates this padding routine. Padding signals in such a manner imposes zero acceleration values at boundaries, making it useful for decreasing end point errors whenever acceleration values at the boundaries are negligible. However, it should be noted that the procedure certainly leads to large end point errors if this is not the case.

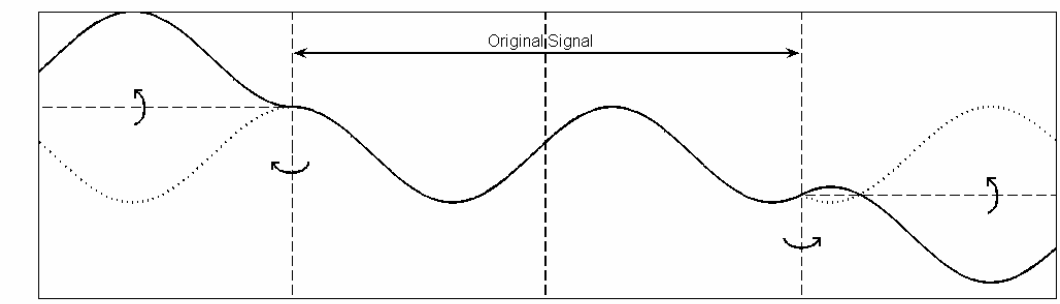

Figure 44. Padding procedure applied to signals before adaptive Butterworth filtering.

MATLAB code of the adaptive Butterworth filter is included in Appendix D.

5.5. Performance Assessment of the Adaptive Butterworth Filter

This section aims to reveal the superiority of the adaptive formulation over the regular one. The demonstration is done by processing sample signals with both Butterworth filters and then to compare their results with actual acceleration curves. Displacement signals, which are direct outputs of the filters, are not evaluated here as they do not yield as valuable information about filter performances as acceleration signals do.

The sample signals are those introduced in the previous chapter, namely four benchmark signals from literature and three artificial gait signals obtained by manipulating marker trajectories captured by KISS. Of the seven displacement

signals, only three (Pezzack et al.'s, Dowling's and foot impact signals) were acquired during actual experiments, implying that they are readily contaminated by noise. The remaining four (running simulation and three marker signals); however, are free of noise, which is why they were artificially contaminated with Gaussian noise. This way, 100 different noisy signals were obtained for each of the four signals. The standard deviation of the random numbers added to running simulation displacement signal is 0.5 mm, which is within the range used by Giakas and Baltzopoulos (1997b). As for the standard deviation of the contamination in marker displacements, it was selected to be 1.5 mm on the assumption that such a value was representative of the noise level in KISS.

The whole assessment routine is based on selection of suitable filter parameters with trial and error. Parameters that minimized acceleration errors for each signal were determined through experimentation. Here, it should be noted that initial and final two points of acceleration histories were excluded in performance assessments as it is a known fact that acceleration values at signal ends are bound to deviate from reference values. This phenomenon is referred to as end point error. The padding method described above eliminates end point errors only if actual acceleration boundaries are zero. Since this is often not the case, RMSE calculations were not performed on entire lengths of the calculated acceleration signals. Such an approach is not considered inappropriate because measures against end point error are out of the scope of the current study.

Table 3 shows these parameters along with the RMSE values they yielded[20]. Values of standard deviation of errors, are also included whenever applicable to show that both filters operate in a consistent manner. A quick examination of error values indicate that the adaptive Butterworth filter always performed better than the regular Butterworth filter.

Here, it should be noted that initial and final two points of acceleration histories were excluded in performance assessments as it is a known fact that acceleration values at signal ends are bound to deviate from reference values. This phenomenon

is referred to as end point error. The padding method described above eliminates end point errors only if actual acceleration boundaries are zero. Since this is often not the case, RMSE calculations were not performed on entire lengths of the calculated acceleration signals. Such an approach is not considered inappropriate because measures against end point error are out of the scope of the current study.

Table 3. Performance comparison of the regular and adaptive Butterworth filter formulations. [f_c: Cut-off frequency of the regular filter (Hz). f_1: Minimum cut-off frequency used by the adaptive filter (Hz). $f_1 + f_2$: Maximum cut-off frequency used by the adaptive filter (Hz). # Iter.: Number of iterations in adaptive filtering. RMSE: Root Mean Squared Error between the actual acceleration signal and the second derivative of the filter output (rad/s^2 or m/s^2).]

	Regular		**Adaptive**			
Data	f_c	RMSE	f_1	$f_1 + f_2$	# Iter.	RMSE
Pezzack et al.'s	6.1	4.39	3.5	7.5	2	3.99
Dowling's	18.6	21.88	6.4	27.4	6	12.67
Foot Impact	75.5	6.58	8.0	84.2	5	3.65
Running Sim.	29.6	5.17 ± 0.26	10.4	39.3	3	3.81 ± 0.26
ASIS Marker	4.0	0.22 ± 0.04	-	-	-	-
Knee Marker	5.3	0.49 ± 0.06	3.6	6.4	3	0.45 ± 0.06
Meta. Marker	8.0	1.18 ± 0.14	3.2	9.6	3	0.91 ± 0.12

Table 3 serves as a quantitative performance summary for the two filter formulations. Means of visual investigation of how the filters performed on each test signal is presented in what follows. The figures are organized in such a way that each first subfigure shows how cut-off frequencies used in adaptive filtering process are distributed and in each second subfigure; actual, regularly filtered and adaptively filtered acceleration histories are plotted[21].

Pezzack et al.'s Data: In Figure 45, it is seen that higher cut-off values are synchronized with the quicker swing interval, as expected. Due to the low dynamic range (f_2 - f_1); however, the effectiveness of such a correct distribution remains

[20] For artificial data, each RMSE value is the mean of all errors.

[21] For the running simulation and the three gait signals, the presented acceleration curves are those whose RMSE values are very close to the corresponding mean RMSE values.

rather limited. As a result, outputs of the regular and adaptive filters do not differ much form each other.

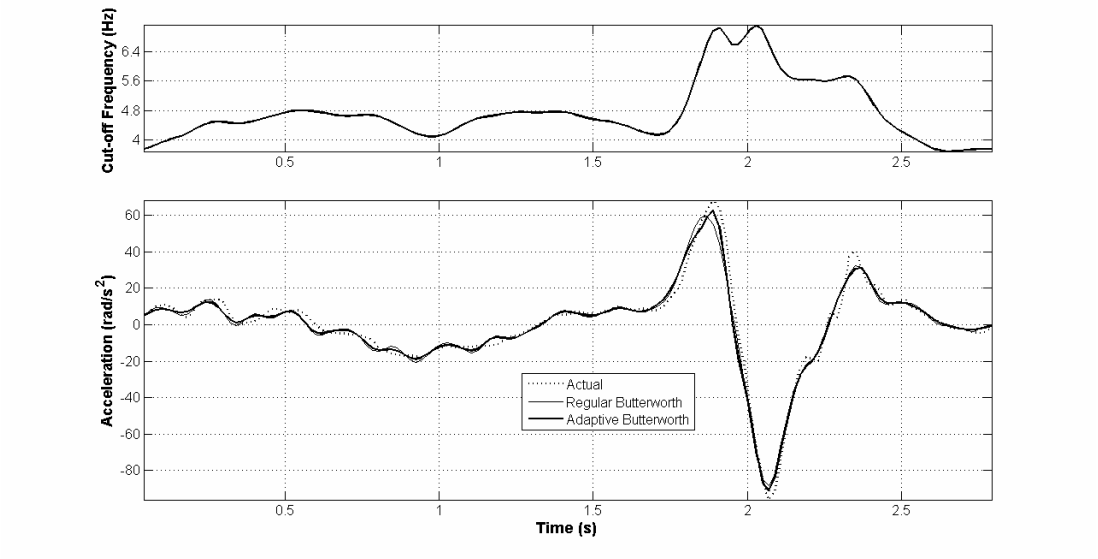

Figure 45. Distribution of the adaptive cut-off frequencies; variations of the actual and estimated acceleration signals (Pezzack et al.'s data).

Dowling's Data: Figure 46 reveals that highest frequency values are assigned to the points of impact phase. For the neighbouring region, the cut-off stays almost constant around the lower limit as this is an interval where there is almost no displacement. Beyond these points, the filter again adjusts itself to the changes in the signal structure, raising frequency values. Since in this case, the dynamic range is sufficiently high, the agreement between the reference acceleration and the adaptive filter output is very good except for slight discrepancies. On the other hand, the regular filter is seen to dramatically underestimate the peak acceleration. It also fails in the stationary parts of the signal, producing intolerable oscillation patterns.

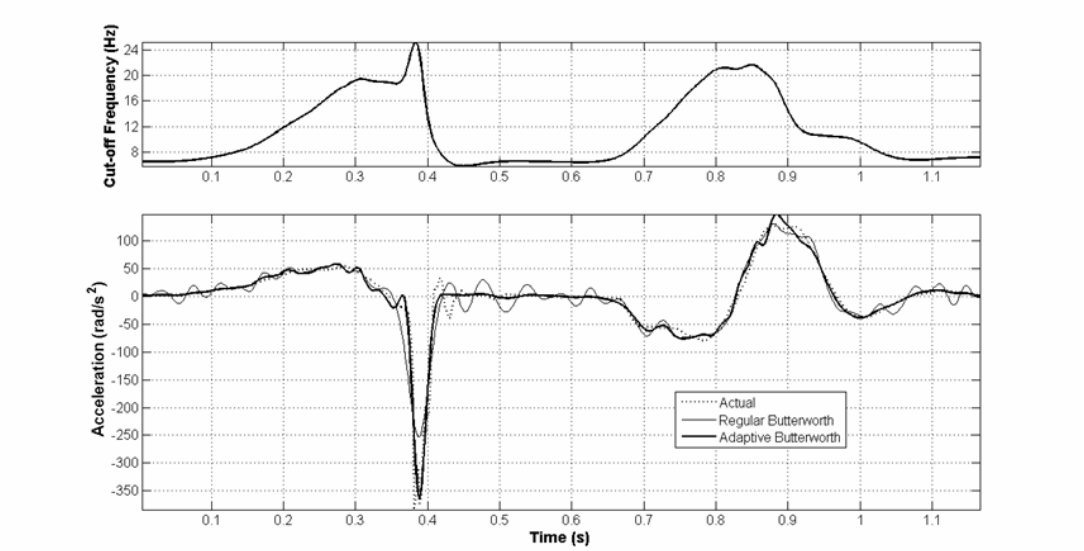

Figure 46. Distribution of the adaptive cut-off frequencies; variations of the actual and estimated acceleration signals (Dowling's data).

Foot Impact Data: As shown in Figure 47, highest frequency values are again assigned to points that have the highest acceleration values. The figure also shows that both filters are able to provide acceptable estimates, the adaptive one being slightly more successful. It might be surprising that the regular Butterworth filter does not fail to process such a non-stationary signal. The rather clean nature of the recorded displacement signal is the explanation why.

Running Simulation Data: In spite of the fact that Figure 48 illustrates the acceptable performance of the adaptive filter, it also indicates that adaptive cut-off frequencies are not distributed quite as would be expected. Maximum cut-off values are not assigned to points around the highest acceleration interval. Both filters are seen to underestimate the peak acceleration; nonetheless, the adaptive filter clearly provides a better match.

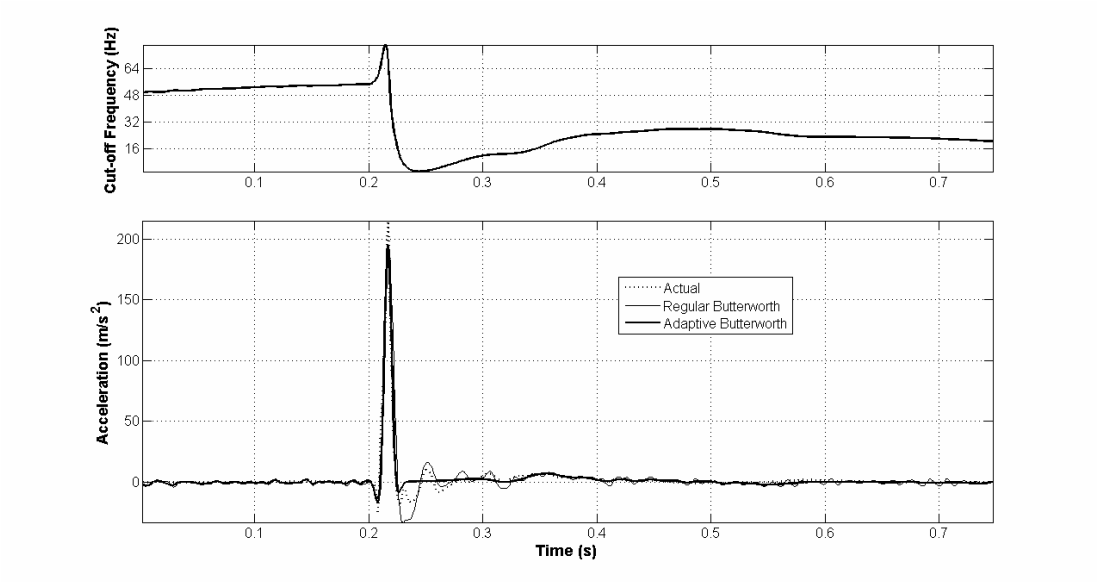

Figure 47. Distribution of the adaptive cut-off frequencies; variations of the actual and estimated acceleration signals (foot impact data).

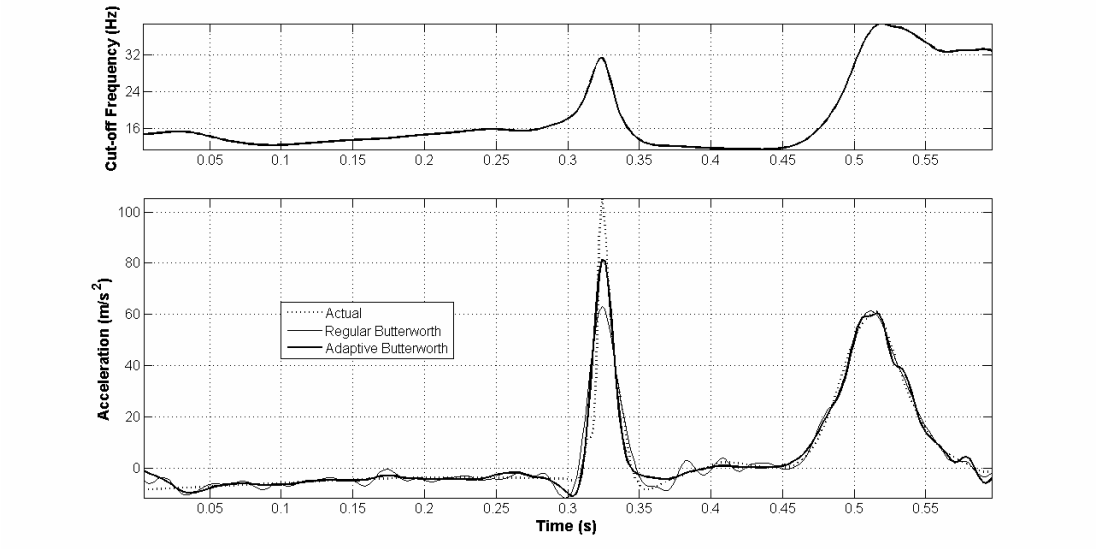

Figure 48. Distribution of the adaptive cut-off frequencies; variations of the actual and estimated acceleration signals (running simulation data).

ASIS Marker Data: Because the data is quite stationary, there is no point in resorting to adaptive filtering. As Figure 49 shows, the regular Butterworth filter can handle the task.

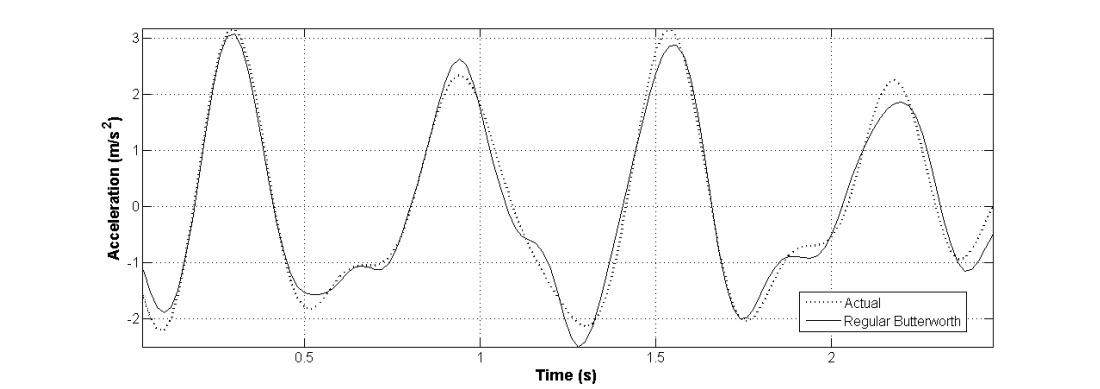

Figure 49. Variations of the actual and estimated acceleration signals (ASIS marker data).

Knee Marker Data: As evident from Figure 50, the regular and adaptive formulations perform equivalently. Although adaptive cut-off frequencies visibly vary in harmony with the frequency content of the signal, they have almost no effect due to the low dynamic range.

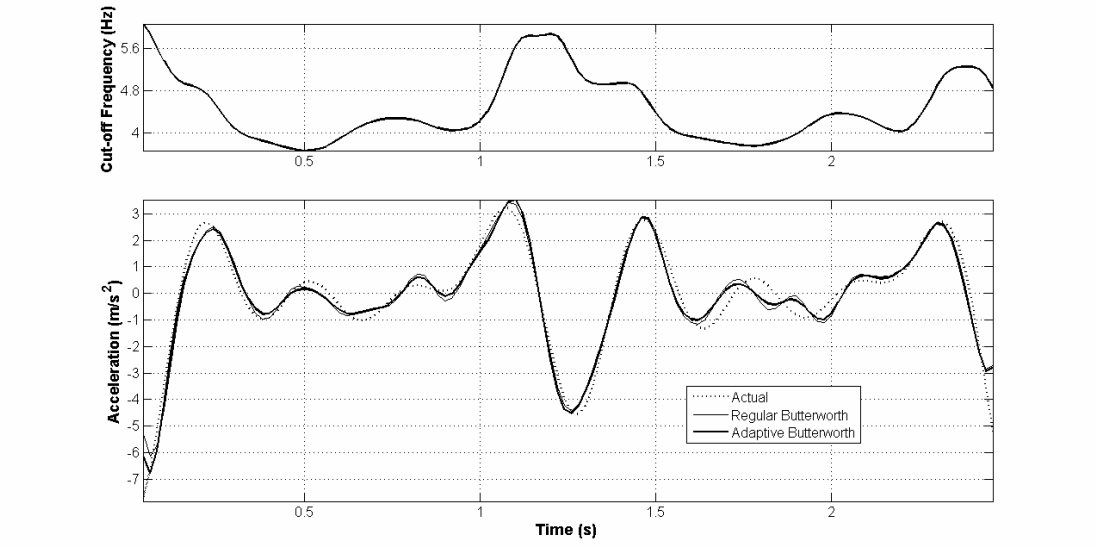

Figure 50. Distribution of the adaptive cut-off frequencies; variations of the actual and estimated acceleration signals (knee marker data).

Metatarsal Marker Data: The cut-off frequency distribution plotted in Figure 51 illustrates the non-stationary nature of the data. Unlike the previous case, the dynamic range is high enough to result in improved acceleration estimation. As seen, intervals of negligible acceleration are accurately replicated by the adaptive filter whereas the regular filter results in oscillations.

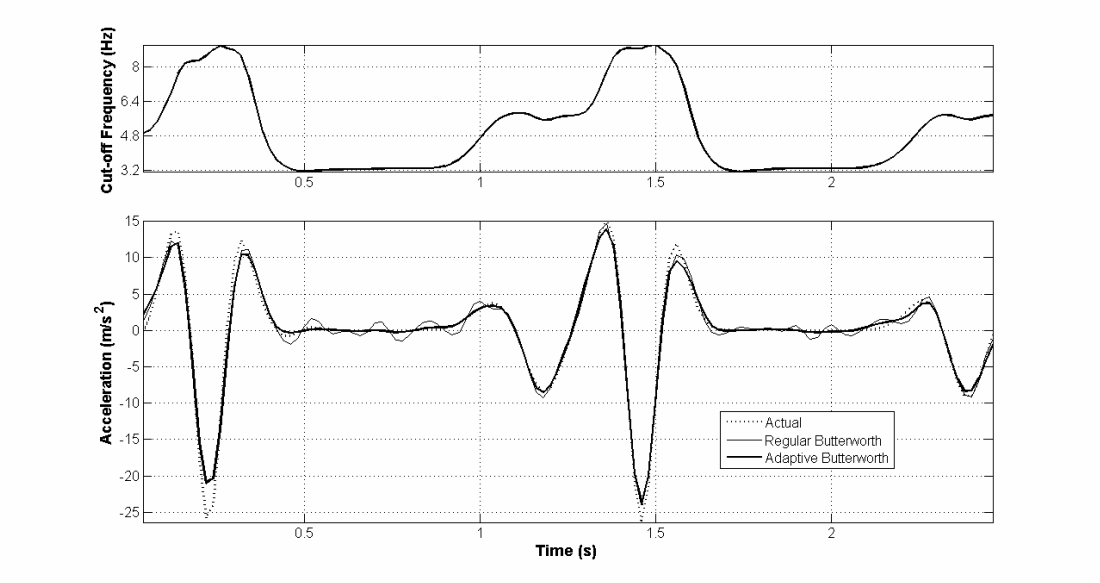

Figure 51. Distribution of the adaptive cut-off frequencies; variations of the actual and estimated acceleration signals (metatarsal marker data).

5.6. Comments on the Performance

Among all test signals the adaptive Butterworth filter was experimented upon, the filter's performance on the running simulation data is somewhat disturbing. Fairly high, prolonged acceleration period near the end of the signal causes simultaneous high velocity values. Because of this, highest cut-off values are assigned to this portion of the signal instead of the short interval where the peak acceleration happens to be. This is responsible for the underestimated peak acceleration; f_2 cannot be raised without causing the acceleration output of this period to get out of control. A similar behaviour can also be seen in the filtering of Dowling's data, but is not as pronounced. After the first half of the signal, the velocity reaches its

maximum value accompanied by some moderate amount of acceleration. However, the peak acceleration value here is so dominant that the maximum cut-off frequency is correctly positioned. The effect is nonetheless visible: There are some unwanted deviations in the interval of positive maximum acceleration. In the case of filtering the foot impact data, the highest velocity values occur before the impact and although these are low in a global view, they consequently give rise to unnecessarily high frequency values, which, however, does not affect the output acceleration much. There are no such considerations for Pezzack et al.'s and the three gait experiment data. Velocity histories of the signals (except for the ASIS Marker) derived by integrating acceleration histories can be seen in Figure 52.

In Figure 53, error variations versus number of iterations are plotted for each test signal. All settle to a constant error value except for the running simulation error, which remains bounded around a nearly constant average error. Convergence is quick; usually in the order of a few iterations. The curves never settle to the minimum error value possible, which means that more number of iterations does not mean a better result.

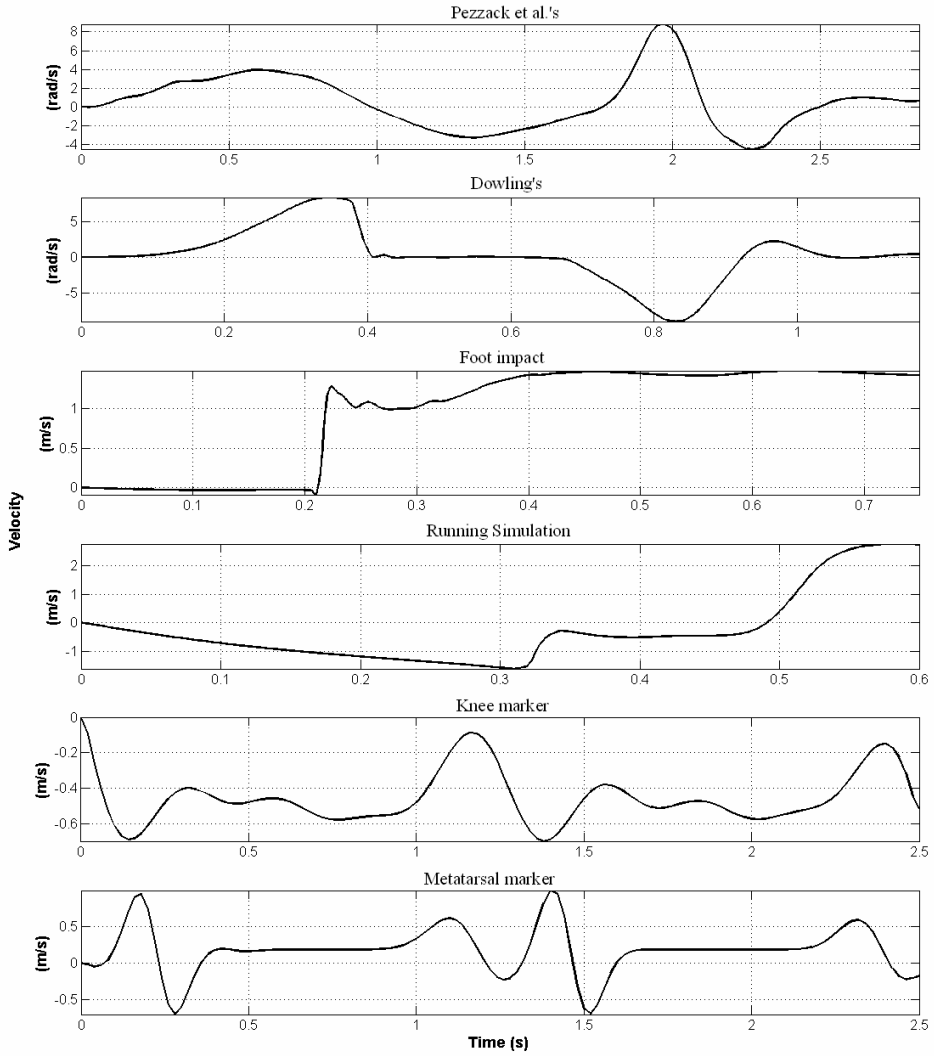

Figure 52. Velocity histories of test data.

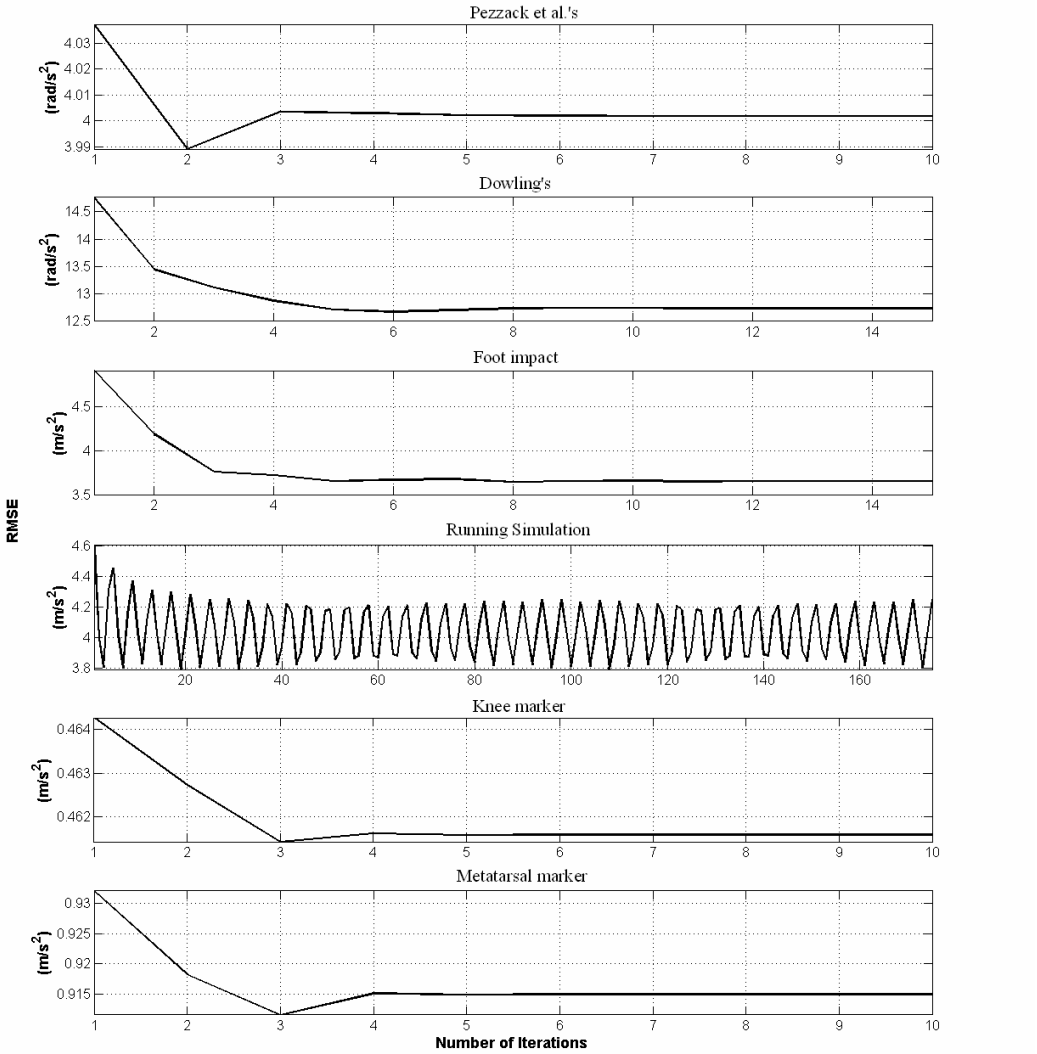

Figure 53. Effect of number of iterations on RMSE.

5.7. Discussion on Practical Aspects

Even if one happens to choose the so-called optimal cut-off frequency (Capello et al., 1996; Yu et al., 1999; Giakas and Baltzopoulos, 1997a), conventional Butterworth filtering either fails in catching extreme accelerations or is unable to eliminate noise when the signal is not stationary. As demonstrated by van den Bogert and de Koning (1996) making use of the running activity, which unquestionably involves impacts, unacceptable errors in intersegmental loads are likely to arise if the correct nature of the phenomenon under investigation is

overlooked. The proposed filter exploits signal features, making it possible for the Butterworth filter to accommodate changes in local frequency content so that errors arising from improper filtering are eliminated as much as possible. The method involves setting upper and lower limits instead of using a single cut-off frequency. Hence, some means of estimating optimal values for these limits would be extremely useful in the absence of reference acceleration signals.

Based on the results presented above, the proposed filter is not expected to work well with signals that have extended acceleration intervals, such as the vertical trajectory of a falling object which is under the continuous action of gravity. In such a case, the cut-off value will theoretically increase linearly over time as the velocity of the object rises. This weakness of the adaptive filter is a natural consequence of the criterion that is used in the calculation of the cut-off frequencies. The velocity affects the calculation being as dominant as the acceleration. The weight of the velocity might be decreased in various ways; yet, this adds another filter parameter to be determined by the user and furthermore, runs with such configurations did not produce superior results.

The idea of employing variable cut-off frequencies is promising; however, because of the continuously changing coefficients of the adaptive filter, final acceleration can easily assume a highly oscillatory pattern, especially when the dynamic range f_2 - f_1 is too high, if filtering of the cut-off frequencies and postfiltering of the already smoothed data are not executed. Moreover, Butterworth filters have defined attenuation behaviours in frequency domain as shown in the beginning of this chapter. Whether such a definition is possible for the modified version is a question which might be the subject of another study. Nonetheless, the good performance of the filter renders such issues less urgent.

The adaptive filter is expected to perform better with an improved and presumably more complex criterion for determining cut-off frequencies. The current one combines only the velocity and acceleration characteristics of the signal. Higher derivatives or the displacement data itself might contribute to the formation of a superior formulation. This remains an open question.

As for the implementation of the adaptive Butterworth filter into gait analysis applications, the experimentation done here on three representative signals suggests that the new filtering technique is not absolutely necessary for smoothing marker trajectories. Nevertheless, the filter gains some usefulness in smoothing signals which belong to distal segments, e.g. trajectories of markers placed on foot, owing to non-stationary natures of such signals. As illustrated above with the metatarsal marker data, the filter prevents oscillatory acceleration patterns in intervals when markers are at rest. However, this advantage is likely to disappear when kinetic analysis of gait is concerned. Ground reactions are involved in the calculation of forces and moments acting on segments. As the gait to be analyzed gets slower and slower, inertial terms become more dominated by ground reactions. The natural consequence of this is the insensitivity of calculated intersegmental loads to the applied smoothing technique.

The reasoning above does not mean that the usage of the adaptive Butterworth filter is not preferable for gait analysis. Results obtained here imply that it almost always performs better than the regular filter. Since it may not always be possible or desirable to control the gait speed, having ready a superior tool for analysis of quick gait is valuable. It should also be noted that usage of the adaptive filter in processing of slow gait does not have any downsides; the only concern would be to waste most of the filter's potential.

Based on this discussion, the adaptive Butterworth filter was found suitable to be integrated into KissGait-M. The results above show that 3 iterations produce successful, if not optimal, results for gait data. As for the cut-off frequency limits, it seems reasonable not to keep f_1 below 3.5 or 4 Hz while having f_2 around 6 Hz at the foot and to decrease it gradually to 0 (this forms a regular filter) as the progress is made towards the pelvis. An experienced operator should be able to adjust these values depending upon the gait speed of the subject.

CHAPTER 6

KissGaitM: A GAIT ANALYSIS TOOL DEVELOPED IN MATLAB

This chapter is reserved for KissGaitM, a gait analysis tool that makes use of the flexible programming medium provided by MATLAB, which the M at the end stands for.

The graphical user interface of KissGaitM is composed of two windows. The first one, which is shown in Figure 54, is where gait data to be analyzed and the filtering method to be applied on dynamic marker trajectories are selected.

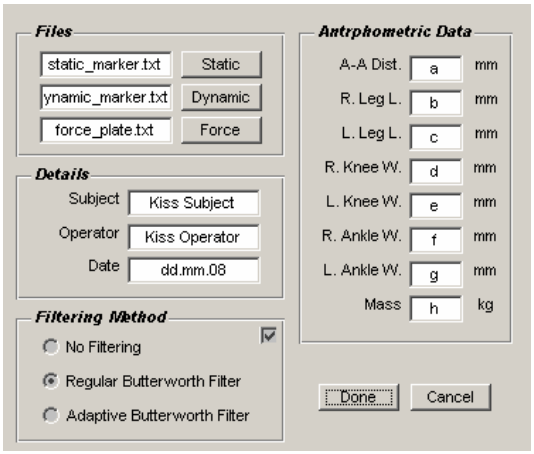

Figure 54. KissGaitM input window.

The second window is the main window of KissGaitM (Figure 55). As is done in Kiss-GAIT, the operator manually marks the gait events based on the visual information provided by the stick-man animation and ground reaction forces. With the gait events specified, KissGaitM can calculate and plot joint variables, which are joint angles, moments and powers. Sample plots are available in Appendix E. It

is also possible to see the time-distance parameters. Moreover, the code lets the user to save any variable such as marker trajectories, segment angular velocities, joint moments, etc. for further analysis.

One important property of KissGaitM is that it does not require to be compiled as it runs under MATLAB. This feature makes the code easily accessible, allowing modifications to be made according to user needs, thus enabling a flexible programming environment.

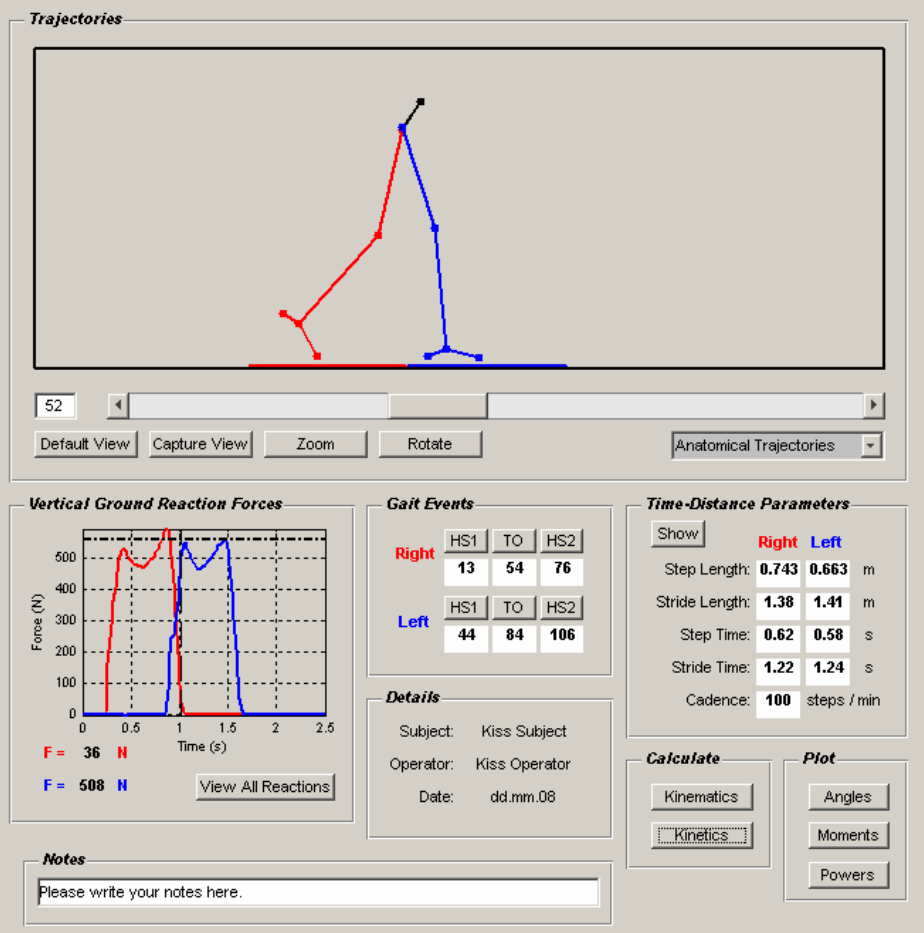

Figure 55. KissGaitM main window.

Figure 56 shows a simplified flowchart of KissGaitM. The code is based on the formulation given by Söylemez (2002), which is the area labelled as *Unmodified*.

Not to fill the text with repetitions, only a very brief account of this portion is given below.

Firstly, static shot data from 19 markers are manipulated so as to establish dynamic trial relationships between segment reference frames and marker trajectories. The process is initiated by constructing technical reference frames using positions of markers that are also present in dynamic trial. After centres of hip, knee and ankle joints are calculated with the help of markers that are not present in dynamic trial, anatomical reference frames are formed. Then, transformation matrices that define angular relationships between technical and anatomical reference frames for static shot are obtained. These constant matrices are assumed to be also valid during dynamic trial between technical and anatomical reference frames. Based on this key assumption, the second task is to construct anatomical reference frames that define orientations of segments with respect to the laboratory reference frame during the gait cycle. As is done with static shot data, marker positions (13 markers in this case) are used to construct technical reference frames. Mathematical representations of these technical frames are multiplied by the constant transformation matrices mentioned above to get anatomical reference frames. Joint angles can finally be calculated using the Hartenberg-Denavit (H-D) convention described in Chapter 3.

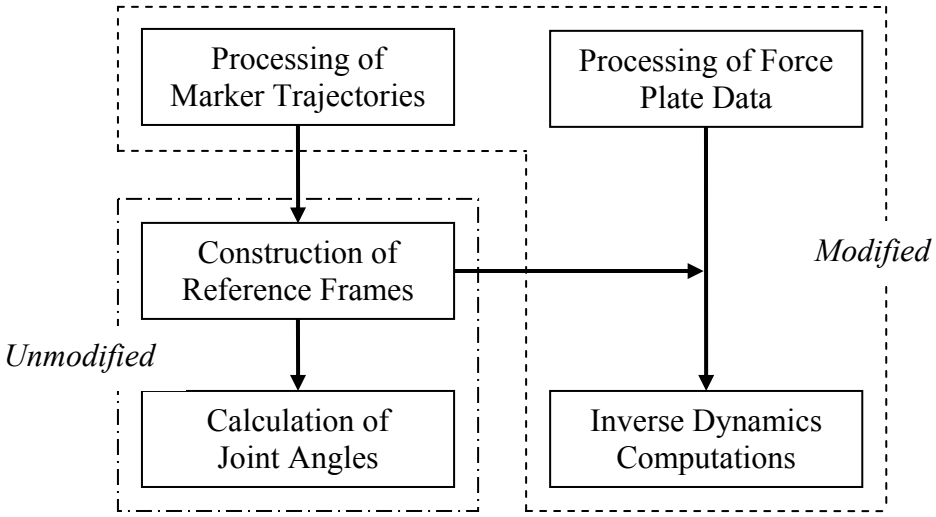

Figure 56. Flowchart of KissGaitM.

Components *Modified* by this new version of Kiss-GAIT are discussed below in detail.

6.1. Processing of Marker Trajectories

Unlike Kiss-GAIT, which applies a double smoothing process; one to raw marker trajectories and the other during the calculation of joint angles, KissGaitM avoids such redundancy by filtering only raw marker trajectories before any subsequent processing. The operator is free to choose between regular and adaptive Butterworth filtering, the default setting being the regular filter. The option of no filtering is also available in order to facilitate understanding as to how filtering affects final outputs.

In Table 4, default values of the filter parameters used by KissGaitM are given. These values are applied only to vertical marker trajectories and were determined based on the results of the previous chapter, also making use of test results performed on data from various gait trials. It is clear how the cut-off frequencies change in positive correlation with distance from the trunk; or in other words, in accordance with the expected frequency contents of trajectories during gait. All horizontal marker trajectories are smoothed by a regular Butterworth filter with a cut-off frequency of 3.2 Hz.

Table 4. Default filter parameters used by KissGaitM.

	Regular	**Adaptive**		
Marker	f_c	f_1	f_2	**Iter. #**
ASIS	4.0	-	-	-
Sacrum	4.0	-	-	-
Thigh	4.4	-	-	-
Knee	5.2	3.6	2.8	3
Shank	6.0	3.6	3.6	3
Ankle	7.2	3.2	6.4	3
Meta.	7.2	3.2	6.4	3

Figure 57 illustrates how filtering choice affects the trajectory of an ankle marker. Although it is not correct to evaluate filter performances in the zeroth derivative level, it is clearly seen in the close-up how the regular filter outperforms the adaptive one around the local maxima and how the adaptive filter smooths the motionless interval better than the regular one. This trade-off is more apparent in the acceleration plot. The adaptive filter underestimates the regions around 10^{th} and 75^{th} data points while it predicts zero acceleration values for the motionless interval as it should be.

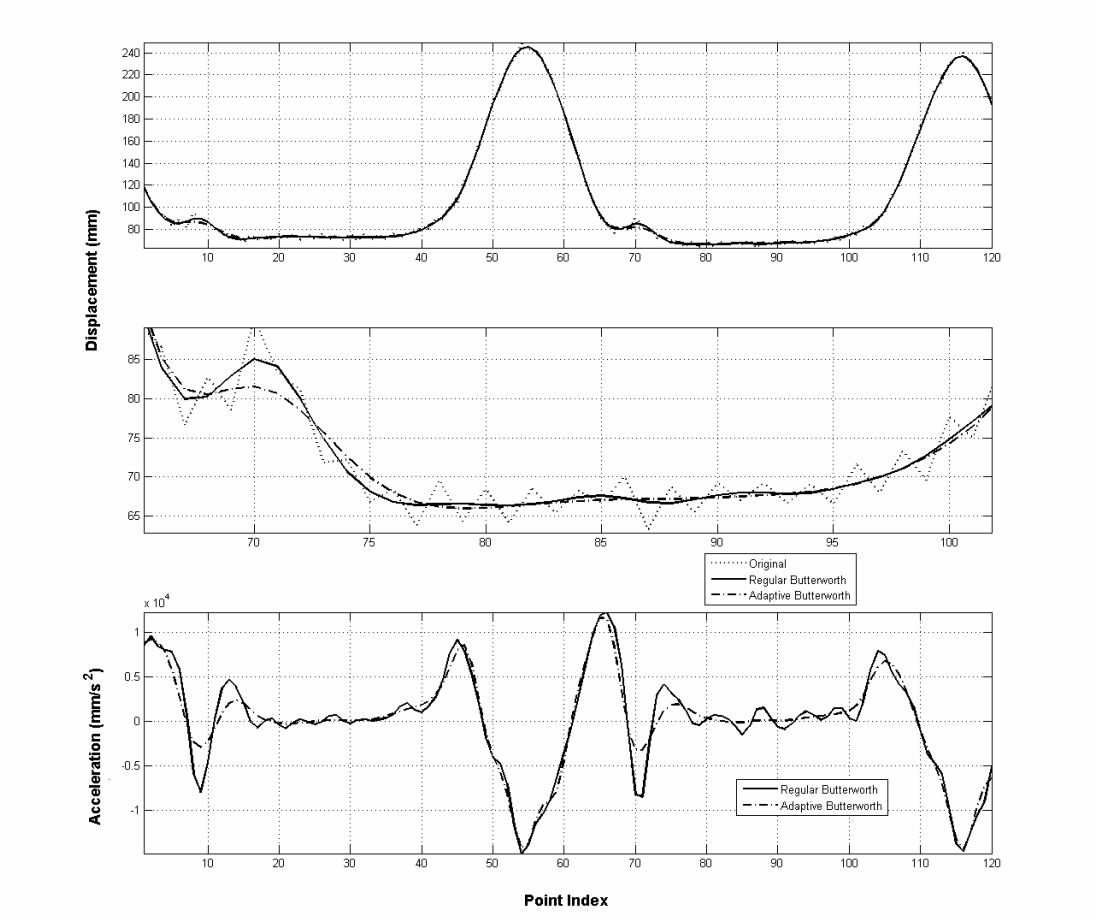

Figure 57. Variations of the displacement and acceleration signals of an ankle marker.

Judging from the overall patterns, it seems that the final decision could be in favour of the regular filter. Nonetheless, as demonstrated in the previous chapter, this is

only so for this specific marker trajectory or for gait trajectories in general. Therefore, the user is advised to be careful in filter selection when analysing other activities such as running or jumping.

6.2. Processing of Force Plate Data

The acquired force plate data must be processed before being used in kinetic calculations. There are three processes as described below.

6.2.1. Bias Removal

Outputs of the force plates involve constant biases, i.e. shifts in the vertical axis, due to calibration errors. No matter how small they are compared to maximum reaction values, they should be removed for better kinetic calculations.

Figure 58 shows a biased vertical reaction force. As seen in the zoomed interval, the reading is around -6 N whereas the actual value is exactly 0 because no forcing acts on the force plate. A manual processing can always compensate the shift; but, the compensation procedure can be made entirely automatic by employing histograms. In the figure, the histogram (with 500 bins) of the reaction force is also plotted. As seen, most of the data points in the signal are valued around -6 N, which indicates with high reliability the bias value. KissGaitM automatically removes biases in force plate signals by subtracting the constant values specified by this probabilistic technique.

6.2.2. Low-Pass Filtering

Even if it is true that outputs of the force plates are cleaner than marker trajectories and they do not undergo the differentiation process, they still might need to be filtered as a precaution against outliers in the signals.

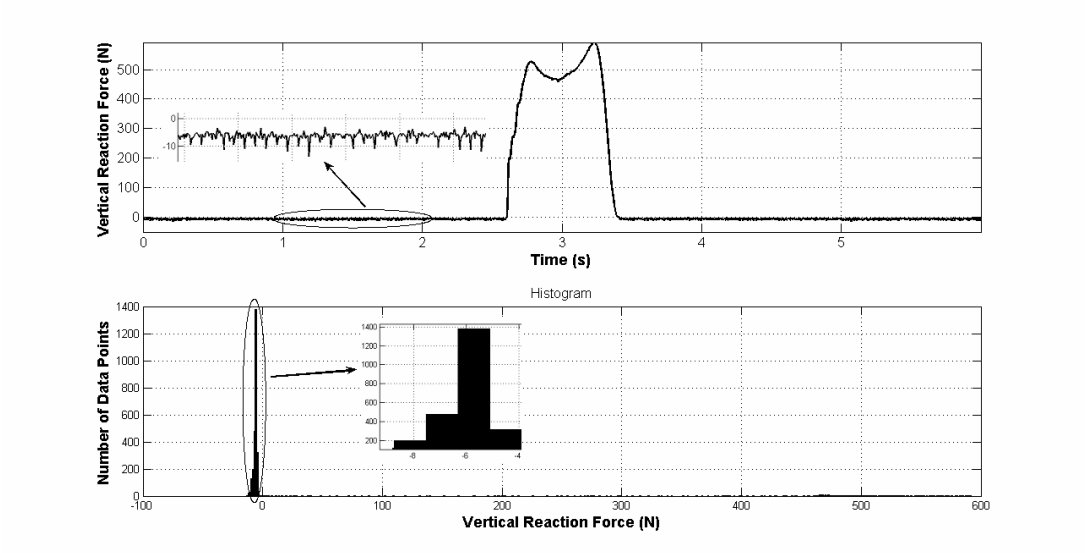

Figure 58. Time variation and histogram of a biased vertical ground reaction force signal.

Since force signals involve rapid transitions, a critically damped filter, which does not over- or undershoot signals, is expected to perform better on this kind of data than a Butterworth filter, which is underdamped (Robertson and Dowling, 2003[22]). Responses of the Butterworth and critically damped filters are plotted in Figure 59. It is seen that the output of the critically damped filter follows the original signal better.

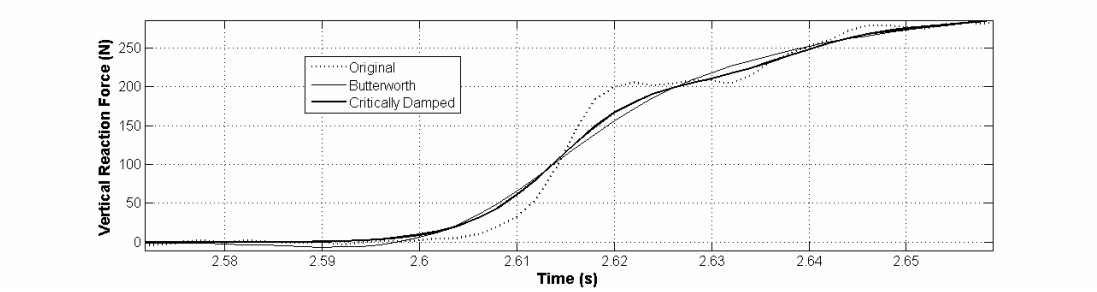

Figure 59. Performances of a Butterworth and a critically damped filter on a vertical ground reaction force signal.

[22] The authors state that a critically damped filter is weaker in noise suppression than a Butterworth filter of the same order and that the Butterworth filter might still be the better choice for data to be differentiated.

A second order critically damped digital low-pass filter (single dual pass) is coded in KissGaitM for smoothing of force plate data. The code calculates the filter coefficients as given by Robertson and Dowling (2003). The default cut-off frequency of the filter is 30 Hz, a value high enough not to cause any information loss as far as human gait is concerned.

6.2.3. Downsampling

Kiss-DAQ does not sample images and force plate signals at the same rate. As is the usual practice in gait analysis, marker trajectories are sampled at a lower rate than force plate signals are[23]. Therefore, ground reactions must be downsampled before continuing with kinetic calculations.

The downsampling procedure KissGaitM utilizes is as given below:

$$l = round\left(\frac{L-1}{c}+1\right),$$
$$i = \begin{bmatrix}1 & 2 & \dots & l\end{bmatrix},$$
$$j = round\left(\frac{L-1}{l-1}(i-1)+1\right),$$
$$r_i = R_j.$$

Here, L is the length of the original signal R and c is the ratio of sampling frequencies, which is greater than unity. After the length l of the downsampled signal r is calculated, j values corresponding to each i value can be computed. i^{th} sample of r then becomes j^{th} sample in R.

To give an example, when R has 100 data points and c is 10, the number of elements in r is calculated to be 11. Then, the sets of indexes become:

$$\begin{bmatrix} i \\ j \end{bmatrix} = \begin{bmatrix} 1 & 2 & 3 & 4 & 5 & 6 & 7 & 8 & 9 & 10 & 11 \\ 1 & 11 & 21 & 31 & 41 & 51 & 60 & 70 & 80 & 90 & 100 \end{bmatrix}.$$

It should be noted that the intervals over which the original and downsampled signals span may not be exactly equal, as in this case.

[23] Default sampling rates of cameras and force plates are 50 and 500 Hz, respectively.

6.3. Inverse Dynamics Computations

With known ground reactions, the solution of equations of motion is initiated from the most distal segment, recursively progressing up to adjacent segments until finally, the forces and moments acting on the desired joint are obtained.

6.3.1. Equations of Motion

The N-E equations of motion are (the derivation is given in Appendix C):

$$\Sigma\vec{F} = m\vec{a}_G,$$
$$\Sigma\vec{M}_G = \breve{J}_G \bullet \vec{\alpha} + \vec{\omega} \times \breve{J}_G \bullet \vec{\omega}.$$

The first equation defines how the sum of forces $\Sigma\vec{F}$ on a rigid body is calculated, knowing its mass *m* and the acceleration vector $\vec{a}_G$ of its centre of gravity. The second equation is the rotational extension of the first one. It says that if the angular velocity and acceleration vectors ($\vec{\omega}$ and $\vec{\alpha}$, respectively) of the body along with its inertia dyadic $\breve{J}_G$ about the centre of gravity are known, the sum of moments $\Sigma\vec{M}_G$ about the centre of gravity can be calculated.

The lower extremity of human body may be approximated as a series of rigid links connected to each other. Figure 60 shows the free-body diagram of such a link. The link is attached to proximal and distal links with joints located at both ends. $\vec{F}_p$ and $\vec{M}_p$, and, $\vec{F}_d$ and $\vec{M}_d$ denote the forces and moments acting on the proximal and distal joints, respectively while $m\vec{g}$ is the weight of the body. Vectors $\vec{r}_p$ and $\vec{r}_d$ respectively define the locations of the proximal and distal joints with respect to the centre of gravity *G*. The equations of motion can be written as:

$$\Sigma\vec{F} = \vec{F}_p + \vec{F}_d + m\vec{g} = m\vec{a}_G,$$
$$\Sigma\vec{M}_G = \vec{M}_p + \vec{r}_p \times \vec{F}_p + \vec{M}_d + \vec{r}_d \times \vec{F}_d = \breve{J}_G \bullet \vec{\alpha} + \vec{\omega} \times \breve{J}_G \bullet \vec{\omega}.$$

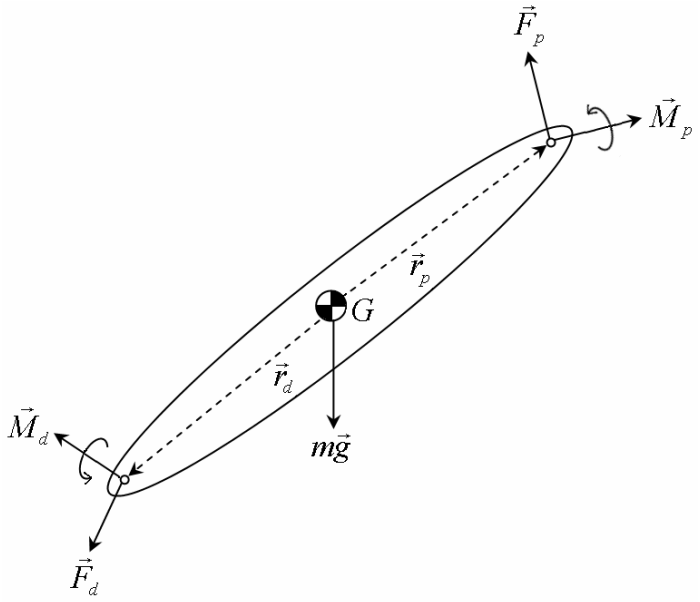

Figure 60. Free-body diagram of a body segment.

Assuming that only $\vec{F}_p$ and $\vec{M}_p$ are unknown, the equations may be rewritten as:

$$\vec{F}_p = m\left(\vec{a}_G - \vec{g}\right) + \vec{F}_d,$$
$$\vec{M}_p = \breve{J}_G \bullet \vec{\alpha} + \vec{\omega} \times \breve{J}_G \bullet \vec{\omega} - \vec{r}_p \times \vec{F}_p - \vec{M}_d - \vec{r}_d \times \vec{F}_d.$$

As stated above, inertial and kinematic quantities must be known before the equations of motion can be solved.

6.3.2. Calculation of BSIP

Kiss accounts for the inertial effects created by the shank and thigh segments while it assumes that mass of the foot is negligible[24]. Table 5 includes the constants for males and females used by KissGaitM for BSIP calculation (de Leva, 1996). Segment masses are expressed as percent fractions of total body mass while centre of gravity positions and radii of gyration are expressed as percent fractions of segment lengths. Here, the length of a segment is defined as the distance between its proximal and distal joints[25]. It should be noted that centres of gravity are closer to

[24] For slow gait, this approach is acceptable; however, it might be unjustifiable in case of fast gait (Woltring, 1985).

[25] Distance information is extracted from marker data.

proximal joints and when squared and multiplied with segment masses, frontal (x), transverse (y) and sagittal (z) radii of gyration form symmetric (no off-diagonal terms) inertia matrices about centres of gravity.

Table 5. BSIP estimation constants given as percents of body mass and segment lengths for males / females (de Leva, 1996).

	Mass	**cg Position**	**Sagittal Radius of Gyration**	**Frontal Radius of Gyration**	**Transverse Radius of Gyration**
Shank	4.33 / 4.81	43.95 / 43.52	25.1 / 26.7	24.6 / 26.3	10.2 / 9.2
Thigh	14.16 / 14.78	40.95 / 36.12	32.9 / 36.9	32.9 / 36.4	14.9 / 16.2

6.3.3. Calculation of Kinematic Quantities

For inverse dynamics calculations[26], the angular velocity and acceleration vectors ($\vec{\omega}$ and $\vec{\alpha}$, respectively) of the body along with the linear acceleration vector $\vec{a}_G$ of its centre of gravity are required. As none of these are directly measured, they have to be estimated using marker trajectories.

The transformation matrix between the inertial frame (the global or the laboratory frame) and a segment frame provides orientation (angular position) information of the segment the reference frame is attached to. The columns of this transformation matrix are the unit vectors of the segment frame as expressed in the global frame. Any vector quantity expressed in the segment frame can be transformed by the transformation matrix to its expression in the global frame. The relation between the angular velocity vector and the transformation matrix is given as:

$\tilde{\omega} = \dot{\hat{C}}\hat{C}^T$.

The equation above states that the skew-symmetric matrix $\tilde{\omega}$ of the angular velocity is obtained when the time derivative $\dot{\hat{C}}$ (the hat indicates a square matrix)

[26] The notation used here can be found in Özgören (2004).

of the transformation matrix $\hat{C}$ is multiplied by its transpose. The skew-symmetric, or cross product, matrix is defined as below:

$$\tilde{\omega} = \begin{bmatrix} 0 & -\omega_3 & \omega_2 \\ \omega_3 & 0 & -\omega_1 \\ -\omega_2 & \omega_1 & 0 \end{bmatrix}.$$

The expression for the angular velocity vector is then:

$$\bar{\omega} = \begin{bmatrix} \omega_1 & \omega_2 & \omega_3 \end{bmatrix}^T.$$

It is important here to notice that the over-bar indicates a column vector and ω_1, ω_2 and ω_3 are the components of the angular velocity vector as observed from the global frame. Now that the angular velocity is available, the angular acceleration is obtained simply by numerical differentiation:

$$\bar{\alpha} = \dot{\bar{\omega}}.$$

As for the linear acceleration vector $\vec{a}_G$, it is obtained by double numerical differentiation of the position vector of the centre of gravity. The position vector is obtained by linearly combining the positions of the proximal and distal joint centres, respectively denoted as $\vec{p}$ and $\vec{d}$. Hence, the expression of the acceleration vector of the centre of gravity as observed from the global frame is:

$$\bar{a}_G = (1-c)\ddot{\bar{p}} + c\ddot{\bar{d}}.$$

Constant *c* is found from Table 5. For instance, it takes the value of 0.4395 for the shank of a male subject.

It should finally be noted that the expression for the inertia dyadic $\breve{J}_G$ in the global frame is not constant due to the orientation difference between the global and anatomical reference frames. Since the equations of motion are solved in the global frame, the anatomical frame expression $\hat{J}_G$ of the inertia dyadic must be transformed into its equivalent in the global frame. The transformation is: $\hat{C}\hat{J}_G\hat{C}^T$. $\hat{J}_G$ is calculated using Table 5, which dictates that the inertia matrix is a diagonal

matrix. After the transformation; however, the inertia matrix is no longer diagonal unless the two frames are parallel.

6.3.4. Calculation of Kinetic Quantities

Vector forms of the equations of motion assume are as given below:

$$\bar{F}_p = m\left[(1-c)\ddot{\bar{p}} + c\ddot{\bar{d}} - \bar{g}\right] + \bar{F}_d,$$
$$\bar{M}_p = \hat{C}\hat{J}_G\hat{C}^T\bar{\alpha} + \tilde{\omega}\hat{C}\hat{J}_G\hat{C}^T\bar{\omega} - \tilde{r}_p\bar{F}_p - \bar{M}_d - \tilde{r}_d\bar{F}_d.$$

These equations yield a three element force and a three element moment acting on the distal joint, where the elements are expressed in the laboratory frame. $\bar{g}$ is taken to be $[0\ -9.81\ 0]^T$ m/s^2.

Accepting marker trajectories and force plate data as inputs, KissGaitM computes the forces and moments in ankle, knee and hip joints. As the foot segment is assumed to be massless, ankle joint forces are nothing but those that are exerted by the force plate. Ankle moments; however, are calculated by taking into account the distance between the centre of the force plate and the ankle joint centre as the moment arm. The ankle joint is the distal joint of the shank. Knowing the forces and moments at the distal joint, those at the proximal joint, which is the knee joint, can be calculated using the formulation presented above. The recursion continues for the thigh segment in the same manner. This time, the knee joint is the distal joint and the hip joint is the proximal one.

It should be underlined that moments produced by this algorithm are global reference frame representations of three dimensional vectors. These need to be converted into some form that is more meaningful from a clinical point of view. This purpose can be achieved by expressing the moments in anatomical reference frames, the relative angular motions of which are the actual cause behind the movement. Unit vectors defined by the H-D convention are natural candidates for such a representation. Lower extremity joint moments[27] (T_i) and unit vectors ($\vec{u}^{(i-1)}$) they act about are illustrated in Figure 61. One important point is that hip and knee

[27] The term torque might be a better choice; however, the clinical convention states otherwise.

joint moments are resolved in reference frames defined by the H-D convention whereas ankle joint moments are expressed in the orthogonal shank frame[28]. Accordingly, joint moments are calculated as:

$$T_i = \begin{cases} \vec{M}_{d,i} \bullet \vec{u}_3^{(i-1)} = \bar{M}_{d,i}^T \bar{u}_3^{(i-1)} \text{ for } i = 1,2,...,7 \\ \vec{M}_{d,i} \bullet \vec{u}_1^{(i-2)} = \bar{M}_{d,i}^T \bar{u}_1^{(i-2)} \text{ for } i = 8 \\ \vec{M}_{d,i} \bullet \vec{u}_2^{(i-3)} = \bar{M}_{d,i}^T \bar{u}_2^{(i-3)} \text{ for } i = 9 \end{cases} .$$

Here, $\vec{M}_{d,i}$ is the moment vector acting on the corresponding segment at its distal joint. More specifically, $\vec{M}_{d,i}$ is the moment exerted on the thigh by the pelvis for i = 1, 2, 3; it is the moment exerted on the shank by the thigh for i = 4, 5, 6; and the moment exerted on the foot by the shank for i = 7, 8, 9.

In this convention, right and left sides of the lower extremity are assigned reference frames which are directionally equivalent, i.e. their third unit vectors ($\vec{u}_3^{(0)}, \vec{u}_3^{(3)}, \vec{u}_3^{(6)}$) are directed towards (nearly) the same direction (+z) at all times. As a result, joint moments thus obtained may not be easy to interpret clinically. KissGaitM converts them into representations consistent with the literature (Schache and Baker, 2007). This conversion is explained for in Table 6. It is seen that sagittal plane (extension / flexion) moments have the same sign while frontal (abduction / valgus / inversion) and transverse (internal rotation) plane moments have opposite signs.

[28] This is because of the fact that Kiss does not define a H-D transformation between the shank and the foot.

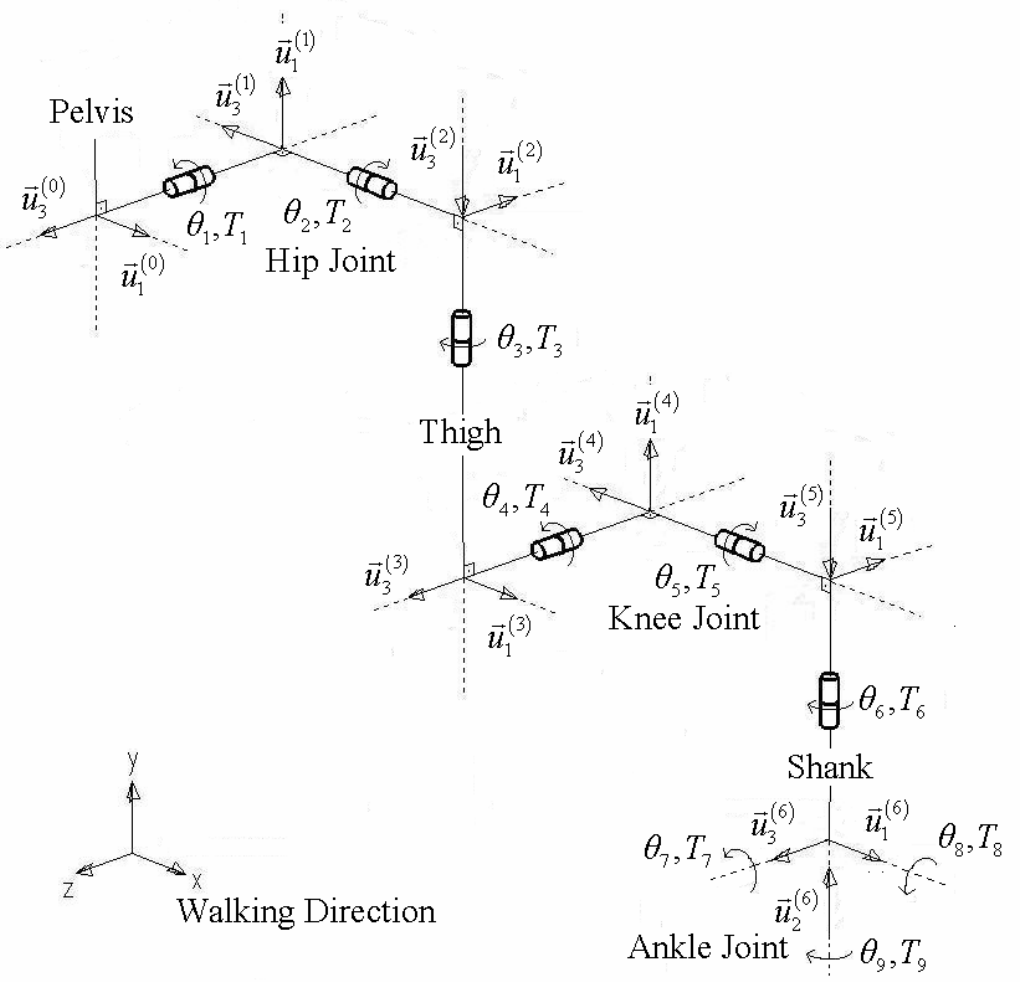

Figure 61. Kinetic model of the lower extremity.

Table 6. Clinical interpretation of joint moments.

Moment	Right	Left
Hip Extension	$-T_1$	$-T_1$
Hip Abduction	T_2	$-T_2$
Hip Internal Rotation	$-T_3$	T_3
Knee Extension	T_4	T_4
Knee Valgus	T_5	$-T_5$
Knee Internal Rotation	$-T_6$	T_6
Ankle Plantarflexion	$-T_7$	$-T_7$
Ankle Inversion	T_8	$-T_8$
Ankle Internal Rotation	T_9	$-T_9$

The last set of kinetic variables KissGaitM calculates is joint powers, which provide additional information on how joints are actuated. Power variation in a joint throughout the gait cycle can be calculated by a simple dot product of the moment vector acting on the joint and the relative angular velocity vector between the two segments connected by the joint. However, such a calculation yields total joint power instead of individual components corresponding to axes defined by the H-D convention. Denoting the relative angular velocity with $\Delta\vec{\omega}$, which is distal segment velocity minus proximal segment velocity, expressions for the joint powers (P_i) that are consistent with the moment definitions become:

$$P_i = \begin{cases} T_i \Delta\vec{\omega}_i \bullet \vec{u}_3^{(i-1)} = T_i \Delta\overline{\omega}_i^T \overline{u}_3^{(i-1)} \text{ for } i = 1,2,...,7 \\ T_i \Delta\vec{\omega}_i \bullet \vec{u}_3^{(i-2)} = T_i \Delta\overline{\omega}_i^T \overline{u}_3^{(i-2)} \text{ for } i = 8 \\ T_i \Delta\vec{\omega}_i \bullet \vec{u}_3^{(i-3)} = T_i \Delta\overline{\omega}_i^T \overline{u}_3^{(i-3)} \text{ for } i = 9 \end{cases} .$$

In the equations above, $\vec{\omega}_i \bullet \vec{u}_3^{(i-1)}$ (i = 1, 2, …, 6) is nothing but the derivative $\dot{\theta}_i$ of the H-D joint variable θ_i. A positive value indicates mechanical power generation while a negative one indicates mechanical power consumption.

6.4. Kinematic and Kinetic Results Produced by KissGaitM

To assess the reliability of its results, KissGaitM was tested on gait data acquired in METU Gait Analysis Laboratory. Caused by unavailability of additional sources that allow a complete analysis[29], only 9 data sets were used. The data sets belong to 3 healthy male subjects, each of which were asked 3 times to walk on the walkway at self selected speeds. The mean height and mass of the subjects are respectively 180.3 cm and 70.3 kg, the mean age being unknown; but, likely to be not more than 25. Calculations were performed as explained above. Each sub-figure in the figures below contains information from 9 x 2 (right and left sides) moment histories.

[29] There are many data sets available which allow only kinematic analysis due to synchronization problems between cameras and force plates.

6.4.1. Joint Angles

Curves of mean and standard deviation values of joint angles are presented in Figure 62. These are H-D joint variables rather than their clinical equivalents. Such a presentation is thought to be more convenient in this text since joint powers are defined in terms of rates of these angles. It is seen that only the sagittal plane angles θ_1, θ_4, θ_7 and the frontal plane hip joint angle θ_2 exhibit consistent patterns for all subjects. The remaining angles either display entirely inconsistent patterns around toe-off (θ_5, θ_8, θ_9) or their standard deviations are at unacceptable levels (θ_3, θ_6). Only the angles that possess consistent patterns throughout the entire gait cycle (θ_1, θ_4, θ_7, θ_2) are in harmony with data in the literature (Kadaba et al., 1990). Kinematic results provided here bolster the conclusions arrived by Güler (1998): angles in the frontal (except θ_2) and transverse planes are more prone to errors than sagittal plane angles, the reason probably being their relatively low dynamic ranges. In other words, the signal-to-noise ratio is lower for these angles.

It is true that the joint angle curves plotted above are smoother than normal outputs of KissGaitM. The reason for this appearance is the averaging of data among subjects, which acts as a low-pass filter. An example of actual angle plots produced by the program KissGaitM is provided in Appendix E.

6.4.2. Joint Moments

The obtained joint moment patterns are plotted in Figure 63. The curves present the means and standard deviations of joint moment histories in each of the sagittal, frontal and transverse planes.

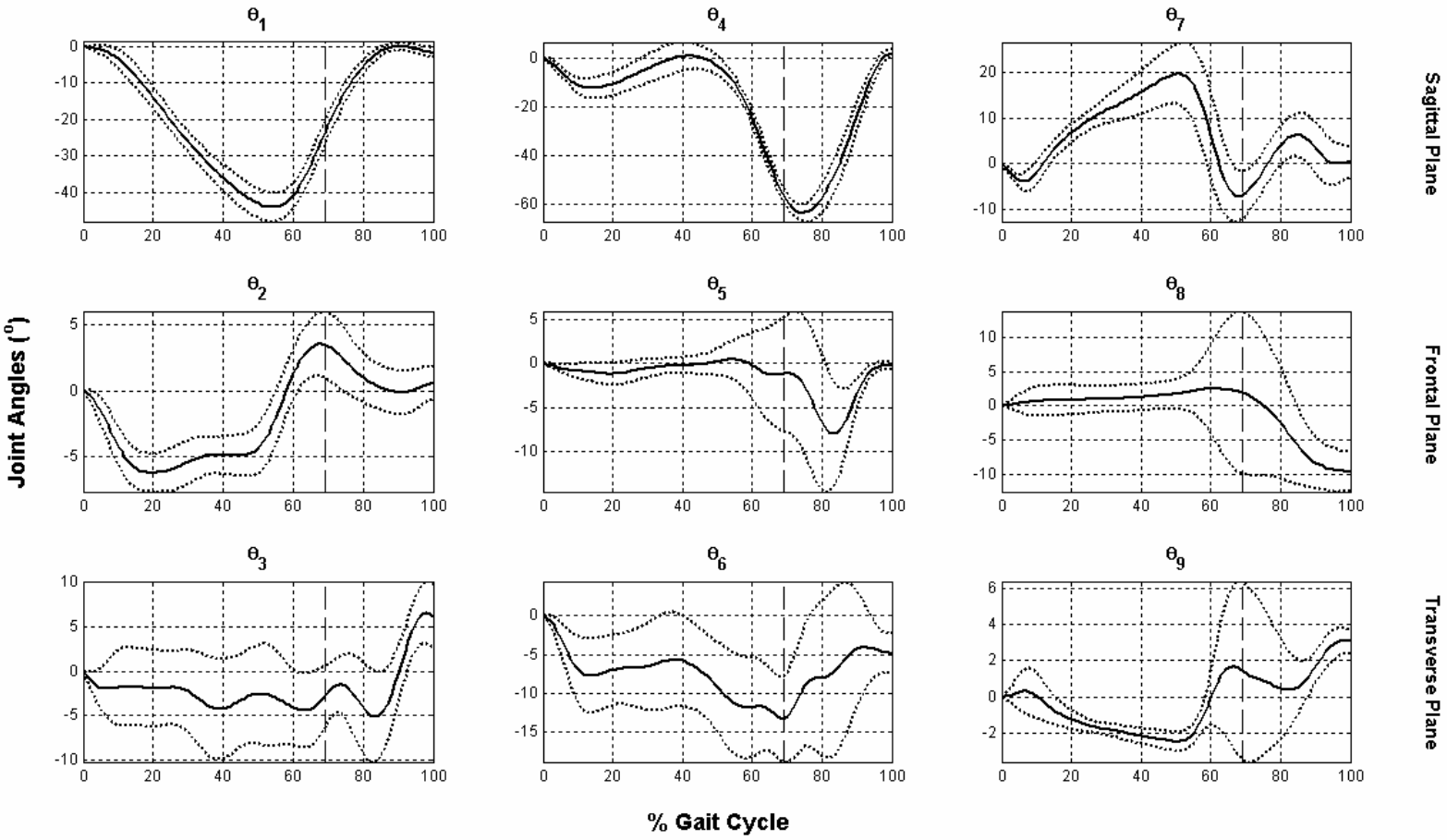

Figure 62. Means (solid lines) and standard deviations (dotted lines) of joint angles produced by KissGaitM.

It is immediately striking that standard deviations tend to disappear after toe-off. This is a clear indication of the fact that individual differences drop to a minimum when the foot leaves the ground. Therefore, investigation of stance phase kinetics may be claimed to contain more valuable information as far as normal human gait is concerned. It is also true that almost all standard deviations reach their maximal values approximately at the end of the first half of the gait cycle. This implies that individual differences are pronounced the most when the foot initiates the process of leaving the ground. This point in the gait cycle directly corresponds to the second local maximum of the vertical ground reaction force (Figure 64).

Moment results presented here are consistent with the literature (Chester and Wrigley, 2007; Eng and Winter, 1995; Liu and Lockhart, 2006; Schache and Baker, 2007) except for the swing phase. Slight inconsistencies in this phase of gait are directly attributed to the assumption in Kiss that the foot segment is massless[30]. Among all results, only the ankle inversion moment displays some strange behaviour; it is clearly seen that all standard deviations except that of the ankle inversion moment follow their mean curves within reasonable bounds. As shown by Schache and Baker (2007), this is the result of expressing the ankle inversion moment in the proximal segment (the shank) anatomical reference frame. If the transformation matrix between the shank and foot segments were defined using the H-D convention, it would then be possible to obtain consistent results for the ankle inversion moment. Plantarflexion and internal rotation moments in the ankle joint are also expressed in the shank reference frame; however, they characteristically do not exhibit inconsistent variations (Schache and Baker, 2007).

[30] Visual comparison with literature data indeed reveals that this assumption does not lead to intolerably adverse effects as long as the researcher is aware of it.

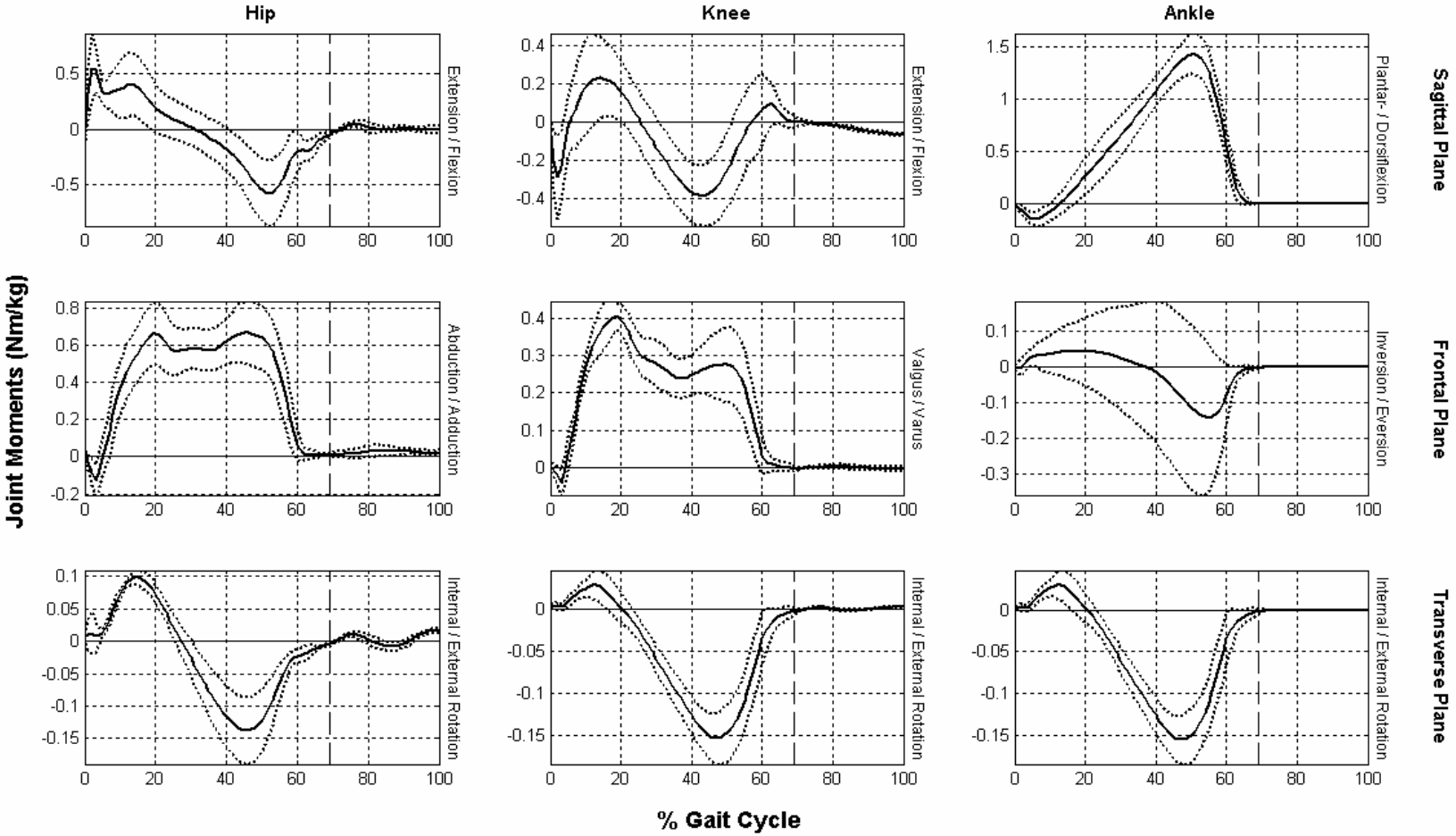

Figure 63. Means (solid lines) and standard deviations (dotted lines) of joint moments produced by KissGaitM.

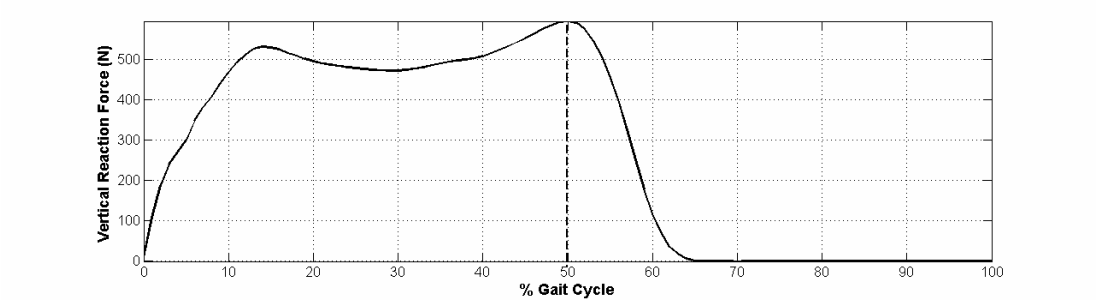

Figure 64. Typical vertical ground reaction force distribution over the gait cycle.

One final note about the joint moment curves plotted above is that they are considerably smooth. It should not be concluded that KissGaitM is able to produce such smooth patterns; the reason for this appearance is, again, the averaging process among subjects. An example of actual moment outputs of KissGaitM is provided in Appendix E.

6.4.3. Joint Powers

The mean and standard deviation curves of joint powers produced by KissGaitM are given in Figure 65.

As seen, power standard deviations decrease after toe-off, consistent with those of joint moment curves. Before toe-off; however, they tend to deviate from mean curves more than moments do. While the deviations for ankle plantarflexion and hip abduction are at tolerable levels, they exceed visual tolerance limits for hip extension, and become disturbing for knee extension. The immediate conclusion should not be that Kiss, and consequently KissGaitM, cannot produce meaningful joint power results. Even with few experimental data sets, the patterns exhibit consistency with power curves from the literature (Eng and Winter, 1995; Vardaxis et al., 1998) except for, again, the swing phase. Considering that literature data show some visible discrepancy among themselves, the results presented here may be said to be acceptable. Nonetheless, care must be taken when interpreting joint power curves produced by KissGaitM.

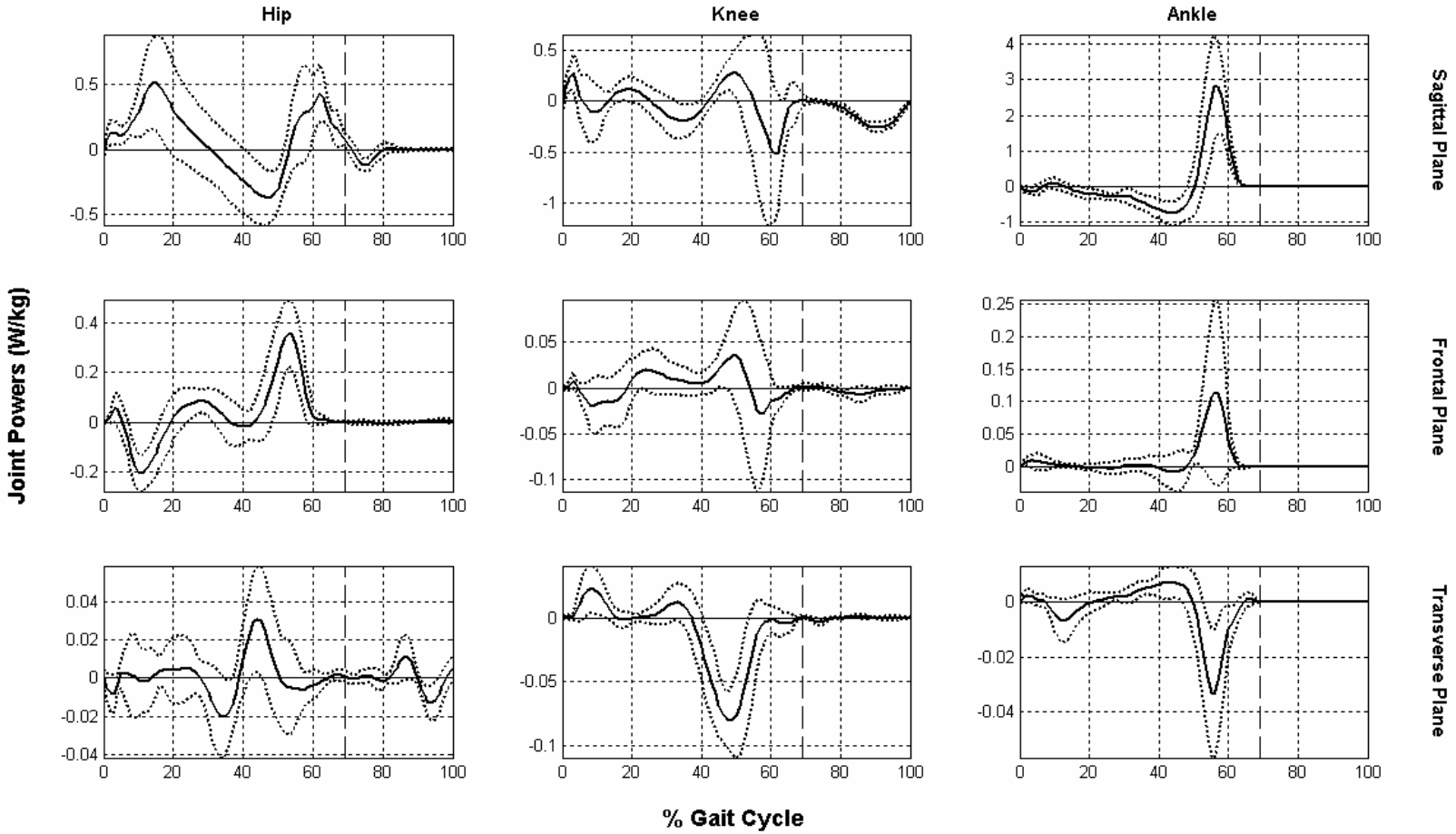

Figure 65. Means (solid lines) and standard deviations (dotted lines) of joint powers produced by KissGaitM.

Like the angle and moment patterns above, the power curves vary quite smoothly. An example of actual power outputs of KissGaitM is provided in Appendix E.

6.5. Sensitivity of Kinetic Results to BSIP Estimation and Filtering Methods

Valuable insight into what role BSIP estimation methods play in kinetic estimations might be gained by carrying out an inverse dynamics analysis routine where segment masses are set to zero, and than to compare the results with those of another routine where BSIP are estimated.

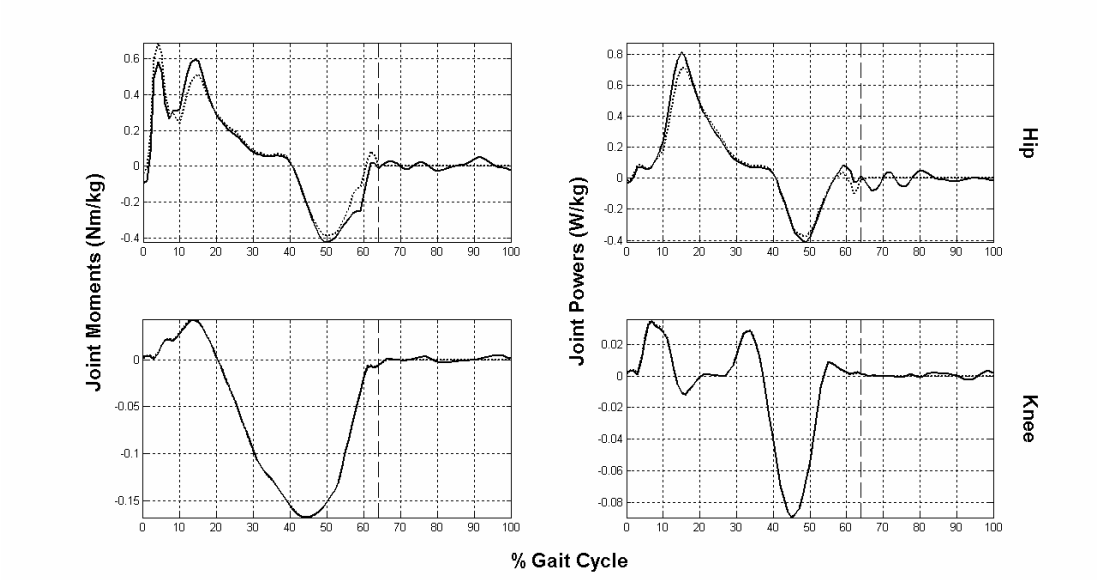

Figure 66. Sagittal plane joint moments and powers calculated by including (solid lines) and excluding (dotted lines) inertial effects.

Such a comparison is given below. Figure 66 shows a subject's sagittal plane joint moments and powers estimated with inertial effects are both included and excluded. The figure does not contain ankle joint kinetic variables since the foot is already assumed massless in Kiss. Apart from the natural fact that all kinetic variables during the swing phase are calculated to be zero by the latter routine, it is seen that discrepancies are not distinguishable for the knee joint, which is somewhat

surprising. There are, however, visible deviations in the patterns for the hip joint. The immediate conclusion is certainly not that static analysis is sufficient. Solving static equilibrium equations may only be justified when the gait speed is so slow that inertial effects are safely neglected. The presented results only imply that accuracy needed in BSIP estimations might not be critical for gait analysis. Of course, the condition is that the estimation technique produces reasonable estimates.

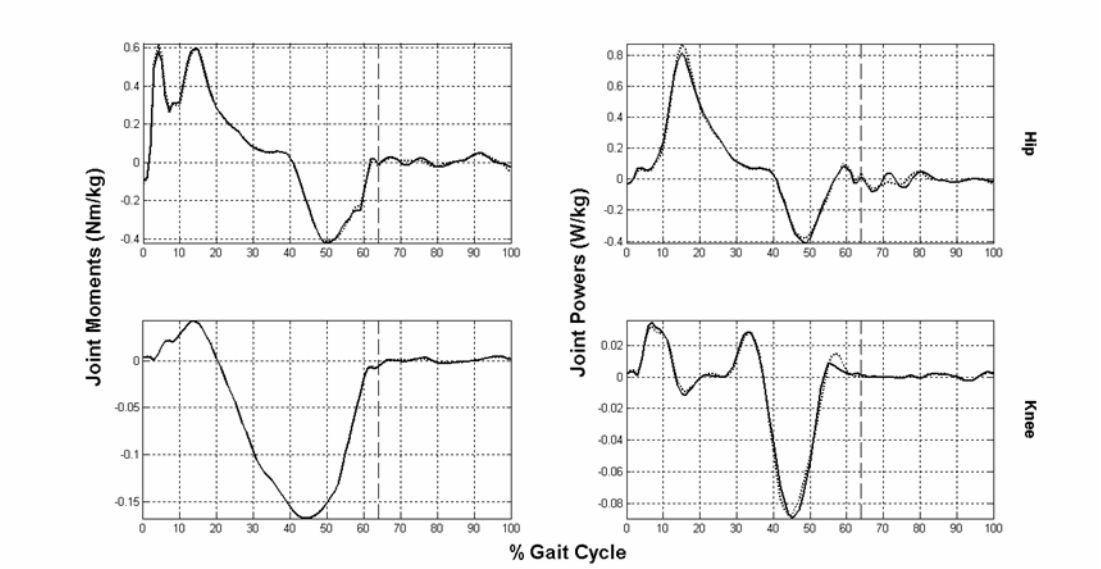

Figure 67. Resulting sagittal plane joint moments and powers after regular filtering (solid lines) and adaptive filtering (dotted lines).

Performance difference, demonstrated in the previous chapter, between the regular and adaptive filters is not effective in inverse dynamics calculations. Figure 67 clearly illustrates this fact. Moment and power results derived after regular and adaptive filtering of marker data yielded results with no appreciable differences. This originates from the dominancy of ground reactions in human gait, which is further evidenced by the fact that static analysis results only fail in the hip. It can be concluded that the choice of filtering method is not critical for kinetic analysis of normal human gait provided that sufficient noise suppression is achieved. However, when jerky, pathological gait is to be analyzed, the adaptive Butterworth filter might prove its usefulness.

6.6. Comparison of Kinetic Results between KissGaitM and Kiss-GAIT

The same gait data, kinetic analysis results of which as produced by KissGaitM are presented above, were analyzed using Kiss-GAIT. In Figure 68, joint moment results of both tools are plotted, where the ankle inversion moment is missing because it is not calculated by Kiss-GAIT. The resemblance of the curves suggests that there is negligible difference between the outputs. Moreover, deviations between the results increase after toe-off since Kiss-GAIT does not perform bias removal on force plate data.

Acceptable differences in joint moment patterns disappear when it comes to joint power curves as seen in Figure 69, where only sagittal plane and the hip frontal plane power curves are plotted as only these are calculated by Kiss-GAIT. There are significant deviations between the results of the two gait analysis tools. While sagittal plane powers show some harmony, the frontal plane hip moment results are only vaguely related.

Employment of different BSIP estimation techniques and downsampling procedures of force plate data and probably a few more unknown factors are certainly effective in the deviations of moment and power patterns presented above. Besides all these, the fact that power results are not consistent while moment results imply the existence of a crucial factor: angular rates calculated by the programs unquestionably differ. Figure 70 exhibits this phenomenon.

As shown in Chapter 3, smoothing and differentiation routines of Kiss-GAIT are unreliable; joint angles and rates are not even consistent within themselves. Hence, results, especially power results, as presented by KissGaitM are likely to be more accurate.

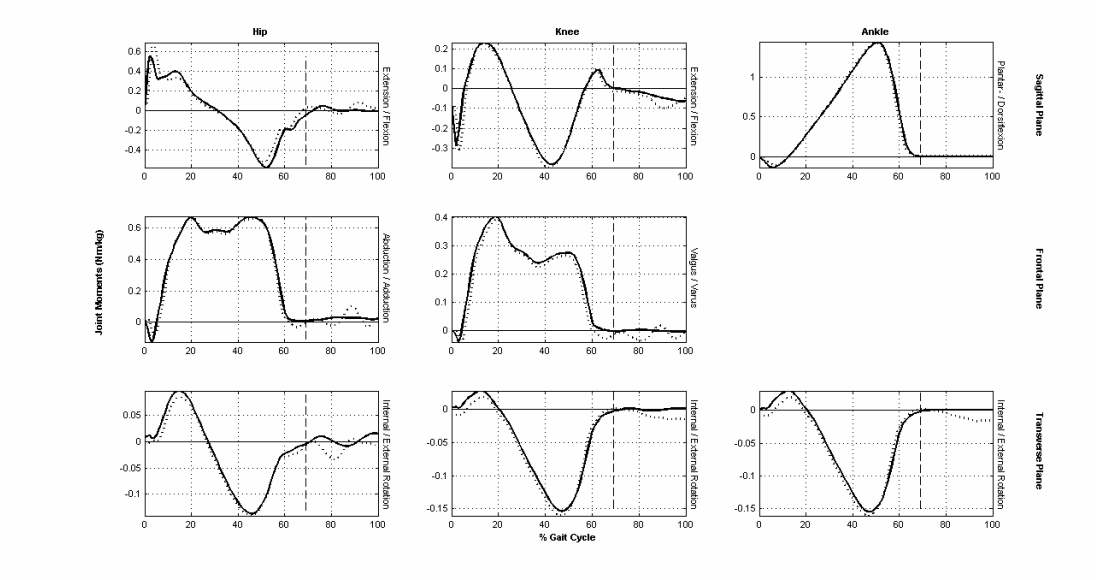

Figure 68. Joint moment outputs of KissGaitM (solid lines) and Kiss-GAIT (dotted lines).

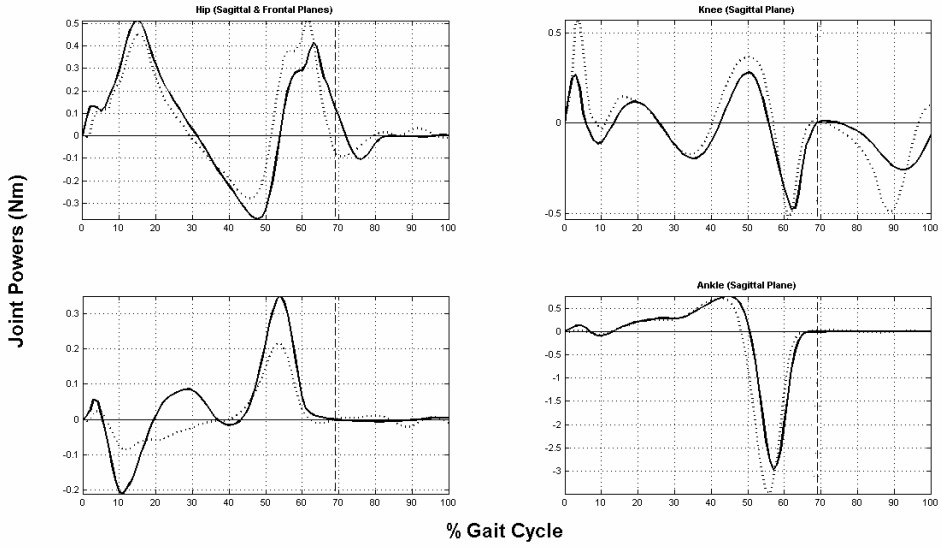

Figure 69. Joint power outputs of KissGaitM (solid lines) and Kiss-GAIT (dotted lines).

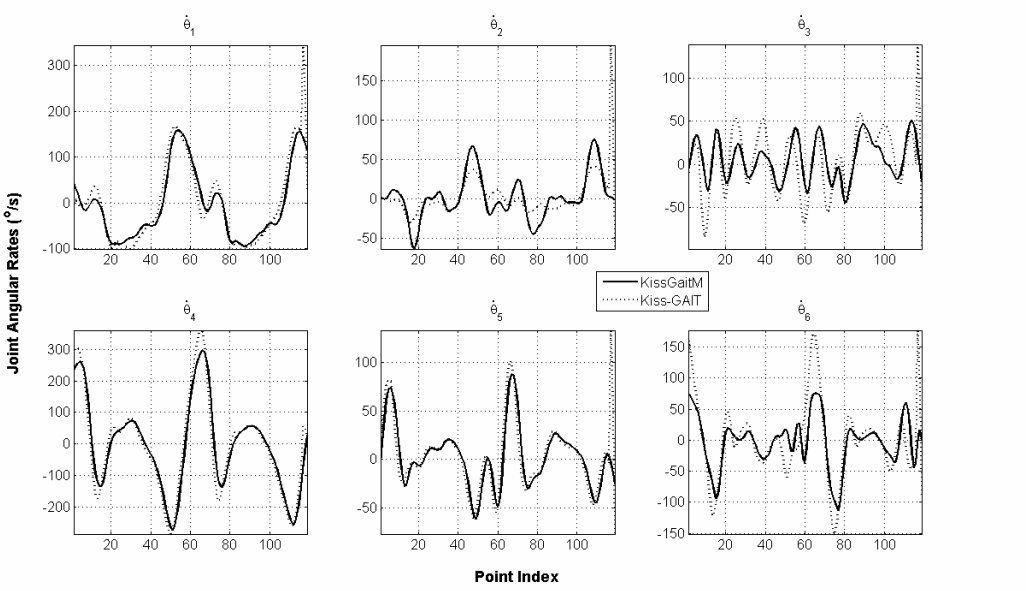

Figure 70. Joint angular rates as calculated by KissGaitM (solid lines) and Kiss-GAIT (dotted lines).

CHAPTER 7

DISCUSSIONS AND CONCLUSIONS

7.1. General Remarks

This thesis work provides an assessment of kinetic analysis capabilities of the METU Gait Analysis System and suggests several software based improvements, which are finally implemented in the developed gait analysis program named KissGaitM.

The work is composed of two main parts the first one of which focuses on the second order Butterworth filter, which, owing to the acceptable quality of its outputs, has been widely utilized in biomechanical applications. Proper filtering of experimental data is an essential process especially if subsequent differentiation is to follow. Judging from a gait analysis point of view, it can easily be concluded for normal gait that owing to dominancy of ground reactions, filter performance is not a critical factor for final kinetic results, provided that outputs of a selected smoothing and differentiation technique remains within reasonable bounds; that is, it should be guaranteed that no harmful amount of noise leaks to derivatives. The fair performance of the Butterworth digital filter in smoothing noisy gait marker data is demonstrated in this text. Nonetheless, such a conclusion is not possible to uphold for other applications such as running or jumping that have significantly varying frequency contents. Consideration of activities other than gait may seem strange, especially in a work committed to gait analysis. However, it should be noted that results in this study indicate that the regular Butterworth filter is likely to be unable to process gait signals that have pronounced impact intervals. It is not uncommon in a gait analysis laboratory to conduct experiments in which data from jerky, pathological gait are examined or in which subjects are instructed to walk faster

than their normal gait for any reason. Such cases necessitate usage of advanced tools that can handle non-stationarities inherent in the signals. Being aware of this fact, the Butterworth filter was modified during the course of the study. The modified version is an adaptive formulation which adjusts filter coefficients based on the local frequency content of the signal being processed. This work confirms that the adaptive formulation almost always performs better than the regular formulation. The performance enhancement is due to the adaptive cut-off frequency distribution, which is obtained through fusion of information from first and second derivative levels. Nonetheless, it is true that the adaptive filter does not all the time yield completely satisfying outputs. As demonstrated, it tends to produce oscillations when data involve extended acceleration intervals. It is convenient to repeat here that some other, superior criterion for calculating cut-off frequencies is likely to improve the performance of the adaptive filter. The criterion presented in this text is sufficient to give clues as to how powerful the concept of adaptively using cut-off frequencies of the Butterworth filter is. This issue is advised to be further investigated to see whether any other criterion is able to outperform the current one, which already yields impressive results.

The second part of the thesis is essentially related to the reformulation of the inverse dynamics algorithm of Kiss. As known, the N-E equations of motion need to be fed with kinematic variables, a task which Kiss-GAIT realizes by adopting the recursive approach of forward progression of kinematics[31]. This approach is suitable for robot manipulators with numerous components; however, it is hardly appropriate for calculating kinematic variables of lower extremity. This state of inappropriateness does not mean that the formulation leads to incorrect results. Rather, it stems from the fact that it is an indirect approach and the corresponding computer code is in a form which may not be easily interpreted by someone who is not acquainted with conventions used in robotics. As a result, there is a non-recursive kinematic formulation present in KissGaitM which calculates kinematic variables directly from marker data without firstly obtaining joint angles. There are some other improvements in the calculation routine the most important of which is the

[31] A recursive kinematic formulation is not the prerequisite of a recursive N-E formulation.

implementation of a consistent smoothing and differentiation algorithm. Kiss-GAIT uses an unjustified dual smoothing process; and furthermore, it introduces artificial temporal shifts in calculated derivatives. Such incompatibility of kinematic variables is directly reflected to calculated kinetic variables, especially to joint powers which are obtained by multiplication of joint moments with angular rates. The digital Butterworth filter, regular or adaptive, is a suitable tool for noise suppression purposes. Naturally, KissGaitM is equipped with a smoothing and differentiation algorithm that uses second order Butterworth filters along with subsequent application of numerical differentiation. The last modification for better kinetic results is how force plate data are processed. In addition to the required downsampling process, bias removal and filtering processes are applied to ground reaction signals by KissGaitM so as to improve their reliability.

The presented kinetic results of KissGaitM are in general agreement with data from the literature. Especially, when joint moment results are evaluated, it can readily be concluded that outputs (tracked marker trajectories and measured ground reactions) of Kiss-DAQ as accepted by KissGaitM are of sufficient quality. However, it is seen that kinematic results are far from being satisfactory. This unquestionably implies problems related to processing of acquired marker trajectories or to trajectories themselves. Either case is bound to lead to poor kinematic accuracy. The reason for acceptable moment patterns in the presence of low quality kinematic data is nothing but the dominancy of ground reactions in normal human gait, which is illustrated by performing kinetic analyses with and without inertial effects included. The fact that no significant deviations are observed between the cases is a clear evidence of ground reaction dominancy. As for joint power results, some other point of view should be adopted when assessing them. Power patterns in the literature show variations between studies, unlike moment patterns. This may imply that normative power patterns do not exist, which is somewhat unlikely. Another explanation, which is more likely, is that powers are more sensitive to estimated kinematic variables than moments. It should be expected that extents of systematic and non-systematic errors that contaminate motion data captured by different systems are different; which, in turn, severely affects estimated kinematic variables,

especially in first and second derivative levels. Noting that joint power is defined as joint moment multiplied by joint velocity, it would not be unexpected that accuracy in powers does not match accuracy in moments. In the light of the discussion above, it can be concluded that joint moment outputs of KissGaitM are expected to be reliable while its joint power outputs should be approached with care.

7.2. Suggestions for Further Research

The phenomenon of the presence of unreliable kinematic results of Kiss in frontal and transverse planes still remains inexplicable after this thesis study. Expecting consistent results, Kafalı (2007) found significant deviations in kinematic quantities when obtained through different analysis protocols and using different hip joint centre estimation methods. Along with conclusions of Güler (1998) about low signal-to-noise ratios preventing angles in frontal and transverse planes from being correctly estimated, this implies that kinematic results are sensitive also to analysis methodology as well as to accuracy of marker trajectories. Consequently, any error caused by incompatible marker placement is expected to propagate into kinematic results. A thorough investigation of the issue is required. A couple of suggestions on what can be done so as to gain insight into the problem are presented below:

- Several tests may be conducted using apparatus that to some extent simulates relative rotations of lower body segments. Calculation of joint angles via captured marker coordinates needs to replicate the known rotation angles in this case. A simple robot arm or a multi-axis turn table can be utilized for the purpose. It should be noted that such tests would be free of skin artefacts.
- Gait trials that involve direct gyro measurement of angular velocities of body segments would be extremely useful for validation of angular velocity results derived from marker data.

The kinetic results of the system will certainly be improved if the following are put into practice:

- Compared to kinetic patterns from discrete trials, it is shown in this work that smoother patterns are obtained when data are averaged among subjects.

A similar effect can be achieved for a single gait trial with two couples of force plates instead of one couple. This way, more accurate, and consequently smoother, results are guaranteed.

- This work shows the assumption of the negligibility of inertial effects of the foot segment to be acceptably valid for analysis of normal gait. This assumption; however, does not provide oversimplification in the analysis routine. Considering that it is likely to come across cases (i.e. pathological or fast gait) where the assumption fails, it is suggested that the foot segment be not bypassed when performing kinetic calculations.

Evaluation of marker tracking capabilities of Kiss was performed previously (Karpat, 2000). The corresponding study also contains results of free-falling marker experiments. The aim of such experiments is to find out whether the gravitational acceleration can be correctly estimated from marker data. However, if a second order polynomial is fitted to a marker trajectory, as is presented in the mentioned study, the data happens to be forced into the correct mathematical form. It is therefore not surprising for such cases that reasonable acceleration estimates are obtained. A superior way to assess both the tracking accuracy and the quality of signal processing (smoothing and differentiation) algorithms is to record accelerations of tracked markers that perform predetermined or random movements. This can be done by attaching a marker to an accelerometer unit, which might be a commercial product. As for the problem of synchronization of the displacement and acceleration signals, it can be overcome by having the marker and the accelerometer unit to start from rest.

REFERENCES

Afşar, H., 2001. Evaluation and compensation of soft tissue movement artefacts for the KISS gait analysis system. M.Sc. thesis, Middle East Technical University, Ankara, Turkey.

Angeloni, C., Riley, P.O., Krebs, D.E., 1994. Frequency content of whole body gait kinematic data. IEEE Transactions on Rehabilitation Engineering 2, 40–46.

Alonso, F.J., Del Castillo, J.M., Pintado, P., 2005a. Application of singular spectrum analysis to the smoothing of raw kinematic signals. Journal of Biomechanics 38, 1085–1092.

Alonso, F.J., Pintado, P., Del Castillo, J.M., 2005b. Filtering of kinematic signals using the Hodrick–Prescott filter. Journal of Applied Biomechanics 21, 271–285.

Best, R., Begg, R., 2006. Overview of movement analysis and gait features. In: Begg, R., Palaniswami (Eds.), Computational Intelligence for Movement Sciences: Neural Networks and Other Emerging Techniques, Idea Group, pp. 1–69.

Butterworth, S., 1930. On the theory of filter amplifiers. Experimental Wireless & The Wireless Engineer 7, 536–541.

Bjørnstrup, J., 1995. Estimation of human body segment parameters – Historical background. Not submitted anywhere.

Cahouët, V., Luc, M., Amarantini, D., 2002. Static optimal estimation of joint accelerations for inverse dynamics problem solution. Journal of Biomechanics 35, 1507–1513.

Capello, A., Palombara, P.F.L., Leardini, A., 1996. Optimization and smoothing techniques in movement analysis. International Journal of Bio–Medical Computing 41, 137–151.

Cappozzo, A., Berme, N., 1990. Subject–specific segmental inertia parameter determination – a survey of current methods. In: Berme, N., Cappozzo, A. (Eds.), Biomechanics of Human Movement: Applications in Rehabilitation, Sports and Ergonomics. Bertec, Ohio, pp. 179–185.

Civek, E., 2006. Comparison of kinematic results between METU-KISS & Ankara University-Vicon gait analysis systems. M.Sc. thesis, Middle East Technical University, Ankara, Turkey.

Chapra, S.C., Canale, R.P, 2002. Numerical Methods for Engineers. McGraw-Hill, New York.

Chester, V.L., Wrigley, A.T., 2007. The identification of age-related differences in kinetic gait parameters using principal component analysis. Clinical Biomechanics, In press.

Cooley, J.W., Tukey, J.W., 1964. An algorithm for the machine calculation of complex Fourier series. Mathematics of Computation 19, 297–301.

Craven, P., Wahba, G., 1979. Smoothing noisy data with spline functions. Numerische Mathematik 31, 377–403.

D'Amico, M., Ferrigno, G., 1990. Technique for the evaluation of derivatives from noisy biomechanical displacement data using a model–based bandwidth–selection procedure. Medical & Biological Engineering & Computing 28, Pages 407–415.

Dariush, B., Hemami, H., Parnianpour, M., 2001. Multi–modal analysis of human motion from external measurements. Journal of Dynamic Systems, Measurement, and Control 123, 272–278.

de Leva, P., 1996. Adjustments to Zatsiorsky-Seluyanov's segment inertia parameters. Journal of Biomechanics 29, 1223–1230.

Derrick, T.R., 1998. Circular continuity of non–periodic data. In: Proceedings of the North American Congress on Biomechanics. University of Waterloo, Ontario.

Dohrmann, C.R., Busby, H.R., Trujillo, D.M., 1988. Smoothing noisy data using dynamic programming and generalized cross–validation. Journal of Biomechanical Engineering 110, 37–41.

Dowling, J.J., 1985. A modeling strategy for the smoothing of biomechanical data. In: Johnsson, B. (Ed.), Biomechanics X-B, Human Kinetics, Chicago, pp. 1163–1167.

Dumas, R., Chéze, L., Verriest, J.–P., 2007. Adjustments to Mcconville et al. and young et al. body segment inertial parameters. Journal of Biomechanics 40, 543–553.

Durkin, J.L., Dowling, J.J., 2003. Analysis of body segment parameter differences between four human populations and the estimation errors of four popular mathematical models. Journal of Biomechanical Engineering 125, 515–522.

Eng, J.J., Winter, D.A., 1995. Kinetic analysis of the lower limbs during walking: what information can be gained from a three–dimensional model? Journal of Bio

Erer, K.S., 2007. Adaptive usage of the Butterworth digital filter. Journal of Biomechanics 40, 2934–2943.

Fu et al., 1987, Robotics: Control, Sensing, Vision, and Intelligence, McGraw-Hill, New York.

Georgakis, A., Stergioulas, L.K., Giakas, G., 2002a. Automatic algorithm for filtering kinematic signals with impacts in the Wigner representation. Medical and Biological Engineering and Computing 40, 625–633.

Georgakis, A., Stergioulas, L.K., Giakas, G., 2002b. Wigner filtering with smooth roll–off boundary for differentiation of noisy non–stationary signals. Signal Processing 82, 1411–1415.

Giakas, G., Baltzopoulos, V., 1997a. A comparison of automatic filtering techniques applied to biomechanical walking data. Journal of Biomechanics 30, 847–850.

Giakas, G., Baltzopoulos, V., 1997b. Optimal digital filtering requires a different cut-off frequency strategy for the determination of the higher derivatives. Journal of Biomechanics 30, 851–855.

Giakas, G., Baltzopoulos, V., Bartlett, R.M., 1998. Improved extrapolation techniques in recursive digital filtering: A comparison of least squares and prediction. Journal of Biomechanics 31, 87–91.

Giakas, G., Stergioulas, L.K., Vourdas, A., 2000. Time-frequency analysis and filtering of kinematic signals with impacts using the Wigner function: accurate estimation of the second derivative. Journal of Biomechanics 33, 567–574.

Gold, B., Rader, C.M., 1969. Digital Processing of Signals. McGraw-Hill, New York.

Güler, H.C., 1998. Biomechanical modeling of lower extremity and simulation of foot during gait. Ph.D. thesis, Middle East Technical University, Ankara, Turkey.

Harris, F.J., 1978. On the use of windows for harmonic analysis with the discrete Fourier transform. Proceedings of the IEEE 66, 51– 83.

Hatze, H., 1981. The use of optimally regularized Fourier series for estimating higher–order derivatives of noisy biomechanical data. Journal of Biomechanics 14, 13–18.

Hatze, H., 1990. Data conditioning and differentiation techniques. In: Berme, N., Cappozzo, A. (Eds.), Biomechanics of Human Movement: Applications in Rehabilitation, Sports and Ergonomics. Bertec, Ohio, pp. 237–248.

Hatze, H., 2002. The fundamental problem of myoskeletal inverse dynamics and its implications. Journal of Biomechanics 35, 109–115.

Ismail, A.R., Asfour, S.S., 1999. Discrete wavelet transform: a tool in smoothing kinematic data. Journal of Biomechanics 32, 317–321.

Kadaba, M.P., Ramakrishnan, H.K., Wootten, M.E., 1990. Measurement of lower extremity kinematics during level walking. Journal of Orthopaedic Research 8, 383–392.

Karpat, Y., 2000. Development and testing of kinematic data acquisition tools for a gait analysis system. M.Sc. thesis, Middle East Technical University, Ankara, Turkey.

Kuo, A.D., 1998. A least-squares estimation approach to improving the precision of inverse dynamics computations. Journal of Biomechanical Engineering 120, 148–159.

Lanshammar, H., 1982a. On practical evaluation of differentiation techniques for human gait analysis. Journal of Biomechanics 15, 99–105.

Lanshammar, H., 1982b. On precision limits for derivatives numerically calculated from noisy data. Journal of Biomechanics 15, 459–470.

Liu, J., Lockhart, T.E., 2006. Comparison of 3D joint moments using local and global inverse dynamics approaches among three different age groups. Gait & Posture 23, 480–485.

Macleod, A., Morris, J.R.W., 1987. Investigation of inherent experimental noise in kinematic experiments using superficial markers. In: Biomechanics X-B, Human Kinetics, Chicago, pp. 1035–1039.

McConville, J.T., Churchill, T.D., Kaleps, I., Clauser, C.E., Cuzzi, J., 1980. Anthropometric relationships of body and body segment moments of inertia. Technical Report, Aerospace Medical Research Laboratory, Wright-Patterson Air Force Base, Dayton, Ohio.

Nyquist, H., 1928. Certain topics in telegraph transmission theory. Transactions of the A. I. E. E. 47, 617-644.

Oppenheim, A.V., Schafer, R.W., 1989. Discrete-time signal processing, Prentice-Hall, New Jersey.

Özgören, M.K., 2004. ME 502 Advanced Dynamics Lecture Notes. Middle East Technical University, Ankara, Turkey.

Özgören, M.K., 2004. ME 522 Principles of Robotics Lecture Notes. Middle East Technical University, Ankara, Turkey.

Pearsall, D.J., Costigan, P.A., 1999. The effect of segment parameter error on gait analysis results. Gait & Posture 9, 173–183.

Pezzack, J.C., Norman, R.W., Winter, D.A., 1977. An assessment of derivative determining techniques used for motion analysis. Journal of Biomechanics 10, 377–382.

Robertson, D.G.E., Dowling, J.J., 2003. Design and responses of Butterworth and critically damped digital filters. Journal of Electromyography and Kinesiology 13, 569–573.

Rao, G., Amarantini, D., Berton, E., Favier, D., 2005. Influence of body segments' parameters estimation models on inverse dynamics solutions during gait, Journal of Biomechanics 39, 1531–1536.

Ren, L., Jones, R.K., Howard, D., 2005. Dynamic analysis of load carriage biomechanics during level walking. Journal of Biomechanics 38, Pages 853–863.

Ren, L., Jones, R.K., Howard, D., 2007. Predictive modelling of human walking over a complete gait cycle. Journal of Biomechanics 40, 1567–1574.

Riemer, R., Hsaio-Wecksler, E.T., Zhang, X., 2007. Uncertainties in inverse dynamics solutions: A comprehensive analysis and an application to gait. Gait & Posture, In press.

Schache, A.G., Baker, R., 2007. On the expression of joint moments during gait. Gait & Posture 25, 440–452.

Schache, A.G., Baker, R., Vaughan, C.L., 2007. Differences in lower limb transverse plane joint moments during gait when expressed in two alternative reference frames. Journal of Biomechanics 40, 9–19.

Simons, W., Yang, K.H., 1991. Differentiation of human motion data using combined spline and least squares concepts. Journal of Biomechanical Engineering 113, 348–351.

Shafiq, M.S., 1998. Motion tracking in gait analysis. M.Sc. thesis, Middle East Technical University, Ankara, Turkey.

Shafiq, M.S., Tümer, S.T., Güler, H.C., 2001. Marker detection and trajectory generation algorithms for a multicamera based gait analysis system. Mechatronics 11, 409–437.

Shannon, C.E., 1949. Communication in the presence of noise. Proceedings of the IRE 37, 10-21.

Padding point extrapolation techniques for the Butterworth digital filter. Journal of Biomechanics 22, 967–971.

Söylemez, B., 2002. An investigation on the gait analysis protocol of the "KISS" motion analysis system. M.Sc. thesis, Middle East Technical University, Ankara, Turkey.

van den Bogert, A.J., de Koning, J.J., 1996. On optimal filtering for inverse dynamics analysis. In: Proceedings of the Ninth Biennial Conference of the Canadian Society for Biomechanics, Vancouver.

Vardaxis, V.G., Allard, P., Lachance, R., Duhaime, M., 1998, Classification of able-bodied gait using 3-D muscle powers. Human Movement Science 17, 121–136.

Vint, P.F., Hinrichs, R.N., 1996. Endpoint error in smoothing and differentiating raw kinematic data: An evaluation of four popular methods. Journal of Biomechanics 29, 1637–1642.

Winter, D.A., Sidwall, H.G., Hobson, D.A., 1974, Measurement and reduction of noise in kinematics of locomotion. Journal of Biomechanics 7, 157–159.

Winter, D.A., 1990. Biomechanics and Motor Control of Human Movement. Wiley, New York.

Woltring, H.J., 1985. On optimal smoothing and derivative estimation from noisy displacement data in biomechanics. Human Movement Science 4, 229–245.

Woltring, H.J., 1990. Model and measurement error influences in data processing. In: Berme, N., Cappozzo, A. (Eds.), Biomechanics of Human Movement: Applications in Rehabilitation, Sports and Ergonomics. Bertec, Ohio, pp. 203–237.

Woltring, H.J., 1995. Smoothing and differentiation techniques applied to 3–D data. In: Allard, P., Stokes, I.A.F., Blanchi, J.P. (Eds.), Three-dimensional Analysis of Human Movement, Human Kinetics. Champaign, Chicago, pp. 79–99.

Wood,G.A., 1982. Data smoothing and differentiation procedures in biomechanics. Exercise & Sport Sciences Reviews 10, 308–362.

Yamaguchi, G.T., Pandy, M.G., Zajac, F.E., 1991. Dynamic muscoskeletal models of human locomotion: Perspectives on model formulation and control. In: Patla, A.E. (Ed.), Adaptability of Human Gait, Elsevier Science Publishers B.V., pp. 205–240.

Yu, B., Gabriel, D., Noble, L., An, K., 1999. Estimate of the optimum cutoff frequency for the Butterworth low-pass digital filter. Journal of Applied Biomechanics 15, 318–329.

Zatsiorsky, V.M., Seluyanov, V.N., Chugunova, L.G., 1990a. Methods of determining mass-inertial characteristicsof human body segments. In: Chemyi, G.G., Regirer, S.A. (Eds.), Contemporary Problems of Biomechanics. CRC Press, Massachusetts, pp. 272–291.

Zatsiorsky, V., Seluyanov, V., Chugunova, L., 1990b. In vivo body segment inertial parameters determination using a gamma-scanner method. In: Berme, N., Cappozzo, A. (Eds.), Biomechanics of Human Movement: Applications in Rehabilitation, Sports and Ergonomics. Bertec, Ohio, pp. 186–202.

Zijlstra, W., Bisseling, R., 2004. Estimation of hip abduction moment based on body fixed sensors. Clinical Biomechanics 19, 819–827.

APPENDIX A

THE BILINEAR TRANSFORMATION

An n[th] order filter has the following transfer function in z domain:

$$H(z) = \frac{\sum_{j=0}^{m} b_j z^{-j}}{1 + \sum_{i=1}^{n} a_i z^{-i}}.$$

A filter defined in s domain can be converted to its equivalent in z domain through bilinear transformation (Oppenheim and Schafer, 1989). The first step is to perform the substitution below:

$$s \to \frac{\omega_c}{\tan(\omega_c / 2 f_s)} \frac{z-1}{z+1} = \hat{f} \frac{z-1}{z+1},$$

where f_s is the sampling frequency in Hertz whereas the filter cut-off ω_c is expressed in radians per second. The constant $\hat{f}$ accounts for the phenomenon called frequency warping. It converges to 2 if f_s is much larger than ω_c. After this substitution, the transfer function of a second order filter takes the form below:

$$G(s) = \frac{\omega_c^2}{s^2 + 2\zeta\omega_c s + \omega_c^2} \to H(z) = \frac{\omega_c^2}{\left(\hat{f}\frac{z-1}{z+1}\right)^2 + 2\zeta\omega_c \hat{f}\frac{z-1}{z+1} + \omega_c^2}.$$

Rearrangement results in:

$$H(z) = \frac{b\left(1 + 2z^{-1} + z^{-2}\right)}{1 + a_1 z^{-1} + a_2 z^{-2}}.$$

The following equations yield the digital filter coefficients:

$$b = \frac{\omega_c{}^2}{\hat{f}^2 + 2\zeta\omega_c\hat{f} + \omega_c{}^2},\ a_1 = \frac{2\left(-\hat{f}^2 + \omega_c{}^2\right)}{\hat{f}^2 + 2\zeta\omega_c\hat{f} + \omega_c{}^2},\ a_2 = \frac{\hat{f}^2 - 2\zeta\omega_c\hat{f} + \omega_c{}^2}{\hat{f}^2 + 2\zeta\omega_c\hat{f} + \omega_c{}^2}.$$

APPENDIX B

SOME NUMERICAL METHODS USED IN THE WORK

B.1. Coefficients for the Second-Order Digital Butterworth Filter

Coefficients for a second-order digital Butterworth filter with cut-off frequency ω_c are calculated as shown below (Robertson and Dowling, 2003):

$$\hat{\omega} = \tan\left(\frac{1}{\sqrt[4]{\sqrt[m]{2}-1}}\frac{\omega_c}{2f_s}\right),\ K_1 = \sqrt{2}\hat{\omega},\ K_2 = \hat{\omega}^2,$$

$$b = \frac{K_2}{1+K_1+K_2},\ a_1 = 2b\left(1-K_2^{-1}\right),\ a_2 = \left(4b-a_1\right)-1.$$

In the equations above, m and f_s are respectively the number of passes and the sampling frequency of the digital signal to be filtered. It should be noted that for a zero-lag dual (forwards / backwards) pass, m is equal to 2. Such a practice results in an equivalent of a fourth-order filter.

B.2. Second-Order Central Difference Formulae

The central difference equations are (Chapra and Canale, 2002):

$$\dot{y}_k = \frac{-y_{k+2}+8y_{k+1}-8y_{k-1}+y_{k+2}}{12/f_s},$$

$$\ddot{y}_k = \frac{-y_{k+2}+16y_{k+1}-30y_k+16y_{k-1}-y_{k+2}}{12/f_s^2}.$$

In the equations above, k is point index, f_s is sampling frequency, $\dot{y}$ and $\ddot{y}$ respectively represent first and second derivatives.

B.3. Root Mean Squared Error

The Root Mean Squared Error can be defined as:

$$\mathrm{RMSE} = \sqrt{\frac{\sum_{k=1}^{N}\left(x_k - \hat{x}_k\right)^2}{N}} .$$

Here, x is the signal to be compared to the reference signal $\hat{x}$. k is the point index and N is the total number of points. A value closer to zero indicates better agreement between the signals.

APPENDIX C

THE NEWTON-EULER EQUATIONS OF MOTION

Linear and angular momenta of a rigid body are respectively defined as:

$$\vec{P} = m\vec{v}_G,$$
$$\vec{H}_G = \breve{J}_G \bullet \vec{\omega}.$$

To express in words; the linear momentum $\vec{P}$ is equal to the multiplication of the mass m with the linear velocity vector $\vec{v}_G$ of the centre of mass, the angular momentum (about the centre of mass) $\vec{H}_G$ is the dot product of the inertia tensor $\breve{J}_G$ with the angular velocity vector $\vec{\omega}$.

Time rates of change of momenta are equal to the forcing on the body:

$$\Sigma\vec{F} = D_i\left(\vec{P}\right),$$
$$\Sigma\vec{M} = D_i\left(\vec{H}_G\right).$$

$\Sigma\vec{F}$ and $\Sigma\vec{M}$ are the net force and net moment vectors acting on the body while D_i denotes the time derivative (with respect to an inertial reference frame) operator. The derivative of the linear momentum is simply:

$$D_i\left(\vec{P}\right) = m\dot{\vec{v}}_G = m\vec{a}_G,$$

where $\vec{a}_G$ is the acceleration of the mass centre. The derivative expression of the angular momentum is not that straightforward as it includes two terms which continuously change in time. Taking the derivative with respect to the body frame rather than the inertial frame simplifies the process because the inertia tensor is constant in the body frame:

$$D_i\left(\vec{H}_G\right) = D_b\left(\vec{H}_G\right) + \vec{\omega} \times \vec{H}_G = \breve{J}_G \bullet \vec{\alpha} + \vec{\omega} \times \breve{J}_G \bullet \vec{\omega}.$$

This practice, as seen, results in the additional term $\vec{\omega} \times \vec{H}_G$ as required by the transport theorem. $\vec{\alpha}$ is the angular acceleration vector and D_b denotes the time derivative operation with respect to the body frame.

Finally, the Newton-Euler equations of motion are:

$$\Sigma \vec{F} = m\vec{a}_G,$$
$$\Sigma \vec{M} = \breve{J}_G \bullet \vec{\alpha} + \vec{\omega} \times \breve{J}_G \bullet \vec{\omega}.$$

APPENDIX D

MATLAB CODE OF THE ADAPTIVE BUTTERWORTH FILTER

```
function [out1,out2,out3]=adaptiveB(in,fs,f1,f2,iter)
% out1: filtered signal
% out2: estimated velocity
% out3: estimated acceleration
% in: signal to be filtered (row vector)
% fs: sampling frequency (Hz)
% f1: lower cut-off frequency (Hz)
% f1+f2: upper cut-off frequency (Hz)
% iter: # of iterations

[padded,half]=pad(in); % padding

y=regular(padded,fs,(f1+f2)); % prefiltering

for k=1:iter

    [vel,acc]=differ(y,fs); % differentiation
    vel=abs(vel/max(abs(vel(half+1:half+length(in)))));
    acc=abs(acc/max(abs(acc(half+1:half+length(in)))));

    cri=vel+acc; cri=cri/max(cri); % criterion

    fc=f1+cri*f2; % cut-off frequencies

    ffc=adaptive(fc,fs,fc); % adaptive filtering of cut-off frequencies

    y=adaptive(padded,fs,ffc); % adaptive filtering

    y=regular(y,fs,max(ffc)); % postfiltering

end

[yy,yyy]=differ(y,fs);  % differentiation

out1=y(half+1:half+length(in)); % extraction of region of interest
out2=yy(half+1:half+length(in)); % extraction of region of interest
out3=yyy(half+1:half+length(in)); % extraction of region of interest

% subfunctions_____________________________________________________________

function [out1,out2]=pad(in)

lng=length(in);

a=in(1:floor(lng/2)); % split into two
b=in(floor(lng/2)+1:lng);
a=-a(length(a):-1:1)+2*in(1); % reflect & invert
b=-b(length(b):-1:1)+2*in(lng);
out1=[a(1:end-1) in b(2:end)];
out2=length(a(1:end-1));


function out=regular(in,fs,fc)
```

```
lng=length(in);

f=fc/((2^(1/2)-1)^0.25);
w=tan(pi*f/fs);
K1=2^0.5*w;
K2=w^2;
a=K2/(1+K1+K2);
b1=2*a*(1/K2-1);
b2=1-(4*a+b1);

x=zeros(1,lng); x(1)=in(1); x(2)=in(2);
for k=3:lng
    x(k)=a*(in(k)+2*in(k-1)+in(k-2))+b1*x(k-1)+b2*x(k-2);
end
y=zeros(1,lng); y(lng)=x(lng); y(lng-1)=x(lng-1);
for k=lng-2:-1:1
    y(k)=a*(x(k)+2*x(k+1)+x(k+2))+b1*y(k+1)+b2*y(k+2);
end

out=y;


function out=adaptive(in,fs,fc)

lng=length(in);
f=zeros(1,lng); w=zeros(1,lng); K1=zeros(1,lng); K2=zeros(1,lng);
a=zeros(1,lng); b1=zeros(1,lng); b2=zeros(1,lng);

for i=1:lng
    f(i)=fc(i)/((2^(1/2)-1)^0.25);
    w(i)=tan(pi*f(i)/fs);
    K1(i)=2^0.5*w(i);
    K2(i)=w(i)^2;
    a(i)=K2(i)/(1+K1(i)+K2(i));
    b1(i)=2*a(i)*(1/K2(i)-1);
    b2(i)=1-(4*a(i)+b1(i));
end

x=zeros(1,lng); x(1)=in(1); x(2)=in(2);
for k=3:lng
    x(k)=a(k)*(in(k)+2*in(k-1)+in(k-2))+b1(k)*x(k-1)+b2(k)*x(k-2);
end
y=zeros(1,lng); y(lng)=x(lng); y(lng-1)=x(lng-1);
for k=lng-2:-1:1
    y(k)=a(k)*(x(k)+2*x(k+1)+x(k+2))+b1(k)*y(k+1)+b2(k)*y(k+2);
end

out=y;


function [out1,out2]=differ(in,fs)

lng=length(in);
out1=zeros(1,lng); out2=zeros(1,lng);

for i=3:lng-2
    out1(i)=(-in(i+2)+8*in(i+1)-8*in(i-1)+in(i-2))/(12/fs);
    out2(i)=(-in(i+2)+16*in(i+1)-30*in(i)+16*in(i-1)-in(i-2))/(12/fs^2);
end
```

APPENDIX E

SAMPLE OUTPUTS OF KISS-GAIT AND KISSGAITM

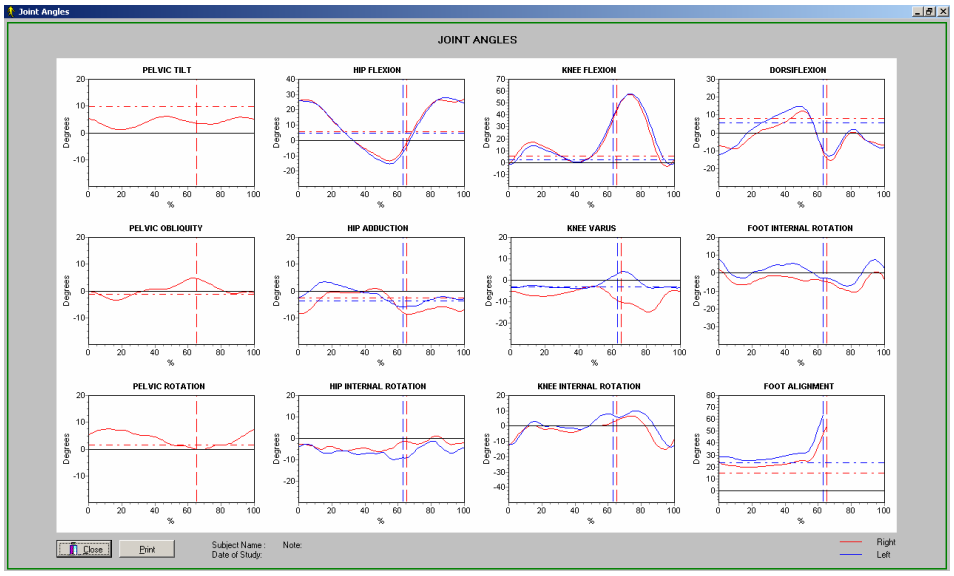

Figure 71. Sample joint angle plots of Kiss-GAIT.

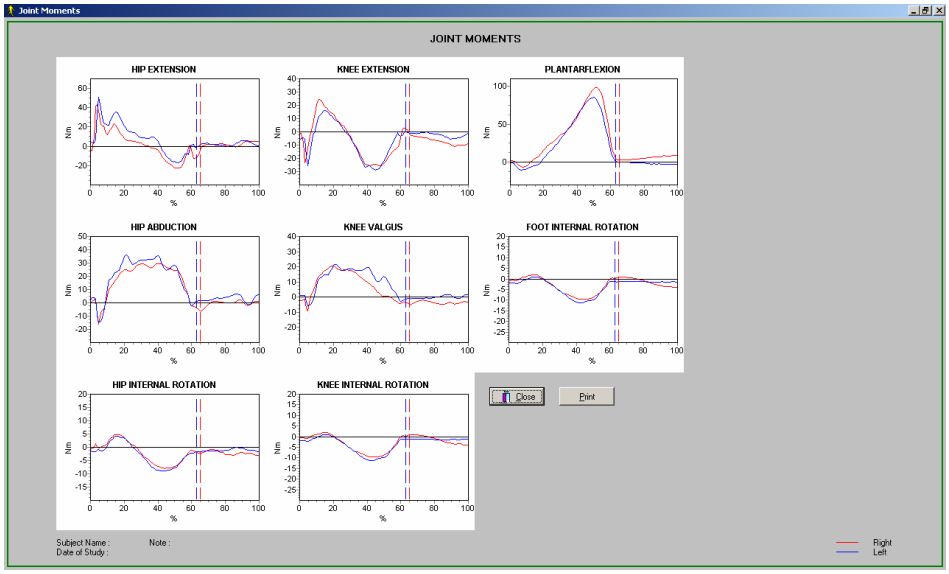

Figure 72. Sample joint moment plots of Kiss-GAIT.

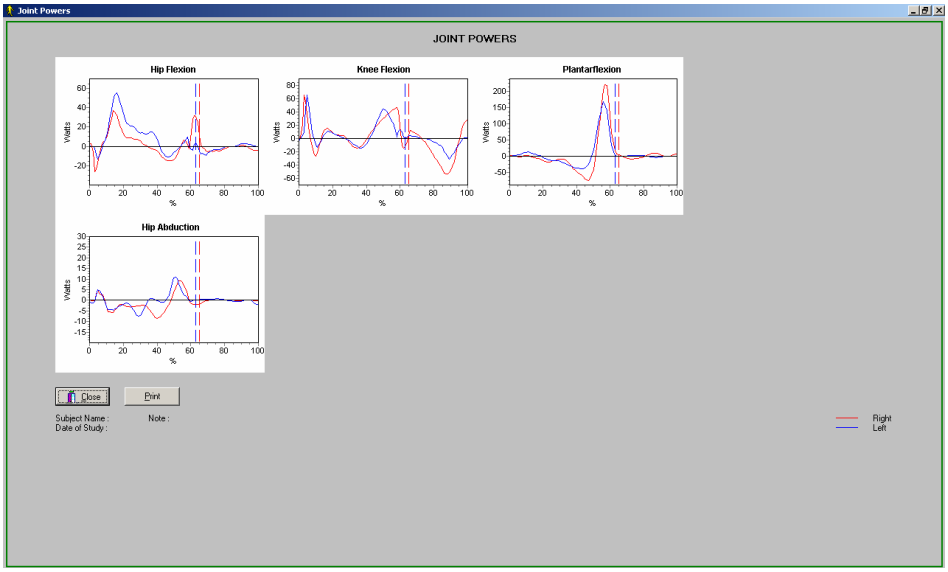

Figure 73. Sample joint power plots of Kiss-GAIT.

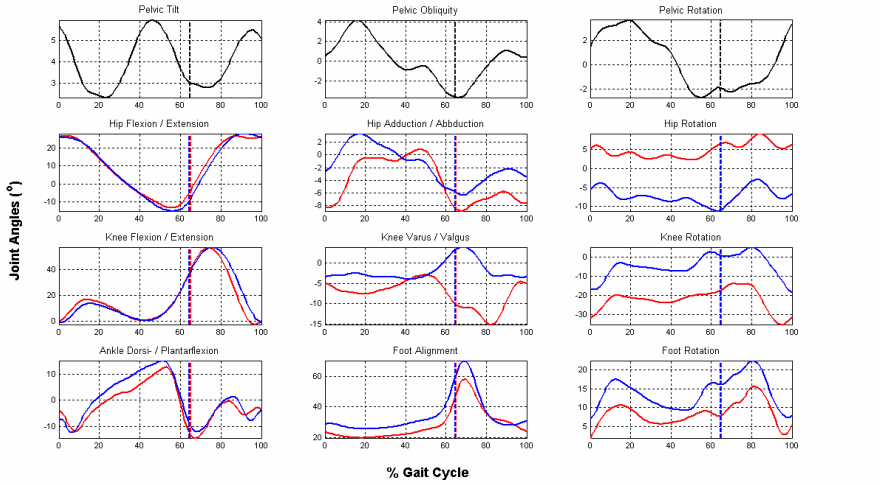

Figure 74. Sample joint angle plots of KissGaitM.

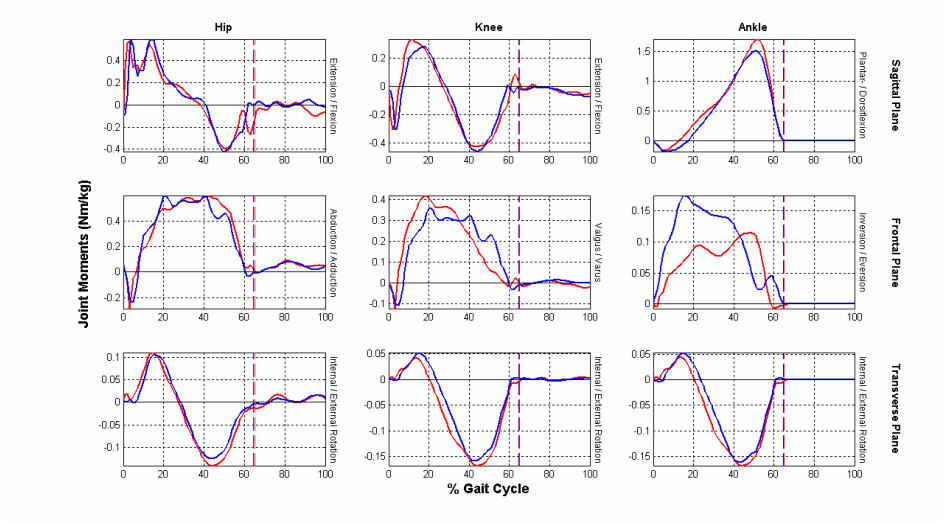

Figure 75. Sample joint moment plots of KissGaitM.

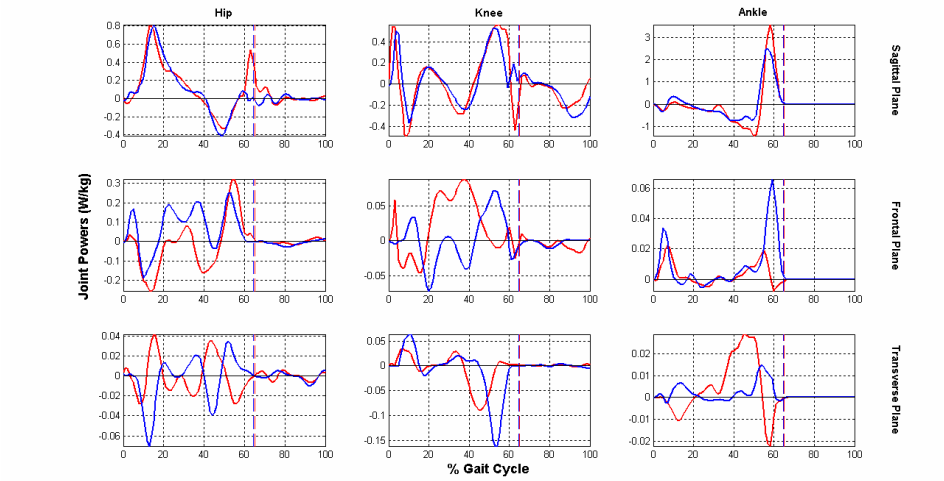

Figure 76. Sample joint power plots of KissGaitM.

APPENDIX E

THE PUBLISHED JOURNAL ARTICLE

ELSEVIER

Journal of Biomechanics 40 (2007) 2934–2943

JOURNAL OF BIOMECHANICS

www.elsevier.com/locate/jbiomech
www.JBiomech.com

Adaptive usage of the Butterworth digital filter

Koray S. Erer*

Mechanical Engineering Department, Middle East Technical University, Ankara, Turkey

Accepted 16 February 2007

Abstract

The Butterworth lowpass filter is a conventional tool that has been commonly used in gait analysis applications. Its operation mainly depends on the selection of the cut-off frequency, which must be done based on the condition of the raw signal assuming that it is stationary. This tool is unable to deal with nonstationary signals especially if impact is involved. In this paper, a modified version of the Butterworth filter that can handle nonstationary signals is presented. The new filter has a variable cut-off frequency distribution defined for each data point, which is determined by local signal characteristics. Because of its adaptive nature, it is possible for the filter to accommodate changes in the frequency content of the signal.

Keywords: Smoothing; Butterworth filter; Nonstationary signals

1. Introduction

Motion capture systems unavoidably introduce errors into marker trajectories. Therefore, raw trajectories must be filtered before they are differentiated; this is because of the noise amplifying feature of the ill-posed derivative estimation process (Woltring, 1985).

Among many tools that have been employed to deal with high-frequency noise, Butterworth filters find wide acceptance owing to their simplicity and acceptable performance. The only parameter which needs to be set by the user is the cut-off frequency, assuming that the order and number of passes are constant. Detailed discussions were given by Robertson and Dowling (2003) and Winter (1990).

Butterworth filters operate on the assumption that the signals to be processed are stationary (Woltring, 1995). However, this is not always the case when gait analysis is concerned. Vertical displacement histories of markers placed on distal segments of lower extremity are far from being so. For instance, an ankle marker comes to rest soon after heel-strike (impact), stays nearly motionless until heel-off, after which it swings in the air. In other words, in certain portions of the gait cycle, the signal contains more high-frequency components than others, meaning that the power of the signal changes in time. This fact limits the usefulness of Butterworth filters since they cannot accommodate changes in local signal structure.

The displacement data provided by Dowling (1985),[1] for which the acceleration history is also available, is a good example of signals which a Butterworth filter fails to handle properly. In the corresponding work, the horizontal pendulum experiment involved impact with a barrier, which is why the data are highly nonstationary. The peak acceleration caused by the impact is noticeably underestimated when the displacement data are low-pass filtered using a low cut-off frequency; if one wants to get a better estimation for the peak value, the cut-off frequency of the filter needs to be increased, which, in turn, results in unacceptable oscillations in the rest of the acceleration output (Giakas et al., 2000).

Based on this need, new filtering techniques have been recently introduced (Alonso et al., 2005; Georgakis et al., 2002a, b; Giakas et al., 2000; Ismail and Asfour, 1999). They were shown to produce better results than those of conventional filters, including the Butterworth filter. These methods are certainly promising; however, are not yet fully established and need further improvement in the sense that

*Tel.: +903124267290; fax: +903122102536.
E-mail address: kserer@gmail.com.

0021-9290/$ - see front matter © 2007 Elsevier Ltd. All rights reserved.
doi:10.1016/j.jbiomech.2007.02.019

[1] http://isbweb.org/data/dowling

selections of their parameters need to be settled on more solid basis.

With some modification, the Butterworth filter can be turned into a more powerful tool that is able to compete with these advanced techniques. This paper shows how the performance of the Butterworth filter can be improved by utilizing an approach that makes use of local signal characteristics. The method will be established with the aid of the data mentioned above and three additional signals will be processed for demonstration purposes.

2. Frequency content of Dowling's data

Frequency spectra up to 50 Hz of the displacement and acceleration data are given in Fig. 1. As seen, the signal gets considerably more contribution from higher harmonics in the second derivative level. However, these do not contribute to the entire signal uniformly, which can be demonstrated as follows: Firstly, the acceleration history was passed through Butterworth filters with increasing cut-off frequencies, f_c. Results can be viewed in Fig. 2. Above 15 Hz, the output was almost unaffected except for the region of impact (around 200th data point, approximately). Secondly, a windowed FFT analysis was carried out on the padded (Derrick, 1998) acceleration data to observe how the local power of the signal changed in time. Fig. 3 shows the plot of power contained within each window. A window length of 41 was selected to provide visual intelligibility. Each value on the vertical axis is a measure of the total power (sum of harmonic magnitudes) of a window whose center is the corresponding point on the horizontal axis. Following these results, it is obvious that the local frequency content of the signal suddenly increases around the impact region. Filters which aim to smooth such signals must accommodate time dependent changes in signal structure; an issue which was previously addressed by Dowling (1985): to be able to have effective noise removal while preserving the correct acceleration pattern, it is necessary to change the filtering method according to the interval being processed.

The following section gives details about how Butterworth filters can be modified so that they are able to handle nonstationary signals.

3. Modification to the Butterworth filter

A second order, recursive digital filter is defined by the following equation:

$$y_n = a_0(x_n + 2x_{n-1} + x_{n-2}) + b_1 y_{n-1} + b_2 y_{n-2}.$$

Filtered data points, y_n, are determined using both previously filtered and raw data points, x_n (n is the point index). For a Butterworth filter, coefficients are functions of the cut-off frequency and number of passes. Robertson and Dowling showed how to calculate them correctly in 2003. The same coefficients are used in the calculation of all data points within the signal. Usually, the data are fed in both forward and backward directions (dual pass) to have zero-lag, which results in a fourth-order filter.

In the preceding section, it was shown that accelerations resulting from impacts cannot be captured with low cut-off frequencies. However, using high cut-offs in regions where signal is weak almost always results in poor noise suppression. The solution might be to vary the cut-off frequency of the filter according to some criterion related to local acceleration, which will result in an adaptive Butterworth filter.

At this point, it is proposed that the cut-off frequency be a function of the point which is being processed. One

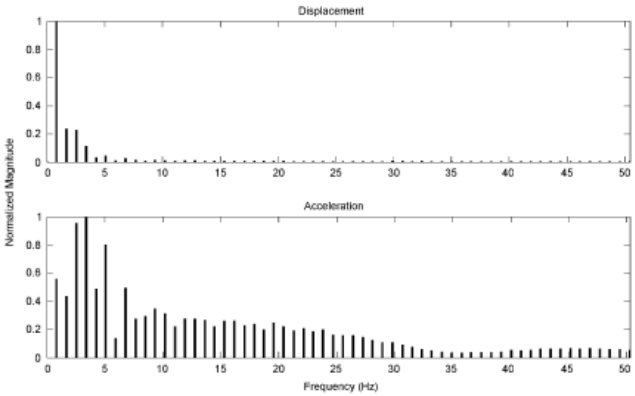

Fig. 1. Frequency spectra of the recorded displacement and acceleration signals.

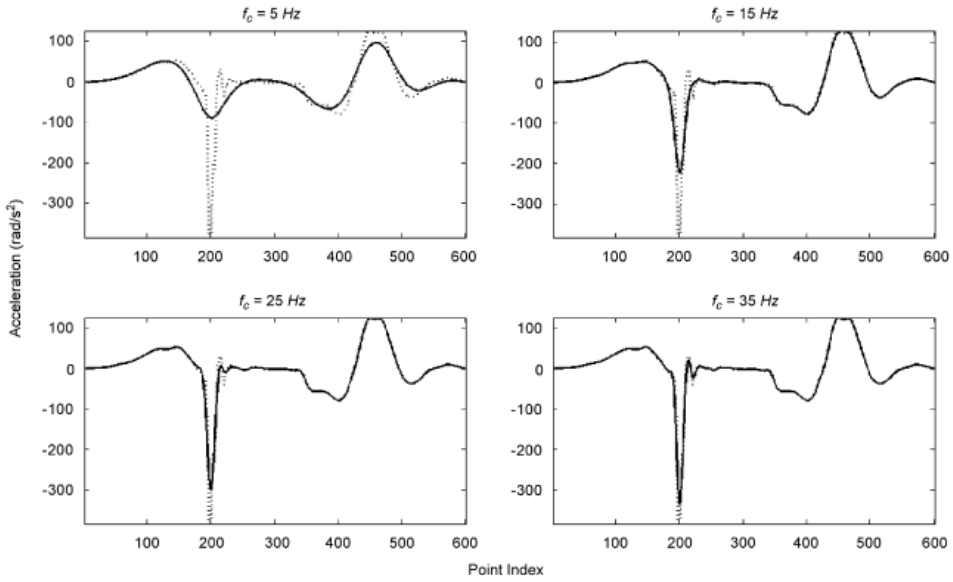

Fig. 2. Results of low-pass filtering (continuous lines) of the acceleration signal (dotted line) with increasing cut-off frequencies.

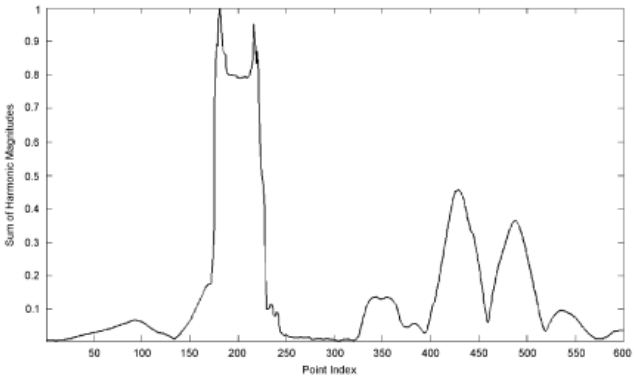

Fig. 3. A measure of the power of the acceleration signal as a function of time.

possible solution is

$$f_n = \omega_1 + \omega_2 c_n.$$

Cut-off frequencies, f_n, take values between ω_1 and $\omega_1 + \omega_2$, which denote the minimum and maximum frequency values to be used in the filtering process. Vector c should be formed such that it leads to cut-off frequencies that are closely correlated to local acceleration values. After exhaustive tests with our motion capture system, KISS (Shafiq et al., 2001), its formulation has been empirically

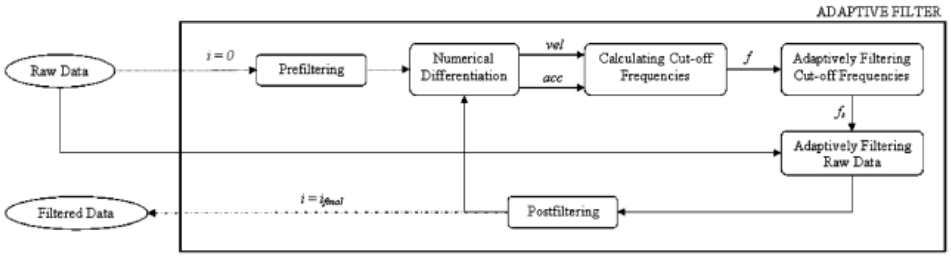

Fig. 4. Steps in the application of the iterative adaptive filter.

determined as

$$d_n = vel_n + acc_n,$$

$$c_n = d_n / \max(d),$$

vel and *acc* are the normalized (ranging between 0 and 1) first and second derivatives of the displacement data derived after filtering the signal. The criterion cannot be solely based on acceleration values because a certain degree of smoothness in the distribution of frequencies is required. Hence, cut-off values of points that have low accelerations but appreciable velocities (e.g. inflection points) are increased by making use of their velocity values. Filtering process needs to be initiated by prefiltering the signal using a standard Butterworth filter with a cut-off frequency f_p, after which the calculation of the adaptive cut-off frequencies follows.

Experimentation with the new filter indicated that iteration increases the performance as it allows the cut-off frequencies to be determined from improved (derived after adaptive filtering) velocity and acceleration estimates; however, it may tend to distort the smooth variation of the frequency distribution. Hence, low-pass filtering of f is necessary if the adaptive filter is to be used in an iterative manner. This filtering is done by employing an adaptive Butterworth filter that uses the elements of f as its own cut-off frequencies. In other words, f is filtered with itself, resulting in f_s. Adaptive filtering of the frequency distribution does not only eliminate the need for a constant cut-off value to be selected by the user, it also renders the total filtering process nearly insensitive to the choice of the prefiltering cut-off; f_p may safely be set equal to $\omega_1 + \omega_2$.

As for the final step, the output of the adaptive filter should be one last time passed through a standard Butterworth filter with a cut-off higher than or equal to the highest element of f_s. This represents a "finishing process", smoothing out small irregularities caused by the adaptive usage of the filter. Obviously, the result is an increase in the filter order.

Fig. 4 summarizes all the steps described above. It should be noted that raw data are padded as described by Derrick (1998) to decrease end point errors, and all four filter passes are single dual pass.

4. Other test signals

4.1. Foot impact data

This is one (S_3) of the nonstationary signals[2] experimentally obtained by Georgakis et al. (2002a). The data represent horizontal displacement that involves impact with an obstacle. The sampling rate is 1000 Hz.

4.2. Running simulation data

The vertical position history of ankle resulting from a running simulation done by van den Bogert and de Koning (1996)[3] is a challenging signal to test filters. The 10,000 Hz data were downsampled to 500 Hz to have a more realistic sampling rate and numerically differentiated to have the reference acceleration signal.

4.3. Gait experiment data

This is an artificial signal created by manipulating a signal of biomechanical origin, which is the vertical displacement of a metatarsal marker recorded at 50 Hz during an experiment with KISS. The reference signal was obtained by applying an eight term Gaussian fit (using MATLAB's Curve Fitting Tool), which, by coincidence, fitted to the data very well. Analytical fitting was used in obtaining the reference signal rather than low-pass filtering, which was preferred by Giakas and Baltzopoulos (1997b), so as to preserve high-frequency components present in the original signal. Fig. 5 shows the original and analytical signals. The resulting signal was differentiated to get the reference acceleration.

5. Results

In obtaining the results below, the limiting cut-off values were selected, after a number of trials, as the ones

[2] http://isbweb.org/c/isb/pub/files/data/filtering/giakas_non_stationary_signals.zip

[3] http://isbweb.org/data/invdyn

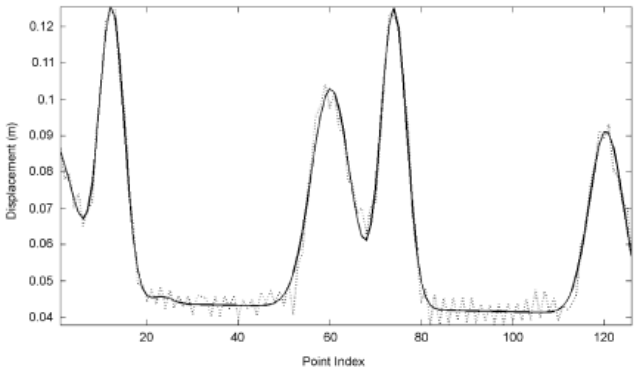

Fig. 5. Original (dots) and analytical (line) gait experiment data.

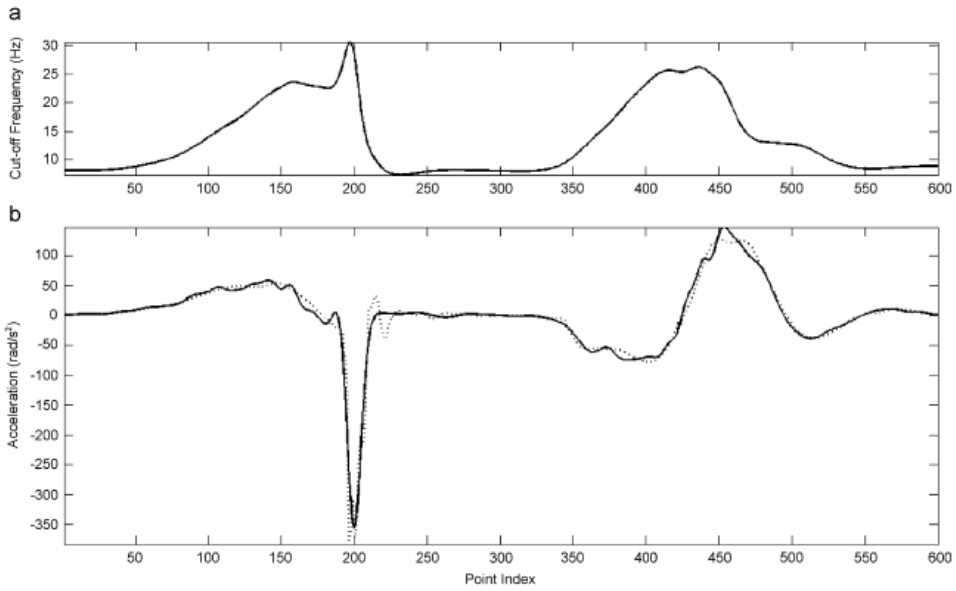

Fig. 6. [Dowling's data] (a) Distribution of the cut-off frequencies. (b) Reference acceleration signal (dotted line) and acceleration calculated after smoothing the displacement signal with the adaptive filter (solid line).

minimizing acceleration errors, where error refers to root mean square error (RMSE). Second-order central differences were used in all derivative calculations as they gave slightly better results than first-order differences did when compared with reference acceleration signals. Calculations were performed with MATLAB.

5.1. Dowling's data

The displacement signal was filtered with the adaptive filter using $\omega_1 = 8$ Hz and $\omega_2 = 25$ Hz. The distribution of cut-off frequencies resulting after six iterations is plotted in Fig. 6a. It is seen that the highest frequency values are

assigned to the points of impact phase. For the neighboring region, the cut-off stays almost constant around the lower limit as this is an interval where there is almost no displacement. Beyond these points, the filter again adjusts itself to the changes in the signal structure, raising frequency values. The error of the acceleration output presented in Fig. 6b is 12.72 rad/s^2. Except for slight discrepancies, the agreement between the curves is very good. This result is considerably better than the one obtained by Alonso et al. in 2005 (23.04 rad/s^2), mostly due to the improved estimation of the peak value. It is possible to approximate this peak acceleration better by increasing ω_1 and/or ω_2; but, the overall agreement would get worse in this case.

5.2. Foot impact data

Lower and upper cut-off frequency limits were selected as 10 and 105 Hz. Fig. 7a shows how the frequencies are distributed between these two values. Again, highest frequency values are assigned to points that have the highest acceleration values. Five iterations with the adaptive filter resulted in the output given in Fig. 7b. The corresponding error is 3.65 m/s^2, which is better than the result obtained in the original work (4.36 m/s^2). The difference between the peaks is 7.5 m/s^2. This value can be improved by tuning cut-off values, which would, however, worsen the overall error.

5.3. Running simulation data

The clean displacement signal was contaminated adding sets of normally distributed random noise with 0.5 mm standard deviation, which is within the range used by Giakas and Baltzopoulos (1997b). By performing a series of runs, $\omega_1 = 14$ Hz and $\omega_2 = 36$ Hz were determined to yield minimal error values for any random noisy set. For most cases, three iterations produced the best results. With this configuration, the filter was applied to 1000 different noisy sets. The mean of all errors was 3.85 m/s^2 with a standard deviation of 0.29 m/s^2. The mean of the differences between the peaks of the reference acceleration signal and differentiated filter outputs were 23.01 m/s^2 with the corresponding standard deviation being 3.57 m/s^2. Figs. 8a and b show the cut-off distribution and acceleration output, respectively, for one of the runs whose error values are the same as the mean values. It is seen that the cut-off frequencies are not distributed quite as would be expected; the maximum cut-off values are not assigned to the points around the highest acceleration interval. Nevertheless, the result is acceptable. Better or worse outputs are possible depending on the noise set.

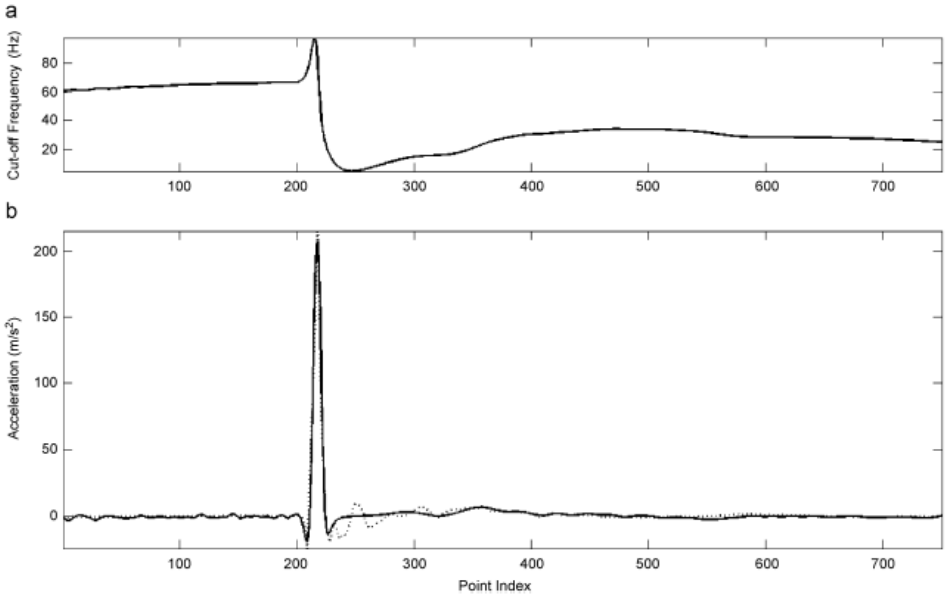

Fig. 7. [Foot impact data] (a) Distribution of the cut-off frequencies. (b) Reference acceleration signal (dotted line) and acceleration calculated after smoothing the displacement signal with the adaptive filter (solid line).

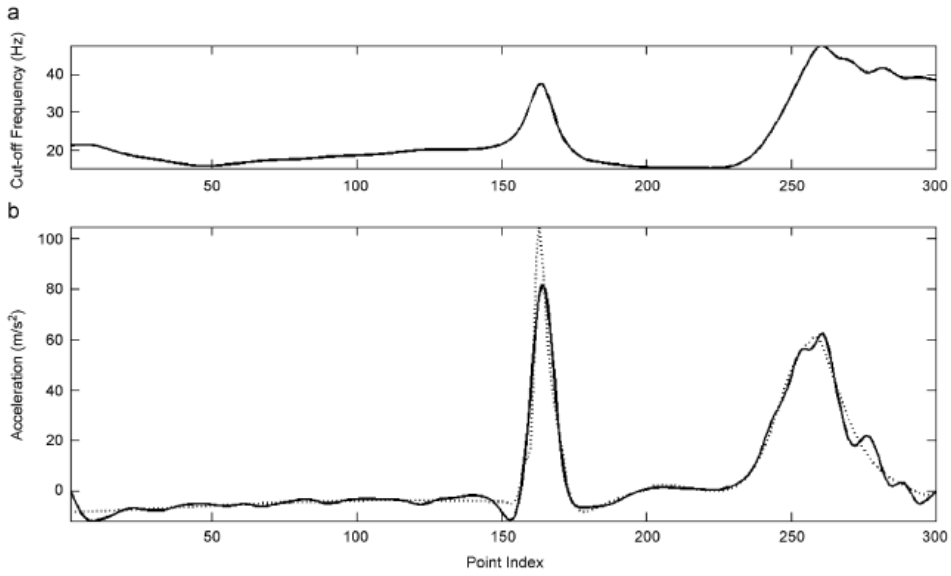

Fig. 8. [Running simulation data] (a) Distribution of the cut-off frequencies. (b) Reference acceleration signal (dotted line) and acceleration calculated after smoothing the displacement signal with the adaptive filter (solid line).

5.4. Gait experiment data

Sets of normally distributed random noise with 1.5 mm standard deviation (consistent with the noise characteristics of KISS) were added to the clean displacement signal. After a number of runs, $\omega_1 = 4$ Hz and $\omega_2 = 8$ Hz were concluded to produce lowest error values for the noisy sets. For most runs, best outputs were obtained after two iterations. Having this configuration, the filter was applied to 1000 different noisy sets. The mean value of the errors was 0.90 m/s^2 with a standard deviation of 0.13 m/s^2. Fig. 9a shows the cut-off frequency distribution of one of the noisy sets for which the error value is the same as the mean value. The acceleration output for the same data can be viewed in Fig. 9b. The agreement with the reference signal is encouraging. Slightly better or worse outputs are possible depending on the noise distribution.

As stated above, the result of filtering the running simulation data is not completely satisfying. Fairly high, prolonged acceleration period near the end of the signal causes simultaneous high-velocity values. Because of this fact, highest cut-off values are assigned to this portion of the signal instead of the short interval where the peak acceleration happens to be. This is responsible for the underestimated peak acceleration; ω_2 cannot be raised without causing the acceleration output of this period to get out of control. A similar behavior can also be seen in the filtering of Dowling's data, but is not as pronounced. After the first half of the signal, the velocity reaches its maximum value accompanied by some moderate amount of acceleration. However, the peak acceleration value here is so dominant that the maximum cut-off frequency is correctly positioned. The effect is nonetheless visible: there are some unwanted deviations in the interval of positive maximum acceleration. In the case of filtering the foot impact data, the highest velocity values occur before the impact and although these are low in a global view, they consequently give rise to unnecessarily high-frequency values, which, however, does not affect the output acceleration much. There are no such considerations for the gait experiment data. The velocity histories of the signals derived after adaptive filtering can be seen in Fig. 10. Subfigures (a–d) correspond to Dowling's, foot impact, running simulation, and gait experiment data, respectively.

In Fig. 11, error variations versus number of iterations are plotted for each test signal. Again, subfigures (a–d) belong to Dowling's, foot impact, running simulation, and gait experiment data. Except for (c), which converges to a nearly constant average error, all settle to a constant error value. Convergence is quick; usually in the order of a few iterations. The curves never settle to the minimum

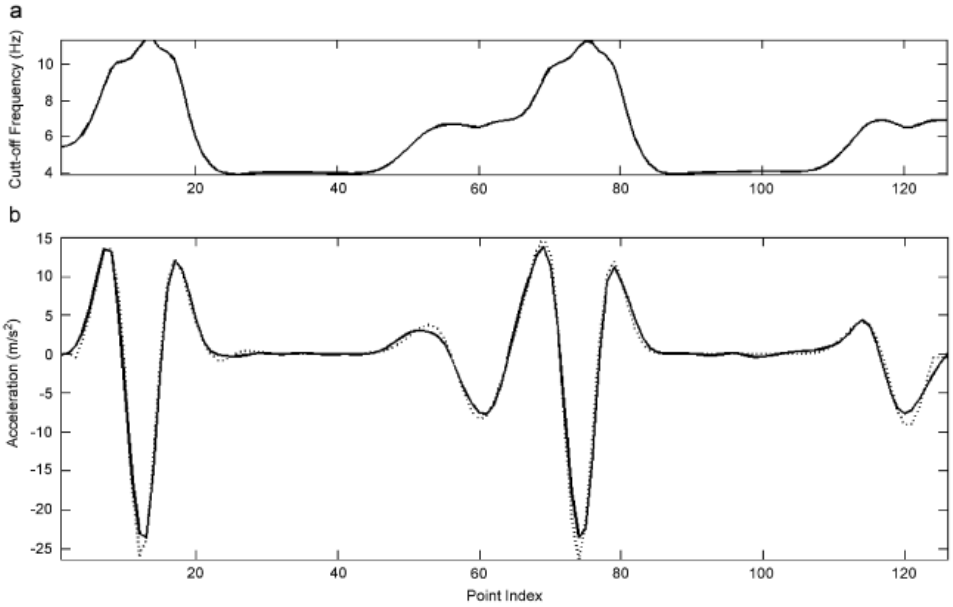

Fig. 9. [Gait experiment data] (a) Distribution of the cut-off frequencies. (b) Reference acceleration signal (dotted line) and acceleration calculated after smoothing the displacement signal with the adaptive filter (solid line).

error value possible, which means that more number of iterations does not mean a better result.

6. Discussion

Even if one happens to choose the "optimal" cut-off frequency (Capello et al., 1996; Yu et al., 1999; also see Giakas and Baltzopoulos, 1997a for a review and comparison of several methods), the conventional Butterworth filter either fails in catching extreme accelerations or is unable to eliminate noise when the signal is not stationary. Such a case was demonstrated by van den Bogert and de Koning (1996). In their work, unacceptable errors in intersegmental loads were caused by the inability to account for the correct nature of the phenomenon under investigation: the movement was "running", which unquestionably involves impacts. The proposed filter exploits signal features, making it possible for the Butterworth filter to accommodate changes in local frequency content so that errors arising from improper filtering are eliminated as much as possible. The method involves setting upper and lower limits instead of using a single cut-off frequency. Hence, some means of estimating optimal values for these limits would be extremely useful in the absence of reference acceleration signals.

Based on the results of the previous section, the proposed filter is not expected to work well with signals that have extended acceleration intervals, such as the vertical trajectory of a falling object which is under the continuous action of gravity. In this case, the cut-off value will theoretically increase linearly over time as the velocity of the object rises. This weakness of the adaptive filter is a natural consequence of the criterion that is used in the calculation of the cut-off frequencies. The velocity enters into the calculation being as dominant as the acceleration. The weight of the velocity might be decreased in various ways; yet, this adds another filter parameter to be determined by the user and furthermore, runs with such configurations did not produce superior results.

The idea of employing variable cut-off frequencies is promising; however, because of the continuously changing coefficients of the adaptive filter, final acceleration can easily assume a highly oscillatory pattern if filtering of the cut-off frequencies and postfiltering of the already smoothed data are not executed. Moreover, Butterworth filters have defined attenuation behaviors in frequency domain. Whether such a definition is possible for the

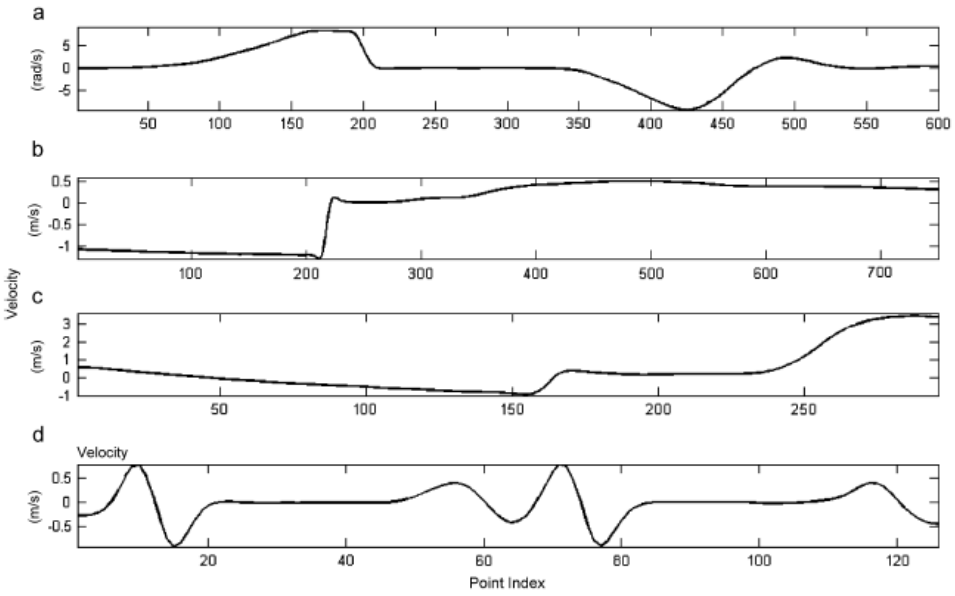

Fig. 10. Velocity histories of (a) Dowling's data, (b) foot impact data, (c) running simulation data, (d) gait experiment data.

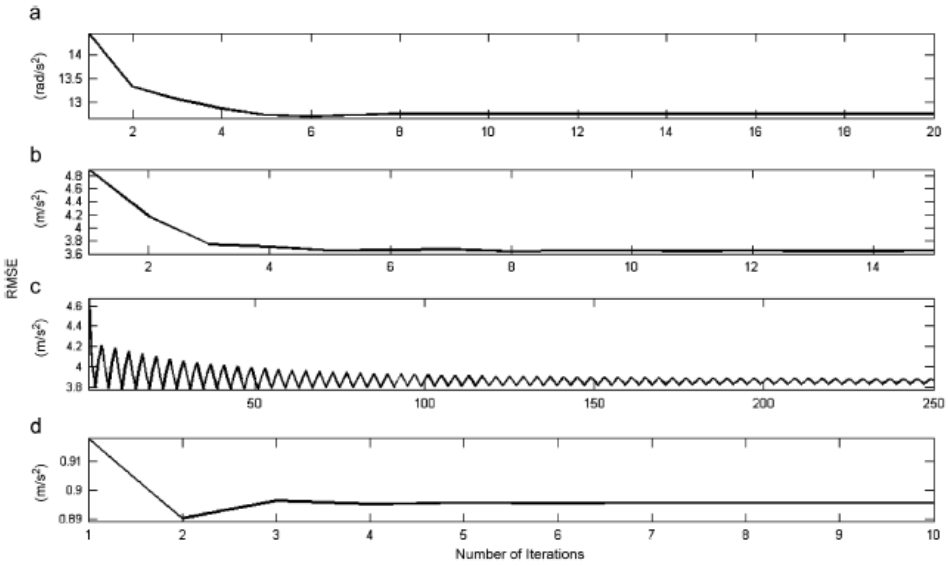

Fig. 11. Effect of number of iterations on RMSE for (a) Dowling's data, (b) foot impact data, (c) running simulation data, (d) gait experiment data.

modified version is a question which might be the subject of another study. Nonetheless, the good performance of the filter renders such issues less urgent.

The adaptive filter is expected to perform better with an improved and presumably more complex criterion for determining cut-off frequencies. The current one combines only the velocity and acceleration characteristics of the signal. Higher derivatives or the displacement data itself might contribute to the formation of a superior formulation. This remains an open question.

Acknowledgements

The author wishes to express his gratitude to Dr. S. Turgut Tümer and Dr. Sibel Tarı for their invaluable contribution.

References

Alonso, F.J., Del Castillo, J.M., Pintado, P., 2005. Application of singular spectrum analysis to the smoothing of raw kinematic signals. Journal of Biomechanics 38, 1085–1092.

Capello, A., Palombara, P.F.L., Leardini, A., 1996. Optimization and smoothing techniques in movement analysis. International Journal of Bio-Medical Computing 41, 137–151.

Derrick, T.R., 1998. Circular continuity of non-periodic data. In: Proceedings of the North American Congress on Biomechanics. University of Waterloo, Ontario.

Dowling, J.J., 1985. A modeling strategy for the smoothing of biomechanical data. In: Johnsson, B. (Ed.), Biomechanics X-B, Human Kinetics. Champaign, IL, pp. 1163–1167.

Georgakis, A., Stergioulas, L.K., Giakas, G., 2002a. Automatic algorithm for filtering kinematic signals with impacts in the Wigner representation. Medical and Biological Engineering and Computing 40, 625–633.

Georgakis, A., Stergioulas, L.K., Giakas, G., 2002b. Wigner filtering with smooth roll-off boundary for differentiation of noisy non-stationary signals. Signal Processing 82, 1411–1415.

Giakas, G., Baltzopoulos, V., 1997a. A comparison of automatic filtering techniques applied to biomechanical walking data. Journal of Biomechanics 30, 847–850.

Giakas, G., Baltzopoulos, V., 1997b. Optimal digital filtering requires a different cut-off frequency strategy for the determination of the higher derivatives. Journal of Biomechanics 30, 851–855.

Giakas, G., Stergioulas, L.K., Vourdas, A., 2000. Time-frequency analysis and filtering of kinematic signals with impacts using the Wigner function: accurate estimation of the second derivative. Journal of Biomechanics 33, 567–574.

Ismail, A.R., Asfour, S.S., 1999. Discrete wavelet transform: a tool in smoothing kinematic data. Journal of Biomechanics 32, 317–321.

Robertson, D.G.E., Dowling, J.J., 2003. Design and responses of Butterworth and critically damped digital filters. Journal of Electromyography and Kinesiology 13, 569–573.

Shafiq, M.S., Tümer, S.T., Güler, H.C., 2001. Marker detection and trajectory generation algorithms for a multicamera based gait analysis system. Mechatronics 11, 409–437.

van den Bogert, A.J., de Koning, J.J., 1996. On optimal filtering for inverse dynamics analysis. In: Proceedings of the Ninth Biennial Conference of the Canadian Society for Biomechanics, Vancouver.

Winter, D.A., 1990. Biomechanics and Motor Control of Human Movement. Wiley, New York.

Woltring, H.J., 1985. On optimal smoothing and derivative estimation from noisy displacement data in biomechanics. Human Movement Science 4, 229–245.

Woltring, H.J., 1995. Smoothing and differentiation techniques applied to 3-D data. In: Allard, P., Stokes, I.A.F., Blanchi, J.P. (Eds.), Three-dimensional Analysis of Human Movement, Human Kinetics. Champaign, IL, pp. 79–99.

Yu, B., Gabriel, D., Noble, L., An, K., 1999. Estimate of the optimum cutoff frequency for the Butterworth low-pass digital filter. Journal of Applied Biomechanics 15, 318–329.